Global budget of black carbon aerosol and implications for climate forcing

Global budget of black carbon aerosol and implications for climate forcing

A dissertation presented
by
Qiaoqiao Wang
to
The School of Engineering and Applied Sciences

in partial fulfillment of the requirements
for the degree of
Doctor of Philosophy
in the subject of
Engineering Sciences

Harvard Unversity
Cambridge, Massachusetts
November 2013

Global budget of black carbon aerosol and implications for climate forcing

Abstract

This thesis explores the factors controlling the distribution of black carbon (BC) in the atmosphere/troposphere and its implications for climate forcing. BC is of great climate interest because of its warming potential. Estimates of BC climate forcing have large uncertainty, in part due to poor knowledge of the distribution of BC in the atmosphere. This dissertation first examines the factors controlling the sources of BC in the Arctic in winter and spring using a global chemical transport model (GEOS-Chem). Emission inventories of BC and wet scavenging of aerosols in the model are updated to reproduce observed atmospheric concentrations of BC as well as observed snow BC content in the Arctic in winter-spring. The simulation shows a dominant contribution of fuel (fossil fuel and biofuel) combustion to BC in Arctic spring. Arctic snow BC content is dominated by fuel combustion sources in winter, but has equal contributions from open fires and fuel combustion in spring. The estimated decrease in Arctic snow albedo due to BC deposition in spring is 0.6%, resulting in a regional surface radiative forcing of 1.2 W m^{-2}. The dissertation then extends the evaluation of the BC simulation to the global scale using aircraft observations over source regions, continental outflow and remote regions and ground-based measurements. The observed low BC concentrations over the remote oceans imply more efficient BC removal than is currently implemented in models. The simulation that has total BC emissions of 6.5 Tg C a^{-1} and a mean tropospheric lifetime of 4.2 days for 2009 (vs. 6.8 ± 1.8 days for the AeroCom models) captures the principal

features of observed BC. The simulation estimates a global mean BC absorbing aerosol optical depth of 0.0017 and a top-of-atmosphere direct radiative forcing (DRF) of 0.19 W m^{-2}, with a range of 0.17-0.31 W m^{-2} based on uncertainties in the BC atmospheric distribution. The DRF is lower than previous estimates, which could be biased high because of excessive BC concentrations over the oceans and in the free troposphere.

Contents

List of Figures

List of Tables

Citations to Previously Published work

Chapters 2 has appeared previously as:

Wang, Q., et al. (2011), Sources of carbonaceous aerosols and deposited black carbon in the Arctic in winter-spring: implications for radiative forcing, Atmos. Chem. Phys., 11(23), 12453-12473, doi:10.5194/acp-11-12453-2011.

Acknowledgements

I am deeply grateful for the contribution of many individuals to this work.

Daniel Jacob has been an incredible advisor. He gave me the greatest support throughout my PhD study. He always encouraged me and can inspire me of raising scientific questions and finding out more interesting results. He also gave me lots of suggestions on my paper writing and presentation. He is a scientist that I most respect and hope to emulate in my future professional career.

I would like to thank Loretta Mickley, who has been very nice to share her expertise and ideas with me and give me many suggestions on my PhD study. I would also like to thank Min Shao, my advisor during my master study, who was very instrumental to my early interest and development as an atmospheric chemist.

I have greatly enjoyed the friendly atmosphere since I joined the Atmospheric Chemistry Modeling Group at Harvard in 2008. I would like to thank every group member, and in particular my office mate Amos Tai, classmates Elo ïse Marais and Kevin Wecht, and Tom Breider for friendship and help with my PhD study.

I also enjoyed being a member of the ARCTAS and HIPPO science Teams. In particular I have received many useful suggestions on my work from Jenny Fisher, Jingqiu Mao, Yutaka Kondo, Jose Jimenez, Michael Cubison, Ryan Spackman, Anne Perring, Joshua Schwarz, and David Fahey.

Thanks to all my friends at Harvard for many great weekends we have had together.

I would like to thank my parents and my brother, for their encouragement and support of my study abroad. Lastly, I would like to thank my husband Jianwei Gu for his continuous support and love over the past years!

Chapter 1. Overview

Black carbon (BC) is emitted to the atmosphere from the incomplete combustion of fossil fuel, wood and other biomass. It is only a minor contributor to aerosol mass, but is of great climate interest as a strong absorber of solar radiation both in the atmosphere [*Jacobson*, 2001; *Koch*, 2001; *Quinn et al.*, 2008] and after deposition to snow [*Warren and Wiscombe*, 1985; *Flanner et al.*, 2007; *McConnell et al.*, 2007].

Estimates of BC climate forcing have large uncertainties due to the heterogenous geographical distribution of BC aerosols associated with their relatively short lifetime and complex mechanisms through which BC affects the radiance balance [*Jacobson*, 2001,2004; *Flanner et al.*, 2007; *Koch et al.*, 2009a]. Recent studies have suggested a large direct radiative forcing (DRF) at the top-of-atmosphere (TOA) from BC of up to 1 W m^{-2}, making BC the second most important component of global warming after CO_2 in terms of DRF. However, there exits large uncertainty in BC DRF estimates (0.05-1 W m^{-2}), attributed mainly to a lack of understanding of the global burden and distribution of BC [*Bond et al.*, 2013].

A number of CTM studies have investigated the regional and global atmospheric distribution of BC, but there are large disagreements among models and discrepancies

with observations in the remote atmosphere, including the Arctic [*Koch et al.*, 2007; *Shindell et al.*, 2008; *Koch et al.*, 2009b; *Schwarz et al.*, 2010; *Tilmes et al.*, 2011]. There also exits controversy about the relative importance of wildfires and anthropogenic (fossil fuel and biofuel combustion) sources in the Arctic [*Warneke et al.*, 2010; *Matsui et al.*, 2011; *McNaughton et al.*, 2011].

The discrepancy between models and observations reflects uncertainties mainly in sources and wet scavenging of BC. Global emission inventories, such as from *Bond et al.* [2007] have regional uncertainties of about a factor of 2 as indicated by comparisons with observations in source regions. Wet scavenging, the main BC sink, appears to be a larger cause of discrepancy in model simulations in the remote troposphere. Global models generally use crude parameterizations of wet scavenging because it occurs on subgrid-scales [*Balkanski et al.*, 1993]. Additional uncertainties for BC scavenging relate to its hydrophilicity [*Park et al.*, 2005; *Riemer et al.*, 2010; *J. Liu et al.*, 2011], its ability to serve as a cloud condensation nuclei (CCN) or ice nuclei (IN) [*Croft et al.*, 2010; *J. Liu et al.*, 2011], and the collection mechanisms for in-cloud and below-cloud removal [*Croft et al.*, 2009; *X. Wang et al.*, 2010].

Understanding the factors controlling long-range transport of BC, observed global distributions and vertical profiles is important for reducing uncertainty in the estimates of BC climate forcing and predicting the potential radiative forcing (RF) reduction from BC abatement strategies. The latter is important for the assessment of BC abatement with regard to costs and benefits in a climate context.

Therefore, the motivation of this thesis has been to identify factors controlling the atmospheric BC distribution on both regional and global scales for better estimates of BC climate forcing. To accomplish this, I use my primary tool the GEOS-Chem 3D global chemical transport model (http://www.geos-chem.org) to bridge the gap between observations, model simulations and to better understand the underlying physical mechanisms. In particular, I show the importance of observations for constraining the BC lifetime, global burden and climate effects.

1.1 Research questions and methods

1.1.1 Carbonaceous aerosols in the Arctic

Aerosol pollution in the Arctic peaks in winter-spring, when transport from mid-latitudes is most intense and removal by deposition is slow [*Barrie et al.*, 1981; *Quinn et al.*, 2002; *Law and Stohl*, 2007; *Quinn et al.*, 2007]. This seasonal phenomenon is referred to as Arctic haze. One of the principal submicron aerosol components of Arctic haze is carbonaceous aerosol, including BC and organic aerosol (OA) [*Ricard et al.*, 2002; *Zhang et al.*, 2007]. Observations of Arctic haze date back to early 1980s [*Schnell*, 1984; *Schnell and Raatz*, 1984; *Schnell et al.*, 1989]. Early modeling studies of Arctic BC showed large errors in the model representation of the observed BC [*Shindell et al.*, 2008; *Koch et al.*, 2009b]. The origin of OA in the Arctic has received far less attention and attempts to model OA over the Arctic have been limited.

My work therefore addressed the following questions:

1) Can aircraft observations be used to constrain the simulation of Arctic carbonaceous aerosol in a global model?

2) What are the sources of carbonaceous aerosols in Arctic haze?

3) What are the sources of BC deposited to Arctic snow and how could that affect the Arctic climate?

I answered these questions using the GEOS-Chem global CTM, with constraints from aircraft measurements from the NASA Arctic Research of the Composition of the Troposphere from Aircraft and Satellites (ARCTAS) campaign [*Jacob et al.*, 2010] as well as long-term observations in surface air and in snow.

1.1.2 Global budget of black carbon aerosol

Mitigating BC is often considered a good solution for curbing short-term climate change due to the strong warming potential of BC, combined with its relative short atmospheric lifetime [*Jacobson*, 2002; *Bond*, 2007]. Accurate estimates of the BC climate effect are therefore important for optimizing mitigation strategies. However, there exits large uncertainty in the estimates of BC climate forcing, attributed partly to the poor knowledge of atmospheric BC concentrations [*Bond et al.*, 2013]. There are order-of-magnitude disagreements between models and observations in the remote and upper troposphere [*Koch et al.*, 2009b; *Schwarz et al.*, 2010; *Schwarz et al.*, 2013]. This can critically affect DRF estimates [*Zarzycki and Bond*, 2010; *Samset and Myhre*, 2011].

My work therefore addressed the following questions:

1) Can aircraft observations with vertical profiles be used to constrain global BC distribution and in particular vertical distribution in global models?

2) What is the global budget of BC?

3) What's the implication on BC direct radiative forcing?

I answered these questions using the GEOS-Chem global CTM, with constraints from the aircraft measurements by HIAPER Pole-to-Pole Observations (HIPPO) [*Wofsy et al.*, 2011], ARCTAS [*Jacob et al.*, 2010] and Aerosol Radiative Forcing in East Asia (A-FORCE) [*Oshima et al.*, 2012] campaigns as well as long-term ground-based measurements from the AERONET surface network [*Dubovik et al.*, 2002].

1.2 Dissertation outline and major results

In Chapter 2, I use GEOS-Chem as well as observations from ARCTAS conducted in April 2008, long-term records of surface concentrations in Alaska and snow BC measurements in the Arctic during 2007-2009 to analyze factors controlling sources of atmospheric carbonaceous aerosols and BC deposited in snow in the Arctic in winter-spring. I first update aerosol scavenging in GEOS-Chem by introducing distinction between rain and snow scavenging and applying different below-cloud scavenging efficiencies to individual aerosol modes (e.g. accumulation mode for carbonaceous

aerosols). I also update both open fire and anthropogenic (biofuel and fossil fuel combustion) emissions based on the comparison of simulated and observed OA and BC concentrations and OA versus BC emission ratios in fire plumes. The source attribution in the simulation is achieved by adding tagged tracers from different regions and source types.

I find that the ensemble of ARCTAS and surface observations provides important constraints on the sources of carbonaceous aerosols to the Arctic in winter-spring. GEOS-Chem with the improved representation of aerosol scavenging scheme was able to reproduce both vertical profiles of carbonaceous aerosols and snow BC content in the Arctic. I show here that during ARCTAS open fires were the dominant source of OA, but anthropogenic sources were more important for BC, particularly near the surface. The results suggest that Russian anthropogenic emissions are a major source of Arctic surface BC in winter and that Asian emissions are the main anthropogenic source of BC in the free troposphere. BC deposited in Arctic snow is dominated by anthropogenic sources in winter but is comparably contributed by open fire and anthropogenic sources in spring. The simulation derived a decrease in Arctic snow albedo of 0.6% in spring due to BC deposition, associated with a regional surface radiative forcing of 1.2 W m^{-2}.

In Chapter 3, I use GEOS-Chem as well as observations from HIPPO conducted over the Pacific in 2009-2011, ARCTAS conducted in April 2008, A-FROCE conducted in March-April 2009 and the AERONET network to estimate the global budget of BC and its implication on DRF. I update the aerosol wet deposition in GEOS-Chem to increase

the scavenging efficiency during convective updrafts based on pre-evaluation of the model BC simulation by comparison with HIPPO observations. I find that the updates to aerosol scavenging significantly improve the BC simulation over the remote Pacific, while not degrading the simulation of BC and other aerosols over the Arctic and over source regions. The results suggest much more efficient BC removal than previously implemented in models is required to reproduce the very low observed BC concentrations over the remote Pacific. I find that the simulation with a global source of 6.5 Tg a^{-1} and mean tropospheric lifetime of 4.2 d successfully simulates BC concentrations in source regions, continental outflow and over the remote Pacific. The derived global BC DRF is 0.19 W m^{-2} with a range of 0.17 - 0.31 W m^{-2} based on uncertainties in the BC atmospheric distribution. The DRF in this study is lower than previous estimates, which could be biased high because of excessive BC load over the oceans and in the free troposphere.

Chapter 2. Sources of carbonaceous aerosols and deposited black carbon in the Arctic in winter-spring: implications for radiative forcing

Abstract

We use a global chemical transport model (GEOS-Chem CTM) to interpret observations of black carbon (BC) and organic aerosol (OA) from the NASA ARCTAS aircraft campaign over the North American Arctic in April 2008, as well as longer-term records in surface air and in snow (2007-2009). BC emission inventories for North America, Europe, and Asia in the model are tested by comparison with surface air observations over these source regions. Russian open fires were the dominant source of OA in the Arctic troposphere during ARCTAS but we find that BC was of prevailingly anthropogenic (fossil fuel and biofuel) origin, particularly in surface air. This source attribution is confirmed by correlation of BC and OA with acetonitrile and sulfate in the model and in the observations. Asian emissions are the main anthropogenic source of BC in the free troposphere but European, Russian and North American sources are also important in surface air. Russian anthropogenic emissions appear to dominate the source of BC in Arctic surface air in winter. Model simulations for 2007-2009 (to account for interannual variability of fires) show much higher BC snow content in the Eurasian than the North American Arctic, consistent with the limited observations. We find that anthropogenic sources contribute 90% of BC deposited to Arctic snow in January-March and 60% in April-May 2007-2009. The mean decrease in Arctic snow albedo from BC deposition is estimated to be 0.6% in spring, resulting in a regional surface radiative forcing consistent with previous estimates.

2.1 Introduction

Aerosol pollution in the Arctic peaks in winter-spring, when transport from mid-latitudes is most intense and removal by deposition is slow [*Barrie et al.*, 1981; *Quinn et al.*, 2002; *Law and Stohl*, 2007; *Quinn et al.*, 2007]. The principal submicron aerosol components are sulfate and organic aerosols (OA) [*Ricard et al.*, 2002; *Zhang et al.*, 2007], which

affect Arctic climate by scattering solar radiation and modifying cloud properties [*Kristjansson et al.*, 2005; *Koch et al.*, 2007; *Quinn et al.*, 2007; *Quinn et al.*, 2008]. Black carbon (BC) is only a minor contributor to aerosol mass but is of great climatic interest as an absorber of solar radiation both in the atmosphere [*Jacobson*, 2001; *Koch et al.*, 2007; *Quinn et al.*, 2008] and after deposition to snow [*Warren and Wiscombe*, 1985; *Flanner et al.*, 2007; *McConnell et al.*, 2007; *Quinn et al.*, 2008]. Here we use a global chemical transport model (GEOS-Chem CTM) to interpret aircraft observations of BC and OA from the NASA ARCTAS campaign over the North American Arctic in April 2008 [*Jacob et al.*, 2010], as well as longer-term records of BC observations at surface sites and in snow. Our goal is to better understand the factors controlling the concentrations of carbonaceous aerosols in the Arctic, the deposition of BC to snow, and the implications for snow albedo and associated radiative forcing.

Observations of elevated BC at Arctic surface sites have been reported since the early 1980s [*Rosen et al.*, 1981; *Schnell*, 1984; *Hansen et al.*, 1989]. The early observations were attributed to fossil fuel combustion in northern Europe and Russia, based on air flow back-trajectories and correlations with trace metal tracers [*G.E. Shaw*, 1982; *Djupstrom et al.*, 1993]. BC concentrations in the Arctic decreased from the 1980s to 2000, followed by a slight increase in the past decade [*Sharma et al.*, 2006; *Eleftheriadis et al.*, 2009; *Gong et al.*, 2010; *Hirdman et al.*, 2010]. Recent measurements of BC in Arctic snow show a strong association with biomass burning based on tracer correlations and optical properties [*Hegg et al.*, 2009; *Doherty et al.*, 2010; *Hegg et al.*, 2010]. *Stohl*

et al. [2007] reported an event of extremely high BC concentrations in the Arctic in spring associated with agricultural burning in Eastern Europe.

The origin of OA in the Arctic has received far less attention. A two-year record of OA concentrations in northern Finland shows a minimum in winter and a maximum in summer attributed to biogenic and photochemical sources [*Ricard et al.*, 2002]. Measurements at Barrow show maximum OA in winter-spring, and correlations with chemical tracers suggest a dominance of ocean emissions (winter) and combustion sources (spring) [*P.M. Shaw et al.*, 2010; *Frossard et al.*, 2011].

Surface measurements of aerosols are not representative of the troposphere, particularly in the Arctic because of strong stratification [*Hansen and Rosen*, 1984; *Hansen and Novakov*, 1989; *Klonecki et al.*, 2003]. The vertical distribution of aerosols has important implications for radiative forcing [*Koch et al.*, 2009a]. Two coordinated aircraft campaigns with carbonaceous aerosol measurements were conducted in April 2008 out of Fairbanks, Alaska: the NASA Arctic Research of the Composition of the Troposphere from Aircraft and Satellites (ARCTAS) [*Jacob et al.*, 2010] and the NOAA Aerosol, Radiation and Cloud Processes affecting Arctic Climate (ARCPAC) [*Brock et al.*, 2011]. These two campaigns were part of the international program Polar Study using Aircraft, Remote Sensing, Surface Measurements and Models, of Climate, Chemistry, Aerosols and Transport (POLARCAT) (http://www.polarcat.no). They provided extensive vertical profiling of trace gases and speciated aerosols through the depth of the Arctic troposphere. They showed in particular large enhancements of carbonaceous aerosols in the mid-

troposphere due to open fires in Russia and Kazakhstan [*Warneke et al.*, 2009; *Spackman et al.*, 2010; *Warneke et al.*, 2010; *Kondo et al.*, 2011b; *Matsui et al.*, 2011; *McNaughton et al.*, 2011]. More recent airborne measurements of BC in the Arctic were made in April 2009 during the PAM-ARCMIP campaign [*Stone et al.*, 2010].

A number of CTM studies have investigated the sources of BC in the Arctic, but there are large disagreements among models and discrepancies with observations [*Shindell et al.*, 2008; *Koch et al.*, 2009b; *Tilmes et al.*, 2011]. Emissions in East Asia have grown rapidly in the past two decades and some work has pointed out an impact on winter-spring Arctic BC concentrations, especially in the free troposphere [*Koch and Hansen*, 2005; *Shindell et al.*, 2008; *Tilmes et al.*, 2011]. However, *Stohl* [2006] found little wintertime Asian influence over the Arctic either at the surface or in the free troposphere. *J.F. Liu et al.* [2011] pointed out that simulation of transport of BC to the Arctic is highly sensitive to the model representation of wet and dry deposition.

Attempts to model OA over the Arctic have been more limited. Open fires would be expected to be a dominant source on an annual average basis [*Koch et al.*, 2007]. There is a general tendency for models to underestimate observed OA concentrations in the remote atmosphere [*Heald et al.*, 2005; *Heald et al.*, 2011], and this has been attributed to poor representation of secondary organic aerosol (SOA) formation [*Volkamer et al.*, 2006; *Hodzic et al.*, 2010; *Heald et al.*, 2011].

We show here that the ensemble of ARCTAS and surface observations provide important constraints on the sources of BC and OA to the Arctic in winter-spring, and that the

GEOS-Chem model with improved representation of wet deposition can successfully simulate these observations. Our work builds on previous studies that applied GEOS-Chem to simulate observations of other species over the Arctic during ARCTAS/ARCPAC including CO [*Fisher et al.*, 2010], sulfate-ammonium aerosols [*Fisher et al.*, 2011], HO_x radicals [*J. Mao et al.*, 2010], and mercury [*Holmes et al.*, 2010]. Fires were a dominant source of OA during ARCTAS/ARCPAC, but we show that anthropogenic (fossil fuel and biofuel) sources were more important for BC, particularly near the surface. Anthropogenic BC was mainly of Asian origin in the free troposphere but had comparable contributions from Asia, Europe, North America and Russia near the surface. Our results suggest that Russian anthropogenic sources are a major source of Arctic BC in winter, and that BC concentrations in Arctic air and snow are highest in the Eurasian sector in both winter and spring.

2.2 Model description

We use the GEOS-Chem CTM version 8-01-04 (http://geos-chem.org) driven by assimilated meteorological data from the Goddard Earth Observing System (GEOS-5) of the NASA Global Modeling and Assimilation Office (GMAO). The GEOS-5 data have 6-hour temporal resolution (3-hour for surface quantities and mixing depths), 47 vertical layers, and 0.5 °x0.667 °horizontal resolution. We degrade the horizontal resolution to 2°x2.5° for input to GEOS-Chem. We initialize the model with a one-month spin-up followed by simulation of Jan-May 2008.

The simulation of carbonaceous aerosols in GEOS-Chem is as described by *Park et al.* [2006] and *Fu et al.* [2009], with modifications of wet deposition and emission inventories described below. BC and primary OA (POA) are emitted by combustion. SOA is produced in the atmosphere by reversible condensation of oxidation products of biogenic and aromatic volatile organic compounds [*S.H. Chung and Seinfeld*, 2002; *Henze and Seinfeld*, 2006; *Henze et al.*, 2008], as well as by irreversible condensation of glyoxal and methylglyoxal [*Fu et al.*, 2008; *Fu et al.*, 2009]. We find that SOA formed by either of these pathways is negligible in the winter-spring Arctic and we do not discuss it further here. The simulations of BC and POA in GEOS-Chem are linear (concentrations are proportional to sources) and we isolate the contributions from different sources by tagging them in the model.

Dry deposition in GEOS-Chem follows a standard resistance-in-series scheme [*Wesely*, 1989] as implemented by *Y.H. Wang et al.* [1998], with deposition velocities calculated locally using GEOS-5 data for surface values of momentum and sensible heat fluxes, temperature, and solar radiation. The global annual mean dry deposition velocity is 0.1 cm s^{-1} for BC and OA, typical of current models [*Reddy and Boucher*, 2004; *Huang et al.*, 2010]. Over snow/ice the *Wesely* [1989] parameterization yields a mean dry deposition velocity of 0.08 cm s^{-1}. *Fisher et al.* [2011] previously found that this leads to GEOS-Chem underestimate of sulfate at Arctic surface sites, and we find the same for BC. Following *Fisher et al.* [2011], we impose a constant aerosol dry deposition velocity of 0.03 cm s^{-1} over snow and ice based on eddy-covariance flux measurements in the Arctic by *Nilsson and Rannik* [2001] and *Held et al.* [2011]. With this assumption and as

discussed later, we find in the model that dry deposition contributes only 15% of total BC deposition to the Arctc in winter and 9% in spring. Similar BC dry deposition velocities (0.01-0.07 cm s^{-1}) over snow/ice were adopted in *J.F. Liu et al.* [2011] to improve their BC simulation over the Arctic in the AM-3 global model.

2.2.1 Wet deposition

Proper representation of scavenging by cold (ice) clouds and snow is important for simulation of aerosols in the Arctic. The standard scheme for aerosol scavenging in GEOS-Chem described by *Liu et al.* [2001] includes scavenging in convective updrafts, as well as in-cloud and below-cloud scavenging from convective and large-scale precipitation. However, it does not distinguish between rain and snow. Here we introduce such a distinction as well as other improvements to the scavenging scheme.

In the standard GEOS-Chem model, below-cloud scavenging (washout) of aerosol mass is calculated using a washout rate constant $k = a\,P$, where P is the precipitation rate (mm h^{-1}) and $a = 0.1$ mm^{-1} is a washout coefficient obtained by integrating scavenging efficiencies from impaction, interception, and diffusion over typical raindrop and aerosol size distributions [*Dana and Hales*, 1976]. This overestimates integrated scavenging during a precipitation event because it does not account for the preferential removal of coarse particles, shifting the aerosol size distribution toward the more scavenging-resistant accumulation mode [*Feng*, 2007; *Croft et al.*, 2009; *Feng*, 2009]. Here we use a parameterization $k = a\,P^b$ constructed by *Feng* [2007, 2009] for individual aerosol modes (nucleation, accumulation, and coarse) and for snow as well as rain. We adopt their

accumulation-mode scavenging coefficients for all aerosols except dust and sea salt, for which we adopt their coarse-mode coefficients. The corresponding values for rain ($T \geq$ 268 K) are $a = 1.1\times10^{-3}$ and $b = 0.61$ for accumulation-mode aerosols, and $a = 0.92$ and $b = 0.79$ for coarse-mode aerosols; for snow ($T < 268$ K), they are $a = 2.8\times10^{-2}$ and $b = 0.96$ for accumulation-mode aerosols, and $a = 1.57$ and $b = 0.96$ for coarse-mode aerosols. Here P is in units of mm h^{-1}, k is in unit of h^{-1}, and the units of a depend on the value of b. Scavenging of accumulation-mode aerosols by snow is 5-25 times more efficient than by rain for P in the range 0.01-1 mm h^{-1} because of the larger cross sectional area of snow crystals vs. rain drops [*Murakami et al.*, 1983]. The difference increases as P increases.

In-cloud scavenging (rainout) efficiently removes aerosols serving as cloud condensation nuclei (CCN) or ice nuclei (IN). In the case of warm (liquid) and mixed-phase clouds ($T \geq$ 258 K), we assume 100% incorporation of hydrophilic aerosols in the cloud droplets followed by efficient scavenging when liquid water is converted to precipitation by coalescence or riming. We assume that 80% of BC and 50% of POA are emitted as hydrophobic [*Cooke et al.*, 1999; *Park et al.*, 2003], and convert them to hydrophilic in the atmosphere with an e-folding time of 1 day which yields a good simulation of BC export efficiency in continental outflow [*Park et al.*, 2005]. In the case of cold clouds (T < 258K), we assume that only dust and hydrophobic BC can serve as IN and hence be removed by scavenging [*Chen et al.*, 1998; *Andreae and Rosenfeld*, 2008]. *Cozic et al.* [2007] find that the BC fraction scavenged into cloud droplets decreases with decreasing temperature, from 60% at 0^{o}C to 10% at <-20^{o}C. However, it must be recognized that the

scavenging of BC by cold clouds is highly uncertain [*Karcher et al.*, 2007; *Baumgardner et al.*, 2008; *Cozic et al.*, 2008; *Targino et al.*, 2009; *Stith et al.*, 2011].

Precipitation is a subgrid process on the horizontal scale of GEOS-Chem. A critical variable in the wet deposition parameterization is the areal fraction F_k of a grid box at vertical model layer k that actually experiences precipitation. *Liu et al.* [2001] applied the formulation of *Giorgi and Chameides* [1986] for the areal fraction F'_k over which new precipitation is formed:

$$F'_k = \frac{Q_k}{LC_1} \tag{2.1}$$

where Q_k is the grid-scale formation rate of new precipitation (kg m^{-3} s^{-1}), L is the condensed water content of the precipitating cloud and is assumed to be constant (L = 1.0×10^{-3} kg m^{-3}) [*DelGenio et al.*, 1996], and C_1 is the rate constant for conversion of cloud water to precipitation ($C_1 = C_{1min} + Q_k / L$ with $C_{1min} = 1.0\times10^{-4}$ s^{-1}). The algorithm is initiated for each grid square at the top of the tropospheric column and proceeds downward, computing the actual precipitating fraction F_k in layer k (index decreasing downward) as $F_k = \max(F'_k, F_{k+1})$ to account for precipitation formation overhead. In previous versions of GEOS-Chem, $Q_k > 0$ caused rainout to be applied to the whole precipitation area fraction F_k and washout was only applied when $F_k > 0$ and $Q_k \leq 0$ (negative Q_k indicating net evaporation). This caused an overestimation of in-cloud scavenging and underestimation of below-cloud scavenging, as $F_{k+1} > F'_k$ should be an indication of washout taking place over the fractional area $F_{k+1} - F'_k$ of layer k. In our

present simulation, we apply rainout in layer k to the precipitating fraction F'_k and washout to the additional fractional area F_{diff} = max (0, F_{k+1} - F'_k). The correction slows aerosol scavenging as washout is generally less efficient than rainout.

J.F. Liu et al. [2011] found in the AM-3 model a factor of 100 increase in winter-spring Arctic BC, and better agreement with observations from surface sites and from ARCTAS, by using a photochemically-varying timescale for BC hydrophobic-to-hydrophilic aging (up to 1-2 weeks in winter) and reducing total deposition efficiencies relative to their original model. They found in their model that 30-50% of Arctic BC remained hydrophobic in winter. However, the significant coating of BC particles indicated by aircraft observations of shell/core ratios [*Kondo et al.*, 2011b] and light absorption [*McNaughton et al.*, 2011] in ARCTAS suggests that BC in the Arctic is mainly hydrophilic. In addition, TRACE-P aircraft observations in Asian outflow in March-April provide good constraints that the BC aging time scale is no more than 2 days [*Park et al.*, 2005].

Model transport of aerosol from northern mid-latitudes to the Arctic is highly sensitive to the representation of wet deposition [*J.F. Liu et al.*, 2011]. There are many associated uncertainties including model precipitation and its vertical distribution, the subgrid scale of precipitation coupled to transport and the scavenging efficiencies from washout and rainout. The tropospheric lifetime of BC against deposition in our simulation is 5.9 days, not significantly different from the standard GEOS-Chem model (5-6 days), and within the range of 5-11days from current models [*Koch et al.*, 2009b]. Wet deposition accounts

globally for 77% of annual BC deposition, consistent with the AeroCom multimodel assessment (78.6 ±17%) [*Textor et al.*, 2006]. The tropospheric lifetime of ^{210}Pb aerosol in the model is 10.4 days [*Amos et al.*, 2012], consistent with observational constraints [*Liu et al.*, 2001]. With regard to the Arctic, our successful simulation of observations combined with the relatively good constraints on emissions (see discussion below) gives some confidence to our scavenging parameterization. *Fisher et al.* [2011] previously showed that it allows a successful simulation of sulfate-ammonium aerosol in ARCTAS.

2.2.2 Emissions of BC and OA

Figure 2.1 shows the hemispheric emissions of BC and POA (primary organic aerosol) in April 2008 in the model. Table 2.1 gives regional and global annual totals for 2008.

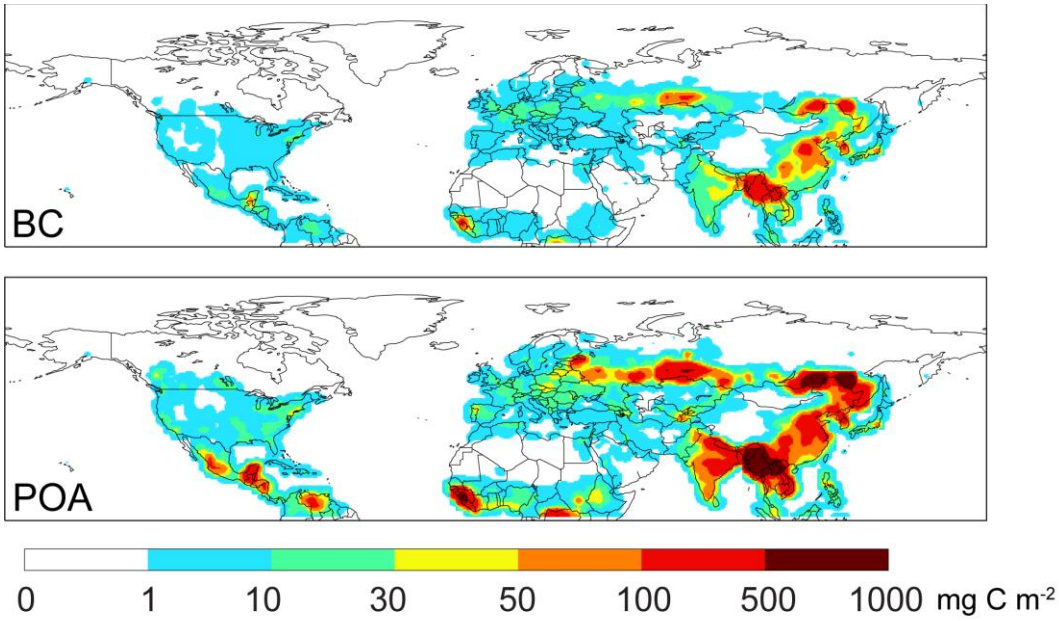

Figure 2.1: GEOS-Chem emissions of black carbon (BC) and primary organic aerosol (POA) in April 2008. Annual regional totals are in Table 2.1.

Table 2.1: Global GEOS-Chem emissions of carbonaceous aerosols in 2008[a]

Source	Black Carbon (Tg C a^{-1})	Organic Aerosol (Tg C a^{-1})
Anthropogenic[b]	7.0	14
North America (172.5–17.5 °W, 24–88 °N)	0.41	0.56
Europe (17.5 °W–30 °E, 50–88 °N & 17.5 °W–60 °E, 33–50 °N)	0.63	1.1
Russia (30–172.5 °E, 50–88 °N)	0.23	0.52
Asia (60–152.5 °E, 0-50 °N)	4.7	9.8
Rest of world	1.0	2.6
Open Fires[c]	11	84
North America (172.5–17.5 °W, 24–88 °N)	0.20	2.7
Europe (17.5 °W–30 °E, 33–88 °N)	0.082	0.63
Russia (30–152.5 °E, 33–60 °N)	0.60	4.5
South Asia (60–152.5 °E, 0-33 °N)	0.77	6.1
Rest of world	9.5	70
Total	18	98

[a] Values are annual means. Different region definitions are used for anthropogenic and open fire sources.

[b] Including fossil fuel and biofuel combustion. Values are from *Bond et al.* [2007] but with doubling of Russian and Asian emissions (see text).

[c] From the FLAMBE inventory of *Reid et al.* [2009] but with major modifications for Russian and Southeast Asian sources as described in the text.

Anthropogenic emissions (fossil fuel and biofuel combustion) are from *Bond et al.* [2007] for 2000, but with doubled emissions in Russia and Asia for both BC and POA to match BC surface observations in China and in the Arctic as discussed below. This doubling is consistent with the strong recovery of the Russian economy since 2000 [*IEA*, 2010] and with the general increase in Chinese emissions over the past decade [*L. Zhang et al.*, 2008; *Lu et al.*, 2010].

Open fires (not necessarily nature) are a major source of carbonaceous aerosols. April 2008 saw exceptionally high forest and agricultural fire activity in Russia and Kazahkstan (hereafter referred to collectively as "Russia") [*Warneke et al.*, 2009; *Fisher et al.*, 2010] as well as typical seasonal fire activity in Southeast Asia (including India and southern China). We specify open fire emissions with the Fire Locating and Monitoring of Burning Emissions (FLAMBE) inventory [*Reid et al.*, 2009], which has 1°x1° spatial resolution and hourly temporal resolution based on MODIS and GOES satellite fire counts. The FLAMBE inventory provides fine particle ($PM_{2.5}$) emissions based on total estimated fuel combustion, carbon fraction in the fuel, and $PM_{2.5}$ emission factors [*Reid et al.*, 2005; *Reid et al.*, 2009]. We partition $PM_{2.5}$ emissions into BC and OA using BC/OA emission ratios from *Andreae and Merlet* [2001] for different vegetation types. *Fisher et al.* [2010] previously used FLAMBE to simulate ARCTAS/ARCPAC CO observations with GEOS-Chem and found that Russian and Southeast Asian emissions needed to be reduced to 53% and 45%, respectively, of the original FLAMBE values. We apply here the same reductions to BC and OA emissions and further correct the emissions to fit the ARCTAS data. Open fires in Russia were the dominant source of OA in ARCTAS [*Warneke et al.*, 2009; *Warneke et al.*, 2010], and we find from tagged source attribution that OA emissions from Russian fires must be reduced by an additional 36% to match the ARCTAS observations. Our resulting OA emission factor from the Russian fires is 6.8 grams carbon per kilogram dry mass burned, consistent with the 3.3-9.7 range reported in the literature for agricultural and extratropical forest fires [*Andreae and Merlet*, 2001; *Akagi et al.*, 2011].

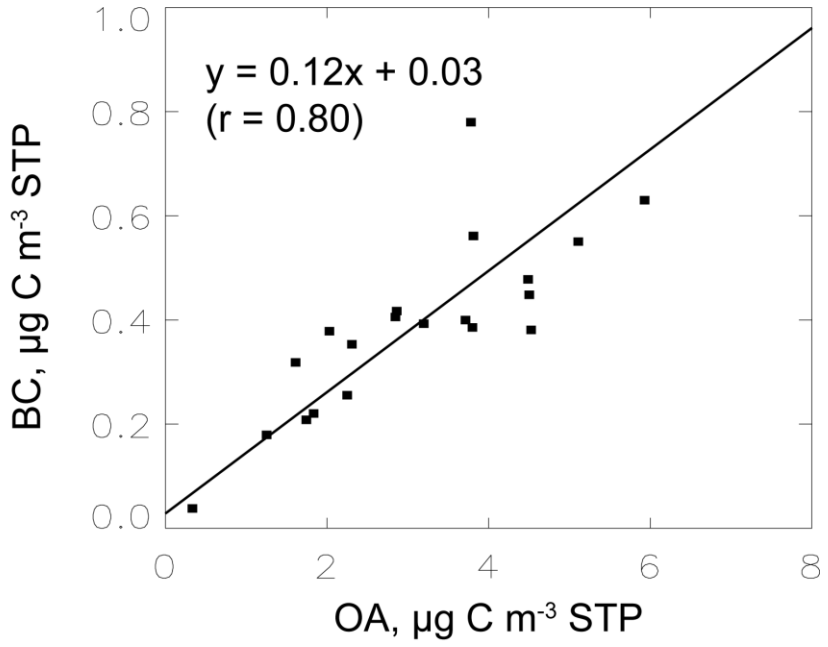

Figure 2.2: Scatterplot of BC vs. OA concentrations in fire plumes diagnosed by [CH_3CN] > 200 ppt for the ensemble of ARCTAS DC-8 flights (1-19 April 2008). STP refers to standard conditions of temperature and pressure (273 K, 1 atm) so that µg C m^{-3} STP is a mixing ratio unit. The reduced-major-axis (RMA) regression is shown by the solid line and the corresponding equation is given in the inset.

From there we use observations of the BC/OA concentration ratio in fire plumes to constrain the BC emission factor. *Warneke et al.* [2009] reported BC/OA ratios of 0.14 (agricultural fires) and 0.15 (forest fires) on a carbon basis for Russian fire plumes sampled in ARCPAC, and we find a similar observed ratio of 0.12 $\pm$0.03 for fire plumes sampled in ARCTAS (Fig. 2.2). The model as specified above, with a BC/OA emission ratio of 0.13, reproduces these observed values in the fire plumes and we have no need to adjust them further. The resulting BC emission factor from the Russian fires is 0.87 g kg^{-1} (gram carbon per kilogram dry mass burned), at the high end of the 0.37-0.82 range

reported in the literature for agricultural and extratropical forest fires [*Andreae and Merlet*, 2001; *Akagi et al.*, 2011].

Figure 2.3 compares annual mean surface air concentrations of BC in the model in 2008 with observations from networks in the US (2008), China (2006), and Europe (2002-2003). Our objective is to diagnose any large model bias in these three major source regions relevant to the Arctic. For the US we use 2008 data from the rural IMPROVE network (http://vista.cira.colostate.edu/improve/Data/IMPROVE/AsciiData.-aspx). For China and Europe we do not have network observations for 2008 and therefore use data for other years with the assumption that interannual variability is small: *X.Y. Zhang et al.* [2008] for rural/regional sites in China in 2006, and the BC/OC campaign in Europe in 2002-2003 (http://tarantula.nilu.no/projects/ccc/-emepdata.html). We diagnose for each region the normalized mean bias:

$$NMB = 100\% \times \sum_i (M_i - O_i) / \sum_i O_i \qquad (2.2)$$

where the sum is over the ensemble of sites i, and M_i and O_i are the modeled and observed values, respectively.

The data in Fig. 2.3 show normalized mean biases of -24% for China, -31% for Europe, and +35% for the US. Without doubling the inventory from *Bond et al.* [2007] the bias for China would be much larger (NMB = -61%). Underestimation in Europe is mainly due to three sites in northern Italy and Belgium. Without these three sites the NMB would decrease to -0.7%. The overestimation of BC in the US can be explained by a 40%

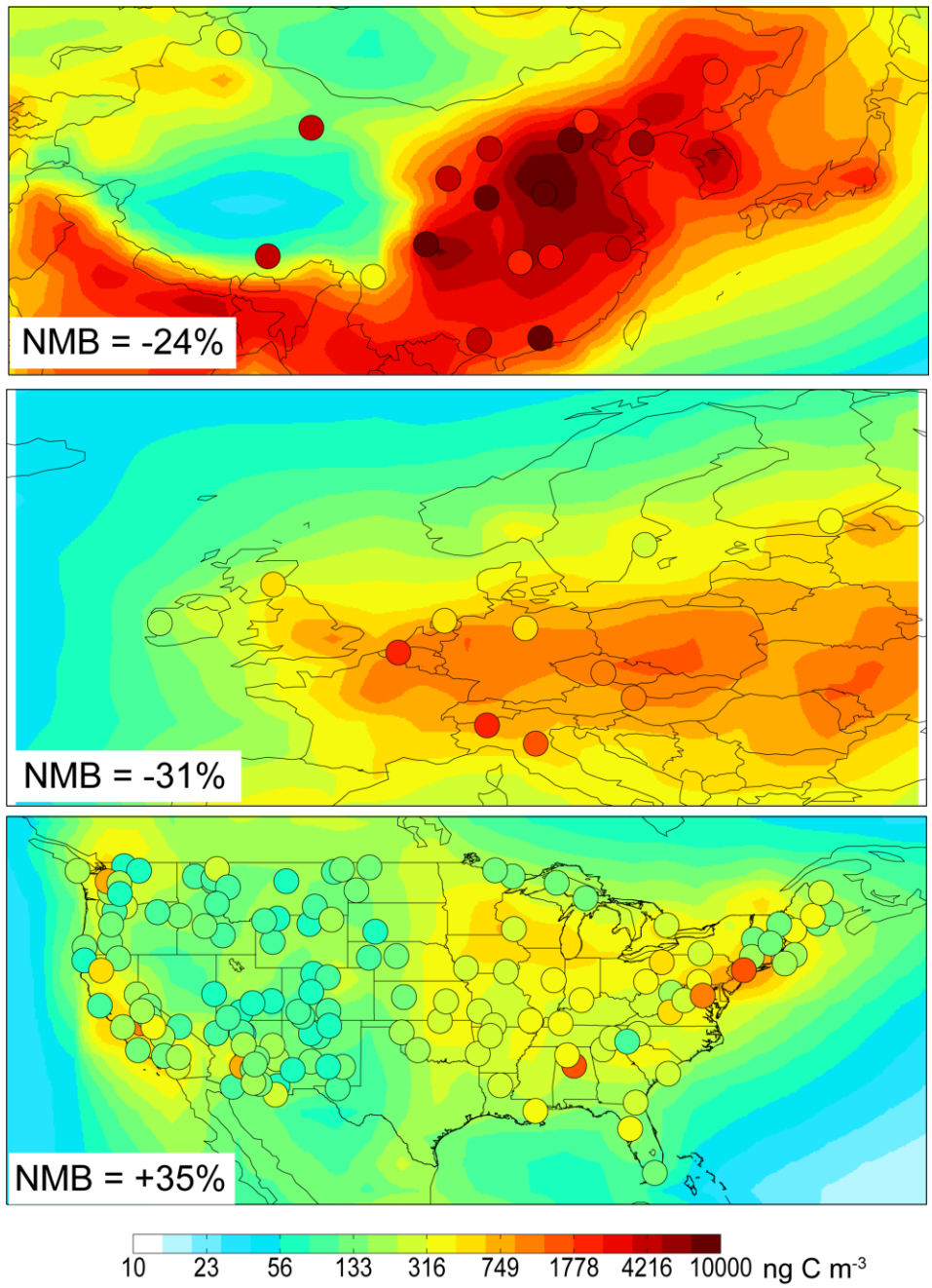

Figure 2.3: Annual mean surface air concentrations of BC aerosol in China, Europe, and the US. Model results for 2008 (solid contours) are compared to observations (circles). Observations are from *X.Y. Zhang et al.* [2008] in China for 2006, from the EMEP network in Europe for 2002-2003 (http://tarantula.nilu.no/projects/ccc/-emepdata.html), and from the IMPROVE network in the US for 2008 (http://vista.cira.-colostate.edu/improve/Data/IMPROVE/AsciiData.aspx). Normalized mean bias (NMB) statistics for each region are shown inset.

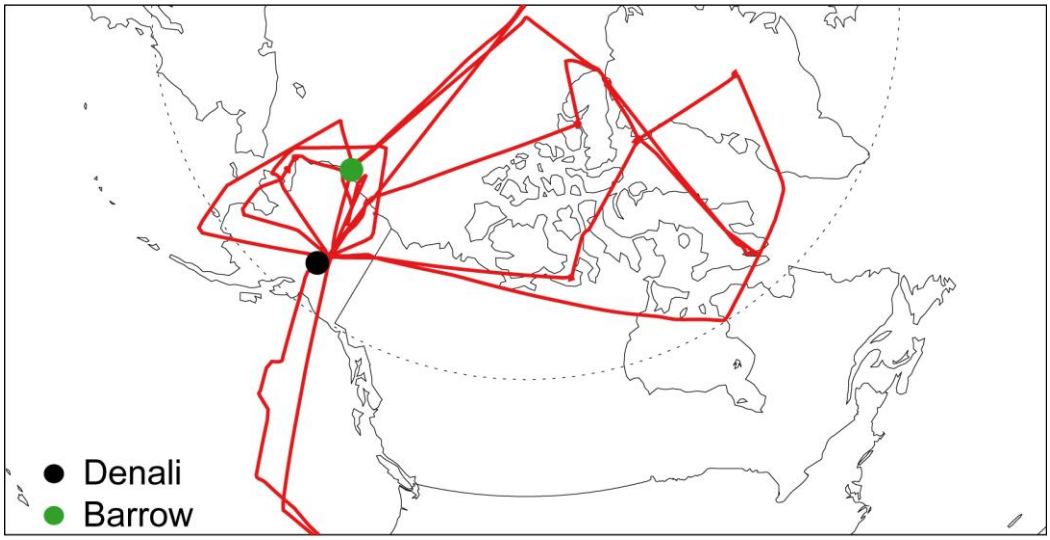

Figure 2.4: DC-8 flight tracks during the April 2008 ARCTAS campaign (red lines). Long-term monitoring sites for BC at Barrow and Denali are also indicated.

decrease in observed concentrations between 2000 (year of the *Bond et al.* [2007] inventory) and 2008, as shown by *Leibensperger et al.* [2012].

2.3 Sources of BC and OA in the Arctic

2.3.1 Constraints from aircraft data

Figure 2.4 shows the DC-8 flight tracks in ARCTAS. BC was measured with an SP2 (Single Particle Soot Photometer) instrument in the size range 0.08-0.860 μm [*Kondo et al.*, 2011b]. OA and other aerosol concentrations were measured by an Aerosol Mass Spectrometer (AMS) in the size range 0.045-1 μm [*Jimenez et al.*, 2003]. We assume that these measurements account for the bulk of BC and OA mass. The AMS measures OA in

units of μg m^{-3} and we convert this to μg C m^{-3} with a scaling factor of 2.1 typical of nonurban aerosols [*Turpin and Lim*, 2001; *Aiken et al.*, 2008]. The model is sampled along the flight tracks at the same time and location as the observations, and the aircraft data are averaged over the GEOS-Chem grid. Observations outside the Arctic (south of 60°N), in the stratosphere ($[O_3]/[CO] > 1.25$ mol mol^{-1}), and in fire plumes ($[CH_3CN] >$ 200 ppt) are excluded. We previously used the information from fire plumes to constrain the BC emission factor (Sect. 2.2).

BC and OA were measured from the ARCPAC aircraft concurrently with ARCTAS, but for fewer flights and a much smaller spatial domain in the Alaskan Arctic. *Fisher et al.* [2011] previously compared the GEOS-Chem sulfate-ammonium aerosol simulation to the ensemble of ARCTAS and ARCPAC observations, and found the ARCPAC data difficult to interpret because of the limited sampling and focus on fire plumes. We limit here our use of the ARCPAC data to the constraints that they provide on biomass burning emission factors [*Warneke et al.*, 2009; *Warneke et al.*, 2010] and BC dry deposition [*Spackman et al.*, 2010].

Figure 2.5 shows the overall fine aerosol composition measured by the ARCTAS DC-8 in 2-km altitude bins, providing context for the relative importance of BC and OA. Sea salt and dust are excluded as only bulk measurements were made in ARCTAS and we expect their coarse-mode fractions to be dominant. OA and sulfate are the dominant components of the fine aerosol. Sulfate is dominant in surface air but OA becomes comparable in the

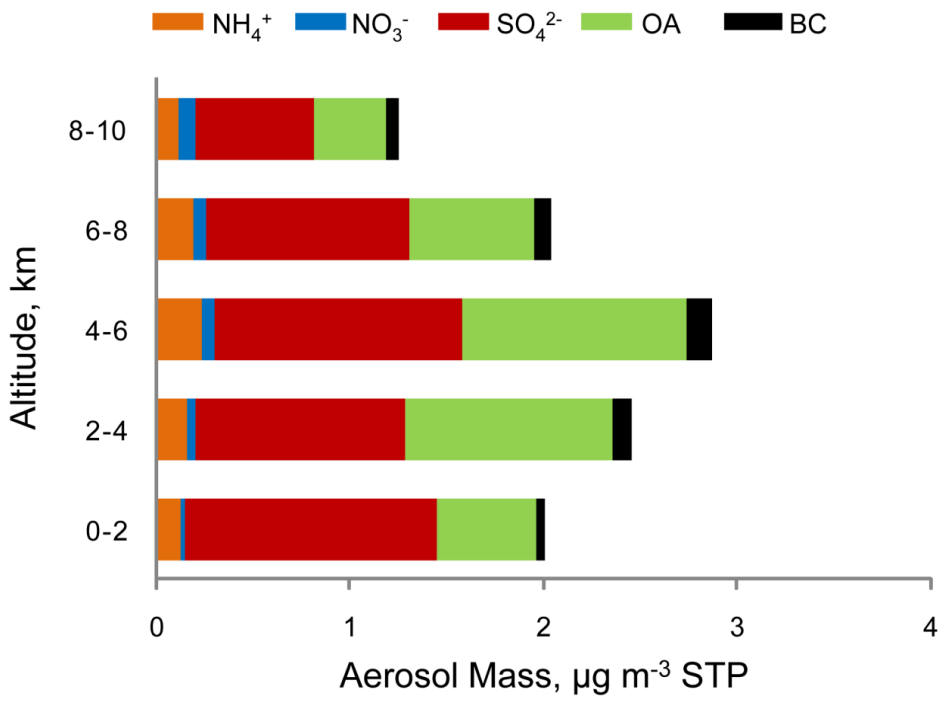

Figure 2.5: Fine aerosol composition observed along the ARCTAS DC-8 flight tracks (1-19 April 2008), averaged over 2-km altitude bins. The averaging excludes data collected south of 60 ºN, in stratospheric air, and in biomass burning plumes (see text).

free troposphere, because sulfate shows little variation with altitude while OA is strongly peaked at 2-6 km.

Figure 2.6 shows scatterplots of simulated vs. observed BC and OA concentrations during ARCTAS, and Figure 2.7 shows mean vertical profiles. The model has some success in reproducing the variability of the individual observations, with a correlation coefficient r = 0.65 for BC and 0.62 for OA. There are some large underestimates in the mid-troposphere associated with elevated CH_3CN, a tracer of biomass burning, but these may reflect the inability of the model to resolve fine plumes not screened by the [CH_3CN]

< 200 ppt filter. Concentrations of BC average 53 ±109 ng C m^{-3} in the observations and 63 ±65 ng C m^{-3} in the model. Concentrations of OA average 0.40 ±0.56 µg C m^{-3} in the observations and 0.35 ±0.37 µg C m^{-3} in the model.

The model successfully reproduces the mean vertical distributions of BC and OA, with peaks in the mid-troposphere. Also shown in Fig.2.7 is the model source attribution using tagged tracers as described in Sect. 2.2 Since the model relationship between sources and concentrations is linear, the source contributions are additive and the sensitivity to source magnitudes can be readily inferred from the data shown here. We see that the mid-troposphere peaks are due to Russian fires, and in the case of BC also to Asian

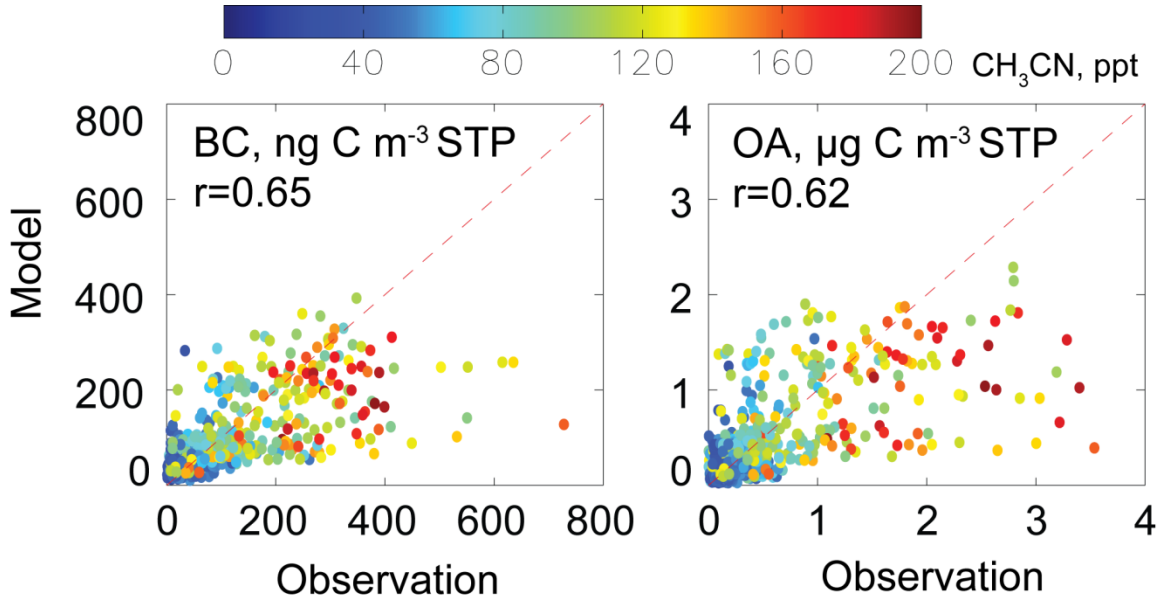

Figure 2.6: Scatterplots of simulated vs. observed BC and OA concentrations along the DC-8 flight tracks during ARCTAS (1-19 April 2008). Colors indicate the corresponding concentrations of CH_3CN, a tracer of biomass burning. The 1:1 line is also shown.

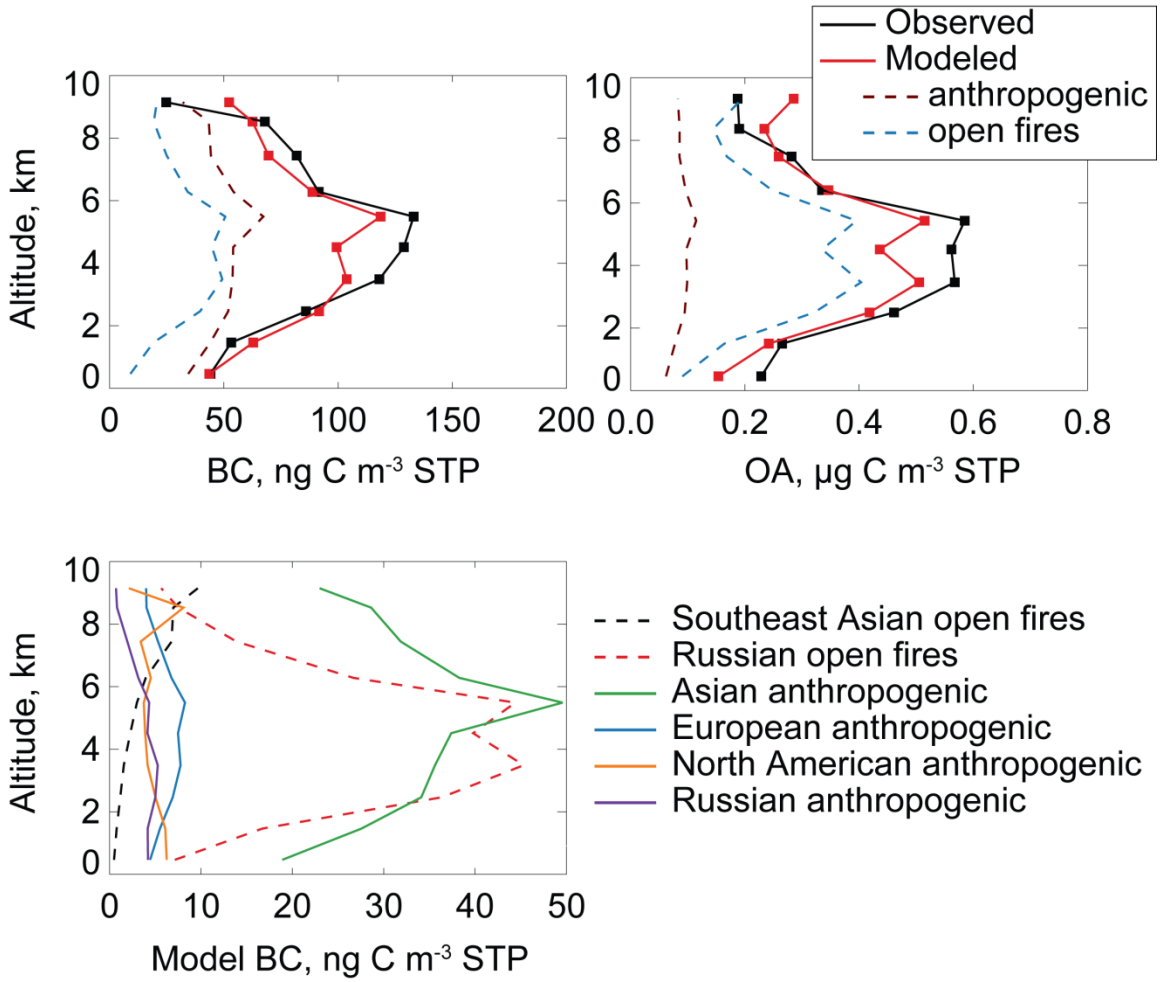

Figure 2.7: Mean vertical profiles of BC and OA concentrations along the DC-8 flight tracks in ARCTAS (1-19 April 2008), averaged over 1-km altitude bins. The top panels compare observations to GEOS-Chem and separate the model contributions from anthropogenic and open fire sources. The bottom panel further separates model BC contributions by source regions. Anthropogenic sources include fossil fuel and biofuel combustion.

anthropogenic influence. Open fires contribute 46% of BC and 84% of OA at 2-6 km altitude in the model. The mid-tropospheric maximum reflects the lifting of Russian fire and Asian pollution effluents by warm conveyor belts (WCBs) originating from the Pacific Rim of the Asian continent [*Liu et al.*, 2003; *Stohl*, 2006; *Fisher et al.*, 2010]. The

strong influence of open fires at 2-6 km is consistent with the observed strong correlations of BC vs. CH_3CN (r=0.74) and OA vs. CH_3CN (r=0.81) and has been reported in previous ARCTAS/ARCPAC analyses [*Warneke et al.*, 2009; *Spackman et al.*, 2010; *Warneke et al.*, 2010; *Kondo et al.*, 2011b; *Matsui et al.*, 2011].

We find that open fires are the dominant source of OA at all altitudes in the model, but anthropogenic sources are more important for BC and dominate near the surface (Fig. 2.7). We evaluate this source attribution by using observed and simulated correlations with sulfate, an aerosol tracer of anthropogenic influence. Simulated GEOS-Chem sulfate is from *Fisher et al.* [2011]. Figure 2.8 shows observed and simulated scatterplots of BC and OA vs. sulfate, indicating good agreement in the correlation coefficients and the slopes of the regression lines at 2-6 km (mid-troposphere) and 0-1 km (near-surface). There is significant correlation between OA and sulfate in the mid-troposphere, consistent with the well-known mixing of pollution and fire influences in Asian outflow lifted by WCBs [*Bey et al.*, 2001] and previously documented in ARCTAS and ARCPAC [*Fisher et al.*, 2010; *Brock et al.*, 2011]. Figure 2.8 shows a population of points at altitude > 6 km with extremely high sulfate concentrations (> 3 μg m^{-3} STP) and low BC and OA concentrations, corresponding to a plume transported from East Asia as indicated by back-trajectories. The strong enrichment of sulfate relative to carbonaceous aerosols in that plume is consistent with Asian pollution having experienced wet scavenging, as previously shown by *van Donkelaar et al.* [2008] and *Dunlea et al.* [2009] in observations from the INTEX-B aircraft campaign.

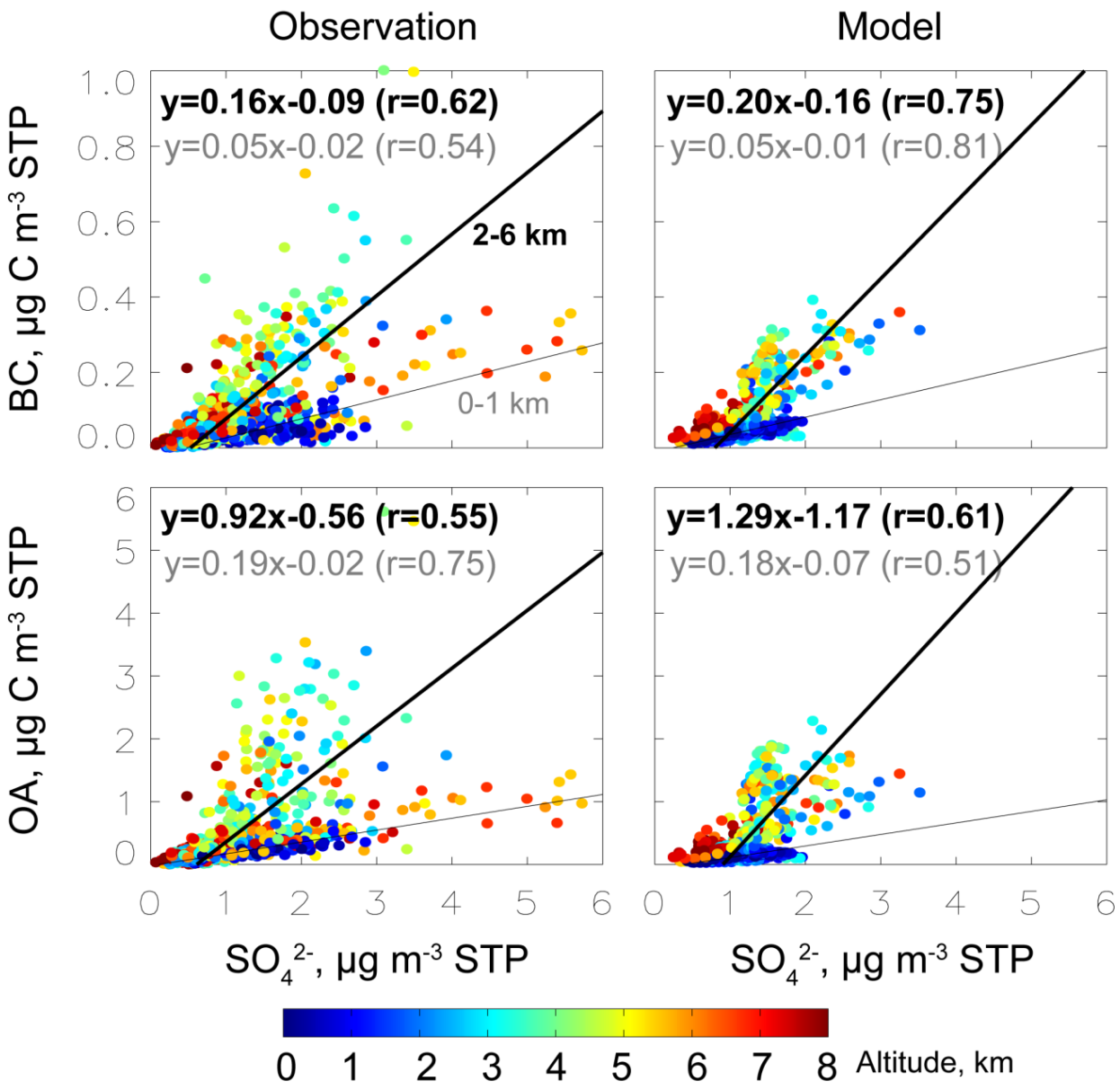

Figure 2.8: Scatterplots of BC and OA vs. sulfate (SO_4^{2-}) concentrations in ARCTAS. Observations from the DC-8 aircraft (left panels) are compared to model values (right panels) sampled along the aircraft flight tracks as described in the text. Individual points are colored by altitude. Reduced-major-axis (RMA) regression statistics and linear fits are shown in thin black for near-surface data (<1 km) and in thick black for mid-tropospheric data (2-6 km).

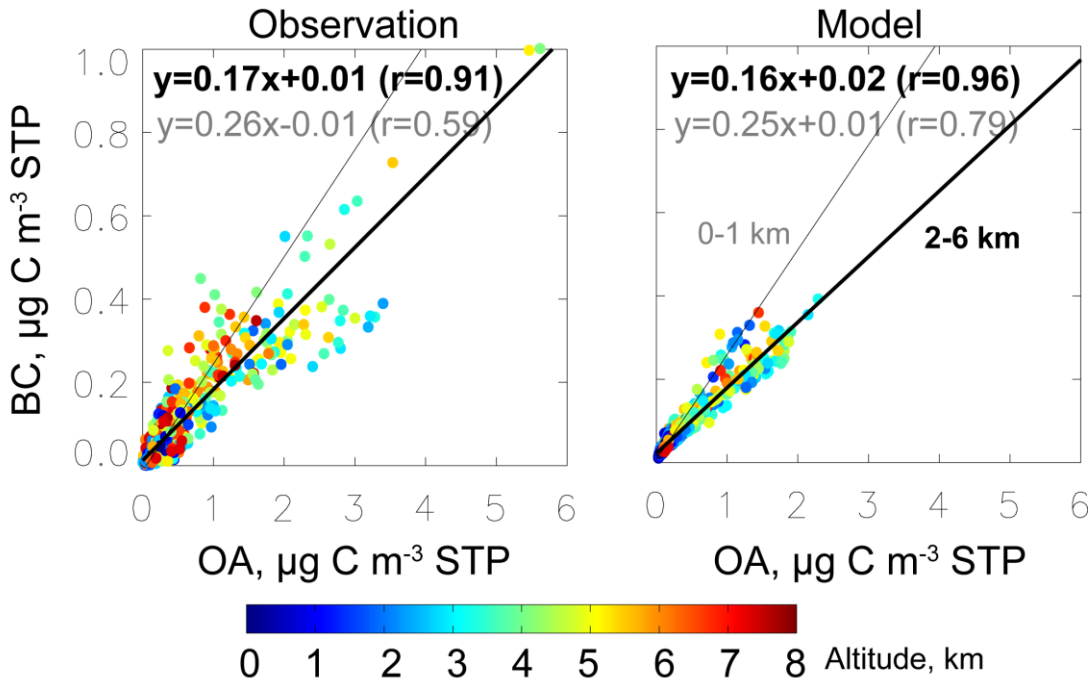

Figure 2.9: Same as Fig. 2.8 but for BC vs. OA concentrations in ARCTAS.

The contribution of open fire emissions in the model decreases from the mid-troposphere to near-surface air (<1 km), where it accounts for 20% of BC and 60% of OA. The concentration ratios relative to sulfate are also much lower in near-surface air than in the mid-troposphere, both in the model and in observations (Fig. 2.8). This is consistent with *Fisher et al.* [2011], who found a major contribution to Arctic boundary layer sulfate from boundary layer transport of European and North American pollution, in contrast to the mid-troposphere where Asian pollution dominates. This boundary layer anthropogenic influence is far more important for BC than for OA because of the much higher BC/OA emission ratio from anthropogenic sources than from open fires (Table

2.1). Consequently, the observed ratio of BC vs. OA increases from 0.17 in the mid-troposphere to 0.26 near the surface (Fig. 2.9), and this is also well captured in the model.

Our estimation of the open fire contribution to BC along the ARCTAS DC-8 flight tracks agrees with the value of 33-41% reported by *McNaughton et al.* [2011] using CH_3CN and the OA/sulfate ratio to classify the data. *Matsui et al.* [2011] attributed most of the BC measured in ARCTAS to Russian fire emissions using CH_3CN and dichloromethane (CH_2Cl_2) to classify the data, but their analysis focused on plumes and ignored background air.

Broader examination of model results over the scale of the Arctic polar cap (north of 60^{o}N) in April 2008 indicates that open fire emissions contribute 50% of total BC in the Arctic tropospheric column and 81% of total OA. Fire influences are the strongest in the Eurasian Arctic (not sampled by the aircraft). Asian pollution dominates the source of anthropogenic BC in the Arctic tropospheric column, but less so in surface air. Our model Asian contribution to Arctic BC in spring is higher than previous studies [*Koch and Hansen*, 2005; *Shindell et al.*, 2008; *Tilmes et al.*, 2011]. This reflects our higher Asian emission inventory, constrained by observations at Chinese sites as discussed in Sect. 2.2.

2.3.2 Surface observations

We now turn to surface observations in Jan-May 2008 to provide broader seasonal context. Figure 2.10 compares model results with monthly average surface concentrations

observed in Alaska at Denali (low Arctic) and Barrow (high Arctic) in 2007-2009 (locations shown in Fig. 2.4). Model contributions from different sources are shown.

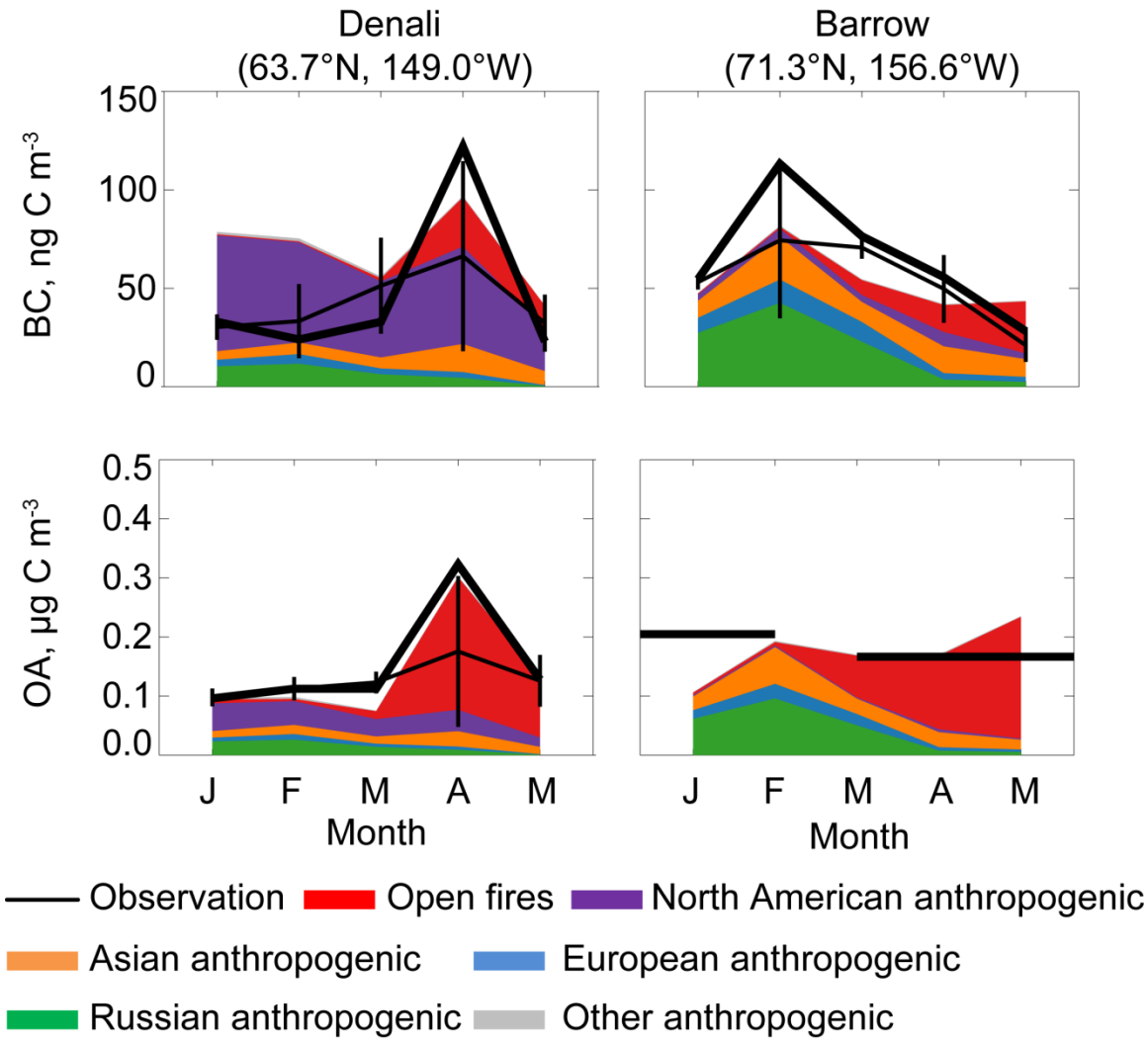

Figure 2.10: Seasonal variation of BC and OA surface air concentrations at Denali and Barrow in Alaska. The thick black lines are monthly mean observations for 2008. The thin black lines are monthly mean observations for 2007-2009 with vertical bars representing interannual standard deviations. The thick line for OA at Barrow represents seasonal mean concentrations in Nov 2008-Feb 2009 and Mar-Jun 2008 from *P.M. Shaw et al*. [2010]. Additive model contributions from different sources in the 2008 simulation are shown in color.

Observations at Denali are from the IMPROVE network (http://vista.cira.colostate.edu/-improve/Data/IMPROVE/AsciiData.aspx) using a thermal/optical reflectance method. Observations at Barrow are from the NOAA Global Monitoring Division (http://www.esrl.noaa.gov/gmd/aero/net/), reported as aerosol light absorption coefficients from a particle soot absorption photometer. We use a mass absorption efficiency of 9.5 m^2 g^{-1} to convert the absorption coefficients to BC mass concentrations based on ARCTAS data [*McNaughton et al.*, 2011]. OA observations at Barrow are from *P.M. Shaw et al.* [2010], who reported seasonal mean concentrations for Mar 2008-Mar 2009.

We find that the BC and OA observations at the surface sites in April 2008 are roughly consistent with the mean near-surface ARCTAS data (Fig. 2.7), but are more affected by Russian fires. The fire influence at Denali is larger than that at Barrow. Observations in April 2008 were anomalously high relative to the 2007-2009 April mean (thin lines in Fig. 2.10), which reflects the anomalously large Russian fires [*Fisher et al.*, 2010].

Observations of BC at Barrow show higher values in winter (Jan-Mar) than spring (Apr-May), even in 2008. In contrast, Denali shows higher values in spring even in the 2007-2009 mean. The model fails to reproduce the seasonal variation at Denali, apparently because it overestimates local pollution influence from nearby Anchorage in winter. It is more successful at Barrow, although this is contingent on doubling of the Russian anthropogenic source from the *Bond et al.* [2007] inventory as described above. The winter maximum at Barrow is explained in the model by the Russian anthropogenic

source, transported to the North American Arctic in the boundary layer around the Siberian High with little dilution and little precipitation. This Russian source influence declines sharply in spring due to vertical mixing and to the weakening of the Siberian High. *Sharma et al.* [2006] found similar source attribution for BC at Barrow using back-trajectory analysis, and *Fisher et al.* [2011] found similar results for sulfate at Barrow using GEOS-Chem.

Observed OA at Denali shows similar winter-spring seasonality as BC. Our model reproduces this seasonality without the spurious local influence from Anchorage seen for BC (the OA/BC emission ratio from Anchorage in the *Bond et al.* [2007] inventory is 50% lower than the anthropogenic mean). Observations of OA at Barrow show little seasonal variation between winter and spring, which is consistent with the model as the decline in the Russian anthropogenic source from winter to spring is compensated by the open fire influence. Both at Denali and at Barrow, we find that we can largely explain the wintertime OA on the basis of anthropogenic sources and the springtime OA on the basis of open fires. The source attribution in spring is consistent with the work of *P.M. Shaw et al.* [2010] and *Frossard et al.* [2011], who identified a dominant combustion source for OA at Barrow on the basis of correlations with combustion tracers. *P.M. Shaw et al.* [2010] attributed most OA at Barrow in winter to oceanic emissions but we find otherwise.

2.4 BC deposition in the Arctic and implications for radiative forcing

BC transported to the Arctic from mid-latitudes can be either removed by deposition or eventually ventilated out of the Arctic. We find in model sensitivity simulations that BC transported to the Arctic below 2 km is mostly deposited within the Arctic, whereas BC transported to the Arctic at higher altitudes is mostly ventilated out. Wet processes in our model account for 85-91% of total BC deposition to the Arctic in winter-spring. This is higher than in the previous model studies of *Huang et al.* [2010] and *J.F. Liu et al.* [2011], but consistent with the studies of *Flanner et al.* [2007]. *Spackman et al.* [2010] inferred a dry deposition flux for BC of 100-5300 ng m^{-2} day^{-1} over snow/ice during ARCPAC on the basis of observed BC depletion in the boundary layer. Our computed dry deposition flux in the Western Arctic (mostly covered by snow/ice) is about 1500 ng m^{-2} day^{-1} in spring, consistent with that estimate.

Figure 2.11 shows the spatial distribution of model BC total deposition in winter (Jan-Mar) and spring (Apr-May) 2008, separately for open fire and anthropogenic contributions. Maximum deposition is in the Eurasian sector due to Russian and European anthropogenic sources, augmented in spring by Russian fires. The fires double BC deposition to the Arctic in spring relative to winter. The Asian anthropogenic contribution to BC deposition is small in winter compared to European and Russian sources but becomes comparable to these sources in the spring.

While ARCTAS data only provide information for the North American Arctic, larger BC deposition in the Eurasian sector is consistent with the work of *Doherty et al.* [2010],

who reported snow BC concentrations from a network of Russian and North American Arctic sites in Mar-May 2007-2009. We compared these observations (http://www.atmos.washington.edu/sootinsnow/) to model values for the corresponding years, using the GFEDv2 fire inventory for 2007 [*van der Werf et al.*, 2006] and the FLAMBE inventory with above scaling factors for 2009.

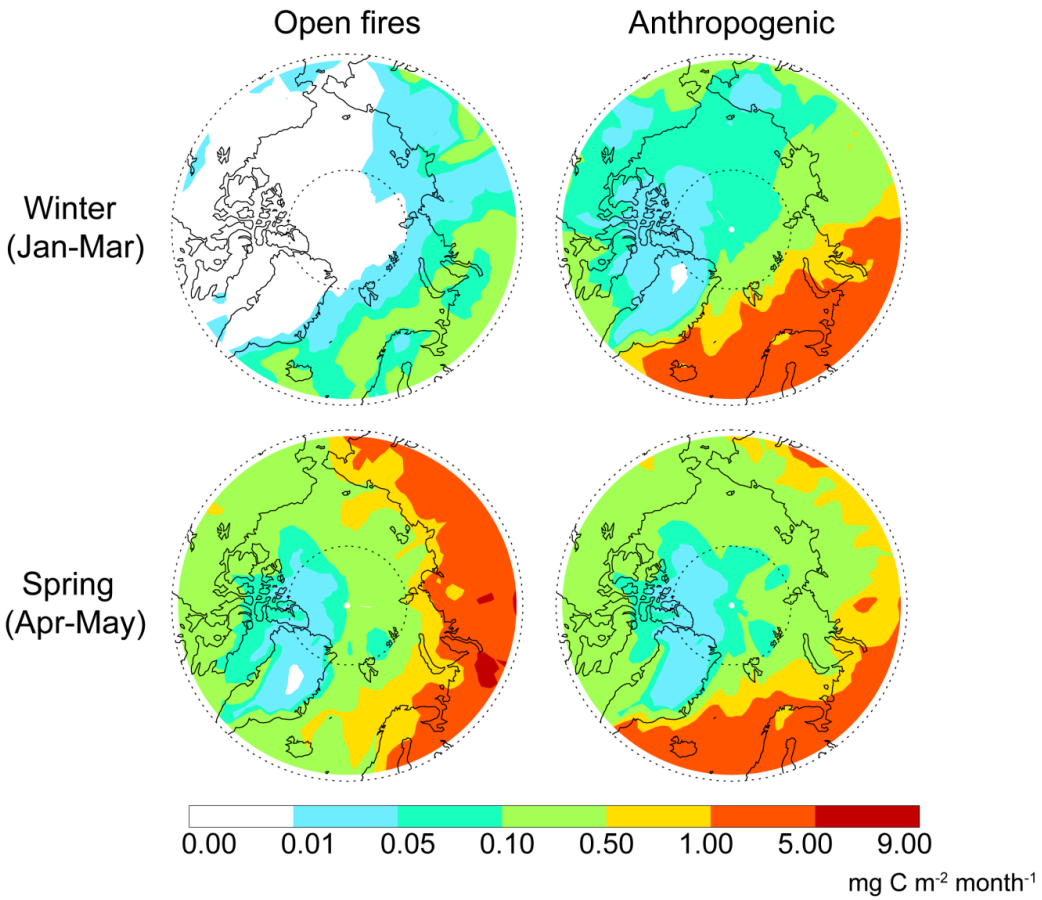

Figure 2.11: Contributions of open fire and anthropogenic (fuel combustion) sources to the BC deposition flux in GEOS-Chem for winter and spring 2008.

Figure 2.12 shows model results for the BC content of snow in winter (Jan-Mar) and spring (Apr-May) 2007-2009, as calculated from the ratio of BC to water deposition fluxes, and Figure 2.13 compares to the *Doherty et al.* [2010] observations for individual sites and months. The observations show mean values of 11 ±5 ng g^{-1} at the North American sites and 23 ±16 ng g^{-1} at the Russian sites, and the corresponding model values for these sites and months are 11 ±3 ng g^{-1} and 31 ±11 ng g^{-1}. Excluding the outlier with observed value of 30 ng g^{-1} in 2007, we find a good model-observed correlation at North

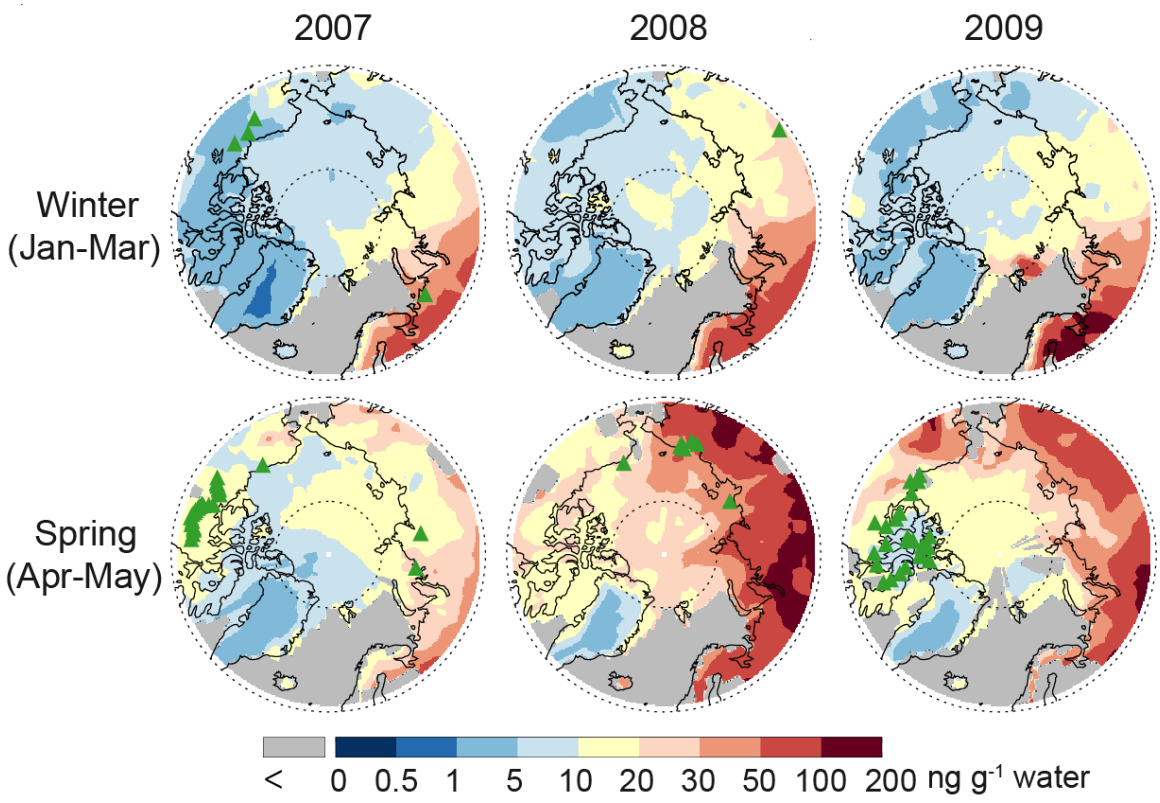

Figure 2.12: Simulated BC content of Arctic snow in winter and spring 2007-2009. Snow-free areas are shown in gray. Green triangles indicate snow sampling sites from *Doherty et al.* [2010] for the corresponding years and seasons.

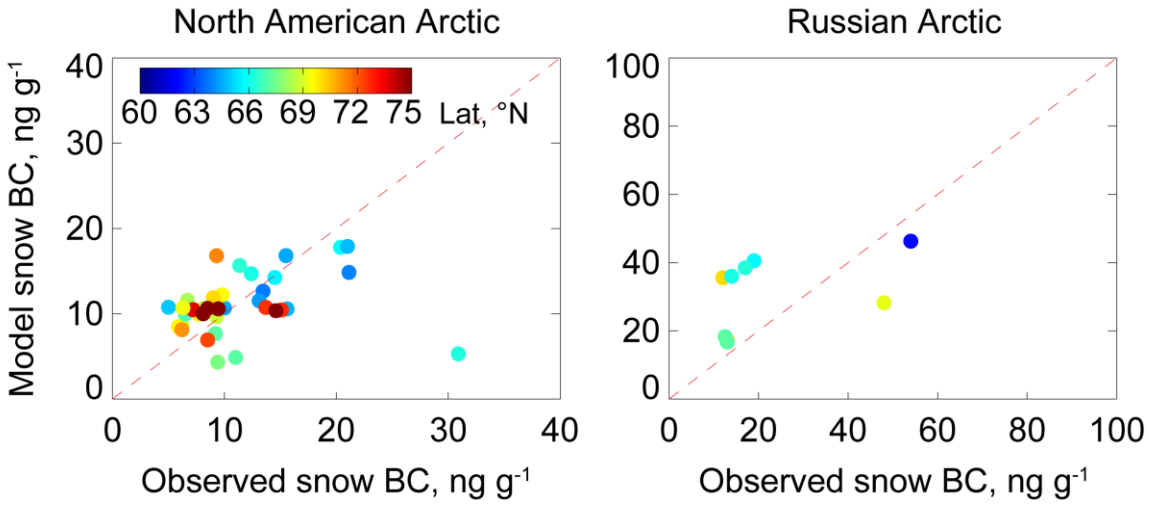

Figure 2.13: Scatterplots of simulated vs. observed BC content in snow for North American and Russian Arctic sites in Mar-May 2007-2009 (Fig. 2.12). Observations from *Doherty et al.* [2010] are averaged over model grid squares, and model results are sampled for the month and year of observations. The data are colored by latitude. Also shown is the 1:1 line.

American sites with r=0.60. Russian data are too sparse to evaluate a correlation. *Spackman et al.* [2010] extrapolated the BC dry deposition fluxes inferred from their aircraft data to BC content in snow and found consistency with the data of *Doherty et al.* [2010], in apparent contradiction with our model results where wet deposition dominates. However, the snowfall used by *Spackman et al.* [2010] in their calculation is only 20% of that used in our model from the GEOS-5 data.

MODIS fire counts show that spring 2007 had lower-than-average Russian fires while 2009 was near average, offering a contrast to spring 2008 which had anomalously high Russian fire activity (http://disc.sci.gsfc.nasa.gov/giovanni/). The total model BC deposition to the Arctic in April-May is 16 Gg month^{-1} for 2007 (including 13% from

open fires), 41 Gg month^{-1} for 2008 (61%), and 34 Gg month^{-1} for 2009 (46%). Deposition in Jan-Mar has little interannual variability (14-19 Gg month^{-1}). The relative contribution of dry deposition to total deposition is 15% in winter and 9% in spring, with little interannual variability. It is smallest over the Eurasian Arctic in spring where the deposition flux is highest.

Model source attribution shows that the mean contribution of open fires to the BC content in Arctic snow is 10% in winter and 60% in spring 2008 (40% for springs 2007-2009). *Hegg et al.* [2009, 2010] and *Doherty et al.* [2010] previously reported a dominant influence from biomass burning in their BC snow content data, based on absorption Ångstrom exponents and correlation with biomass burning tracers. Part of the discrepancy could reflect biofuel combustion, which accounts in the model for 38% of annual anthropogenic emissions in Asia and 25% in Russia, and would be highest in winter-spring due to residential heating. In addition, mixing of anthropogenic and fire influences in Asian outflow discussed above complicates source attribution in the observations; this mixing is apparent in the *Hegg et al.* [2010] analysis as an association of sulfate with biomass burning influence.

Figure 2.14 shows model results for the decreases in snow albedo in winter (Jan-Mar) and spring (Apr-May) 2008 due to BC deposition to snow. We assume a constant snow grain radius of 100 μm [*McConnell et al.*, 2007] with no significant aging, and estimate the effect of BC on snow albedo based on Fig. 2 in *Warren and Wiscombe* [1985]. The resulting decrease in snow albedo averaged over the Arctic is 0.4% in winter and 0.8% in

spring 2008 (0.6% for spring 2007-2009), lower than previous estimates of 1.1-4.7% [*Park et al.*, 2005; *Flanner et al.*, 2007; *Koch et al.*, 2009a]. By convolving this result with the GEOS-5 incoming solar radiation at the surface we deduce a surface radiative forcing over the Arctic (north of 60°N) from deposited BC of 0.1 W m^{-2} in winter and 1.7 W m^{-2} in spring 2008 (1.2 W m^{-2} for spring 2007-2009, including 0.6 W m^{-2} from anthropogenic sources only). A previous model calculation by *Flanner et al.* [2007] reported a surface radiative forcing of 0.02 W m^{-2} in winter and 0.53 W m^{-2} in spring due to anthropogenic BC over the same domain, similar to our values.

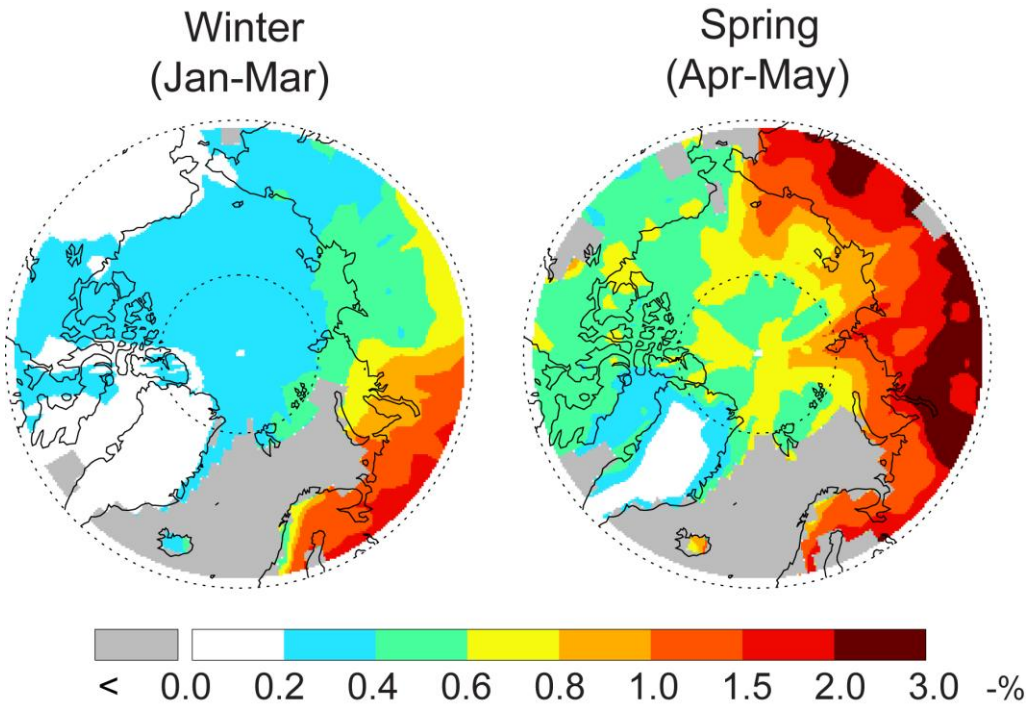

Figure 2.14: Model decreases in snow albedo due to BC deposition in the Arctic (>60°N) in winter and spring 2008. Snow-free areas are shown in gray.

2.5 Comparison to previous global models

Simulation of BC concentrations over the Arctic is considered a difficult problem for global models. Multi-model community (AerocCom and HTAP) intercomparisons show order-of magnitude differences between models and either negative [*Shindell et al.*, 2008; *Koch et al.*, 2009b] or positive bias [*Schwarz et al.*, 2010] compared with observations. These differences between models reflect diversity in both emissions and scavenging efficiency. Considering our general success in reproducing the ensemble of BC observations over the Arctic, it is useful to reflect on what this success implies for modeling BC in that region.

It should be noted that the community intercomparisons cited above involved many models that were not previously evaluated in the Arctic. The order-of-magnitude differences between models may be explained by inadequate representations of wet scavenging, which is particularly important for modeling BC in the Arctic because of multiple e-folding loss during transport from northern mid-latitudes [*J.F. Liu et al.*, 2011]. Individual model studies targeting the Arctic demonstrate much better comparisons to BC observations [*Koch and Hansen*, 2005; *Koch et al.*, 2009b; *Huang et al.*, 2010; *J.F. Liu et al.*, 2011], with our evaluation being the most extensive by encompassing surface air, aircraft, and snow observations. *Huang et al.* [2010] show good comparisons to observed BC concentrations in surface air while *Koch and Hansen* [2005] and *J.F. Liu et al.* [2011] reproduce the seasonality but still underestimate the winter-spring maximum by a factor

of 2-3. Comparisons to ARCTAS vertical profiles show slight underestimation in *Koch et al.* [2009b] and no significant bias in *J.F. Liu et al.* [2011].

Table 2.2 lists the BC sources and global lifetime used by the above models in comparison to ours. Our global anthropogenic emissions are close to *Huang et al.* [2010] but about 50% higher than others, reflecting the major increase in Asian emissions since 2000. Our fire emissions are the highest, though this is mainly weighted by the tropics (Table 2.1) and has little influence on the Arctic. Our Russian fire emissions are high (0.6 Tg C a^{-1}, as compared to 0.3 Tg a^{-1} in *Koch and Hansen* [2005] and *Huang et al.* [2010]), but this reflects the anomalous 2008 fire season [*Fisher et al.*, 2010]. *Koch and Hansen* [2005] implied that their low model bias might be explained by underestimate of Asian anthropogenic emissions.

Table 2.2: Global model representations of atmospheric BC

Reference	Model	Global source, Tg C a^{-1}		Lifetime[b], days
		Anthropogenic[a]	Open fires	
This work	GEOS-Chem	7.0	11	5.9
J.F. Liu et al. [2011]	AM3	5.1	2.6	9.5
Huang et al. [2010]	GEM-AQ	6.0	4.9	9.2
Koch et al. [2009b]	GISS	4.4	2.8	9.2
Koch and Hansen [2005]	GISS	4.7	6.0	7.3

[a] Including fossil and biofuel combustion
[b] Global lifetime in the troposphere against deposition

Our global mean lifetime of BC against deposition (5.9 days) is 20-40% shorter than in the other models of Table 2.2, though within the 5-11 days of the ensemble of models intercompared by *Koch et al.* [2009b]. The global lifetime is of limited relevance to

simulation of the Arctic in winter-spring, where scavenging is principally from cold clouds and snow. There the different models exhibit complicated differences in their scavenging parameterizations. In our model, scavenging from cold clouds is restricted to hydrophobic BC; it is efficient in source regions but inefficient in the Arctic because BC becomes hydrophilic after an aging time of 1 day. The other models in Table 2.2 scavenge hydrophilic BC from cold clouds but not hydrophobic BC. *J.F. Liu et al.* [2011] increased the atmospheric lifetime of BC in their simulation for the Arctic by making the conversion from hydrophobic to hydrophilic contingent on OH levels (as opposed to a fixed 1-day time scale in our model and most others). Below-cloud scavenging from large-scale precipitation removes both hydrophobic and hydrophilic BC in most models in Table 2.2 except *Huang et al.* [2010], which does not scavenge hydrophobic BC at all. In our model, below-cloud scavenging by snow is much more efficient than by rain because of the larger cross sectional area of snow crystals vs. raindrops. *Huang et al.* [2010] and *J.F. Liu et al.* [2011] also include higher below-cloud scavenging efficiency from snow than from rain.

Although dry deposition is a minor contributor to atmospheric removal of Arctic BC, it can significantly affect surface air concentrations. Of most relevance is the deposition to snow/ice. The standard GEOS-Chem model using the resistance-in-series parameterization of *Wesely* [1989] has a mean dry deposition velocity over snow/ice of 0.08 cm s^{-1}, which would cause underestimate of observed Arctic surface air concentrations for BC and also sulfate [*Fisher et al.*, 2011]. In our work and that of *Fisher et al.* [2011], the dry deposition velocity of BC over snow/ice is fixed at 0.03 cm s^{-}

[1], based on the observations of *Nilsson and Rannik* [2001] and *Held et al.* [2011], and this corrects the underestimate. *J.F. Liu et al.* [2011] used a value of 0.04-0.07 cm s^{-1} over snow/ice. The other studies in Table 2.2 used standard resistance-in-series parameterizations but did not report their dry deposition velocities.

2.6 Conclusions

We used the GEOS-Chem chemical transport model (CTM) to interpret aircraft observations of black carbon (BC) and organic aerosol (OA) from the NASA ARCTAS campaign over the North American Arctic in April 2008, as well as longer-term observations of BC concentrations in surface air and in snow. Our focus was to quantify the contributions of different source types and source regions to Arctic BC and OA concentrations in winter-spring, the role of deposition processes, the resulting source attribution for BC in snow, and the implications for radiative forcing.

Our GEOS-Chem simulation includes an improved representation of aerosol scavenging by cold clouds and by snow, anthropogenic (fossil fuel and biofuel) emissions of BC and OA from the *Bond et al.* [2007] inventory for 2000, and open fire emissions from the FLAMBE inventory of *Reid et al.* [2009] with hourly resolution. We evaluated BC sources from the northern mid-latitude continents with data from observation networks. We find that Russian and Asian anthropogenic emissions have to be doubled from *Bond et al.* [2007] to improve agreement with BC observations, as might be expected from

increasing fuel use in these regions since 2000. Unusually large fires occurred in Russia in April 2008. FLAMBE estimates of biomass burned for these fires had to be decreased as previously shown by *Fisher et al.* [2010] from ARCTAS and satellite CO data. We find that BC and OA fire emission factors of 0.87 and 6.8 g carbon per kg dry mass burned, respectively, give a good simulation of observed Russian fire plumes.

The resulting model provides a good fit to the mean observed concentrations and vertical gradients of BC and OA along the ARCTAS flight tracks. Considering that the sources in the model are independently constrained by comparisons to observations over northern mid-latitude continents and in fire plumes, the successful simulation of the ARCTAS data provides some support for the model representation of aerosol deposition. Open fires account for most of OA in the model while anthropogenic emissions are more important for BC. Model and observations show strong peaks in the mid-troposphere for both BC and OA, reflecting the transport of Russian fire and Asian anthropogenic effluents lifted by warm conveyor belts (WCBs). Open fires contribute 46% of BC and 84% of OA in the mid-troposphere (2-6 km) in the model. Near the surface (<1 km), by contrast, fires contribute only 20% of BC and 60% of OA. Anthropogenic BC concentrations in the mid-troposphere are mostly of Asian origin, but in surface air we find comparable contributions from North America, Europe and Russia. These model source attributions are consistent with observed correlations of BC and OA with acetonitrile (a tracer of biomass burning) and with comparisons of simulated and observed correlations of BC and OA vs. sulfate.

Expanding the model results to the scale of the Arctic polar cap in April 2008 indicates that open fire emissions contribute 50% of total BC in the Arctic tropospheric column and 81% of total OA. We find the strongest fire influences in the Eurasian Arctic. Our relatively higher model Asian contribution to Arctic BC in spring compared with previous studies [*Koch and Hansen*, 2005; *Shindell et al.*, 2008; *Tilmes et al.*, 2011] reflects our higher Asian emission inventory, constrained by observations at Chinese sites.

We used surface air observations of BC and OA at two Alaskan sites (Denali and Barrow) in Jan-May 2007-2009 to place the aircraft data in a broader seasonal context. The Denali site shows an increase of BC from winter to spring due to Russian fire and Asian pollution influences. The seasonality is reversed at Barrow with a winter maximum that we attribute to transport from Russia. OA concentrations at Denali and Barrow are well simulated by the model, with similar sources as for BC but with stronger impact of fire emissions in spring.

Spring 2008 was anomalously affected by Russian fires. We conducted simulations for Jan-May 2007-2009 to obtain an interannual perspective and to evaluate the model with a pan-Arctic network of observations of BC snow content [*Doherty et al.*, 2010]. We find in the model that the total BC deposition flux to the Arctic in 2007-2009 averages 17 (14-19) Gg month^{-1} in Jan-Mar and 30 (16-41) Gg month^{-1} in Apr-May, where the range indicates the interannual variability. Higher deposition fluxes in spring are due to fires. The BC content of snow is highest in the Eurasian Arctic, consistent with the *Doherty et al.* [2010] data.

Open fires in the model account on average for 10% of BC content in Arctic snow in Jan-Mar and 40% in Apr-May 2007-2009. *Hegg et al.* [2009, 2010] and *Doherty et al.* [2010] previously inferred a dominant biomass burning influence at most of their Arctic sites on the basis of correlations with tracers and absorption Ångstrom exponents. Some of that difference can be reconciled by the biofuel source of BC, which they would diagnose as biomass burning but must be viewed as anthropogenic. In addition, the well-known mixing of anthropogenic and fire influences in Asian outflow could result in anthropogenic influences being correlated with biomass burning tracers.

We estimate decreases in snow albedo due to BC deposition in 2007-2009 of 0.4% in winter and 0.6% in spring. The resulting mean surface radiative forcing over the Arctic in spring is 1.2 W m^{-2} (including open fires) and 0.6 W m^{-2} (anthropogenic only). This is consistent with the anthropogenic value of 0.53 W m^{-2} previously reported by *Flanner et al.* [2007] for the same region.

Chapter 3. Global budget and radiative forcing of black carbon aerosol: constraints from pole-to-pole (HIPPO) observations across the Pacific

Abstract:

We use a global chemical transport model (GEOS-Chem) to interpret aircraft curtain observations of black carbon (BC) aerosol over the Pacific from 85°N to 67°S during the 2009 - 2011 HIPPO campaigns. Observed concentrations are very low, implying much more efficient scavenging than is usually implemented in models. Our simulation with a global source of 6.5 Tg a^{-1} and mean tropospheric lifetime of 4.2 d (vs. 6.8 ± 1.8 days for the AeroCom models) successfully simulates BC concentrations in source regions and continental outflow, and captures the principal features of the HIPPO data, but is still higher by a factor of 2 (1.48 for column loads) over the Pacific. It underestimates BC absorbing aerosol optical depths (AAODs) from the AERONET network by 32% on a global basis. Only 8.7% of global BC loading in GEOS-Chem is above 5 km, vs. 21 ± 11% for the AeroCom models, with important implications for radiative forcing estimates. Our simulation yields a global tropospheric BC burden of 76 Gg, a global mean BC AAOD of 0.0017, and a top-of-atmosphere direct radiative forcing (TOA DRF) of 0.19 W m^{-2}, with a range of 0.17-0.31 W m^{-2} based on uncertainties in the BC atmospheric distribution. Our TOA DRF is lower than previous estimates (0.27 ± 0.06 W m^{-2} in AeroCom, 0.65 - 0.9 W m^{-2} in more recent studies). We argue that these previous estimates are biased high because of excessive BC concentrations over the oceans and in the free troposphere.

3.1 Introduction

Black carbon (BC) is of climatic interest as a strong absorber of solar radiation both in the atmosphere [*Jacobson*, 2001; *Koch*, 2001; *Quinn et al.*, 2008] and after deposition to snow [*Warren and Wiscombe*, 1985; *Flanner et al.*, 2007; *McConnell et al.*, 2007]. Estimates of BC radiative forcing have large uncertainties reflecting, in part, poor knowledge of atmospheric concentrations [*Bond et al.*, 2013]. Here we use a global

chemical transport model (GEOS-Chem CTM) to interpret aircraft observations of BC from the NSF HIPPO deployments over the remote Pacific from 87°N to 67°S in 2009-2011. We show that the data provide important constraints on BC radiative forcing, implying that recent estimates of the direct radiative forcing (DRF) may be too high.

DRF at the top-of-atmosphere (TOA DRF) of BC refers to the change in the top-of-atmosphere energy balance due to absorption and scattering of solar radiation by atmospheric BC. Global TOA DRF estimates in the literature range from 0.05 to 1.0 W m^{-2} [*Schulz et al.*, 2006; *Ramanathan and Carmichael*, 2008; *Bond et al.*, 2013; *Myhre et al.*, 2013], with recent estimates favoring the upper end of that range [*C.E. Chung et al.*, 2012; *Bond et al.*, 2013]. This can be compared to a present-day radiative forcing from CO_2 of 1.6 W m^{-2}.

Uncertainty in the global burden and distribution of BC is a major factor of variability in DRF estimates [*Bond et al.*, 2013]. Due to limited observations of BC concentrations, particularly in the free troposphere and over the oceans, radiative forcing estimates have been mainly based on model simulations. Estimates by the Intergovernmental Panel on Climate Change (IPCC) [*Forster et al.*, 2007] are predominantly based on the AeroCom (Aerosol Comparisons between Observations and Models, http://aerocom.met.no/) ensemble of CTMs [*Schulz et al.*, 2006; *Myhre et al.*, 2013]. However, there are order-of-magnitude disagreements between AeroCom models and with observations in the remote and upper troposphere [*Koch et al.*, 2009b; *Schwarz et al.*, 2010; *Schwarz et al.*, 2013]. This can critically affect DRF estimates [*Zarzycki and Bond*, 2010; *Samset and Myhre*, 2011].

The order-of-magnitude model errors in simulating BC concentrations in the remote troposphere could reflect errors in emission, transport, or wet scavenging which is the main BC sink. Global BC emission inventories such as that from [*Bond et al.*, 2007] have regional uncertainties of only about a factor of 2 - 3 as indicated by comparisons with observations in source regions [*Park et al.*, 2003; *Koch et al.*, 2007; *Q. Wang et al.*, 2011; *Fu et al.*, 2012; *Leibensperger et al.*, 2012]. Transport in global models is unlikely to induce errors of more than a factor of 2 on large scales [*Jacob et al.*, 1997]. Wet scavenging thus appears to be the largest cause of model error in the remote troposphere [*Schwarz et al.*, 2010; *J.F. Liu et al.*, 2011; *Kipling et al.*, 2013]. Global models must necessarily use crude parameterizations of the scavenging process [*Balkanski et al.*, 1993; *Rasch et al.*, 2000]. Additional uncertainties specific to BC scavenging relate to its hydrophilicity [*Park et al.*, 2005; *Riemer et al.*, 2010; *J.F. Liu et al.*, 2011] and its potential to serve as cloud condensation nucleus (CCN) or ice nucleus (IN) [*Croft et al.*, 2010; *J.F. Liu et al.*, 2011; *Q. Wang et al.*, 2011]. Systematic model errors caused by scavenging will grow with distance from source regions.

Global observations of absorption aerosol optical depth (AAOD) are available from the AERONET surface network [*Dubovik et al.*, 2002] and from satellites [*Remer et al.*, 2005; *Torres et al.*, 2007]. These have been used to constrain radiative forcing estimates and to evaluate models [*Sato et al.*, 2003; *Koch et al.*, 2009b; *C.E. Chung et al.*, 2012; *Bond et al.*, 2013]. However, their value is limited because of low sensitivity, sampling bias (e.g., clear-sky), and difficulty in distinguishing between BC and other light-absorbing

constituents. In addition, AERONET observations are mainly confined to continents, while satellite retrievals are subject to cloud contamination [*C.E. Chung et al.,* 2005]. Aircraft observations can provide important constraints for the vertical and oceanic distribution of BC. The HIAPER Pole-to-Pole Observations (HIPPO) aircraft program [*Wofsy et al.*, 2011] offers a unique resource to test global BC models. It involved near-continuous vertical profiling by the HIAPER aircraft from the surface to 8 km with occasional forays over 14 km altitude over the Pacific from 87^{o}N to 67^{o}S. Five deployments were conducted over the 2009-2011 period. Measurements included BC mass concentrations from a single-particle soot photometer (SP2) instrument [*Schwarz et al.*, 2010; *Schwarz et al.,* 2013] together with a number of gases including CO and acetylene (C_2H_2) [*Wofsy et al.*, 2011]. Here we present a detailed simulation of the HIPPO BC observations with the GEOS-Chem CTM, examining the constraints that these observations provide on the model representation of scavenging and BC source attribution on a global scale. From there we draw implications for BC radiative forcing. GEOS-Chem has been used before with success to simulate BC observations in source regions [*Park et al.*, 2006; *Y.H. Mao et al.*, 2011; *Q. Wang et al.*, 2011; *Leibensperger et al.*, 2012] as well as vertical profiles from aircraft campaigns in Asian outflow [*Park et al.*, 2005], North America [*Drury et al.,* 2010], and the Arctic [*Q. Wang et al.*, 2011].

3.2 Model description

We use the GEOS-Chem CTM version 8-01-04 (http://geos-chem.org) driven by assimilated meteorological data from the Goddard Earth Observing System (GEOS-5) of the NASA Global Modeling and Assimilation Office (GMAO). The GEOS-5 data have 6-hour temporal resolution (3-hour for surface quantities and mixing depths), 47 vertical layers, and 0.5 °x0.667 °horizontal resolution. We degrade the horizontal resolution to 2°x2.5° for input to GEOS-Chem. We initialize the model with a 12-year spin-up to reach steady state in the stratosphere, followed by simulation of Jan 2009 - Sep 2011 for comparison to observations.

The simulation of BC in GEOS-Chem was originally described by *Park et al.* [2003]. BC is emitted by fuel (fossil fuel and biofuel) combustion and open fires. We assume that 80% of freshly emitted BC is hydrophobic [*Cooke et al.*, 1999; *Park et al.*, 2003], and convert it to hydrophilic with an e-folding time of 1 day which yields a good simulation of BC export efficiency in continental outflow [*Park et al.*, 2005]. The wet deposition scheme for aerosols in GEOS-Chem was originally described by *Liu et al.* [2001]. In *Q. Wang et al.* [2011] we introduced several improvements, in particular for snow and cold clouds, to simulate ARCTAS aircraft observations over the Arctic. Here we make further updates to the wet scavenging scheme as described below. Dry deposition is an additional minor sink for BC and its implementation in GEOS-Chem follows a standard resistance-in-series scheme [*Wesely*, 1989] as implemented by *Y.H. Wang et al.* [1998]. The global annual mean dry deposition velocity for BC in GEOS-Chem is 0.10 cm s^{-1}, typical of current models [*Reddy and Boucher*, 2004; *Huang et al.*, 2010].

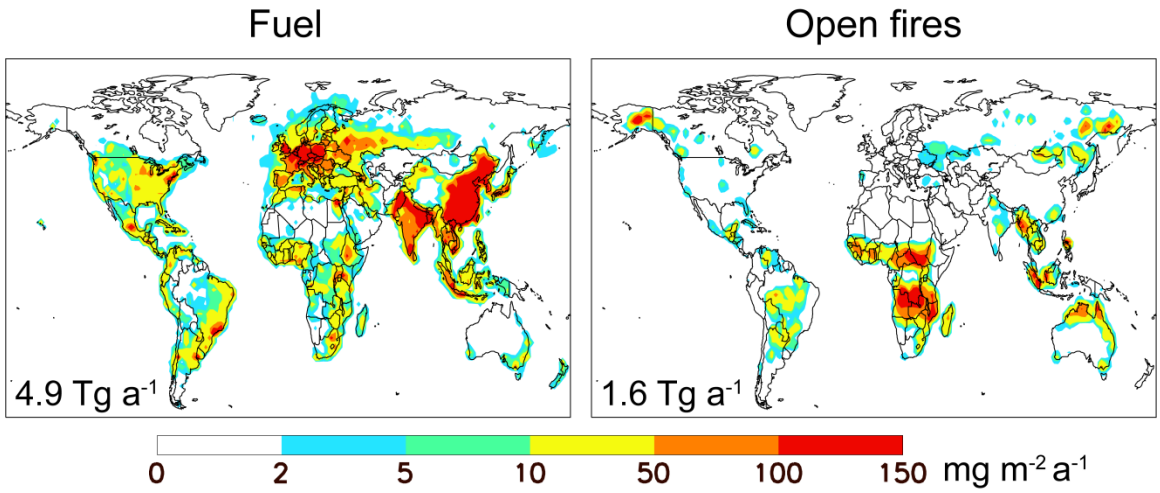

Figure 3.1: GEOS-Chem annual emissions of black carbon (BC) in 2009, separately for fuel and open fire sources. Global totals are inset.

The standard scheme for aerosol scavenging in GEOS-Chem [*Liu et al.*, 2001; *Q. Wang et al.*, 2011] includes scavenging in convective updrafts, as well as in-cloud and below-cloud scavenging from anvil and large-scale precipitation. Here we modify the scheme by scavenging hydrophobic BC in convective updrafts, since this would take place by impaction [*Ekman et al.*, 2004], and by scavenging hydrophilic BC from cold clouds by homogeneous freezing nucleation. See Appendix A for more details. This improves the simulation of HIPPO data without compromising the simulation of other BC data sets as shown below. We conducted a ^{222}Rn-^{210}Pb simulation as a test of global aerosol lifetime and find a lifetime of tropospheric ^{210}Pb aerosol against deposition of 8.6 days, as compared to a best estimate of 9 days constrained by observations [*Liu et al.*, 2001].

Figure 3.1 shows the global emissions of BC in 2009 in the model, separately for fuel and open fire sources. Table 3.1 gives regional annual totals. Fuel emissions are from *Bond et al.* [2007] for the year 2000 with modifications for Russia, North America and Asia. We

Table 3.1: Global emission of black carbon in 2009[a]

Source	Emission (Tg C a^{-1})
Fuel[b]	4.9
North America (172.5-17.5 °W, 24-88 °N)	0.29
Europe (17.5 °W-30 °E, 50-88 °N & 17.5 °W-60 °E, 33-50 °N)	0.63
Russia (30-172.5 °E, 50-88 °N)	0.22
Asia (60-152.5 °E, 0-50 °N)	2.7
Australia (90.0-155.0 °E, 0-40 °S)	0.15
Africa (17.5 °W -60.0 °E, 35 °S -33 °N)	0.45
Rest of world	0.43
Aviation[c]	0.0060
Open Fires[d]	1.6
North America (172.5-17.5 °W, 24-88 °N)	0.056
Europe (17.5 °W-30 °E, 33-88 °N)	0.0027
Russia (30-172.5 °E, 33-88 °N)	0.096
South Asia (60-152.5 °E, 0-33 °N)	0.18
Australia (90.0-155.0 °E, 0 -40 °S)	0.19
Africa (17.5 °W -60.0 °E, 35 °S -33 °N)	0.92
Rest of world	0.13
Total	6.5

[a]Values are annual means. Different regional definitions are used for fuel combustion and open fire sources in Eurasia to improve the model separation between source types.
[b]Including fossil fuel and biofuel. Values are from *Zhang et al.* [2009] for Asia and *Bond et al.* [2007] for the rest of the world but with doubling for Russia and 30% decrease for North America (see text).
[c]AEIC aircraft emission inventory of *Simone et al.* [2013]
[d]GFED3 inventory of *van der Werf et al.* [2010]

double emissions in Russia to account for rapid economic growth since 2000 and as needed to match BC surface observations in the Arctic [*Q. Wang et al.*, 2011]. We decrease North American emissions by 30% to match the observed 2000-2009 decline of surface concentrations in the U.S. [*Leibensperger et al.*, 2012]. For Asia we use the *Zhang et al.* [2009] inventory for 2006, which is 50% higher annually than *Bond et al.* [2007] over China and has greater difference in winter-spring. Aviation emissions are from *Simone et al.* [2013]. Fire emissions are from the GFED3 inventory for 2009-2011 with 3-hour resolution [*van der Werf et al.*, 2010].

3.3 Evaluation in source regions and continental outflow

Before examining model results over the remote Pacific it is important to evaluate the model sources and export by comparison with observations in source regions and continental outflow. Figure 3.2 compares annual mean surface air concentrations of BC in the model with network observations from the US, China, and Europe. These three regions account for over half of the global fuel BC source. For the US we use 2009 data from the rural IMPROVE network (http://vista.cira.colostate.edu/improve/Data/IMPROVE/AsciiData.aspx). For China and Europe we do not have network observations for 2009 and therefore use data for other years: *X.Y. Zhang et al.* [2008] for rural/regional sites in China in 2006, and the BC/OC campaign in Europe in 2002 - 2003 (http://tarantula.nilu.no/projects/ccc/emepdata.html).

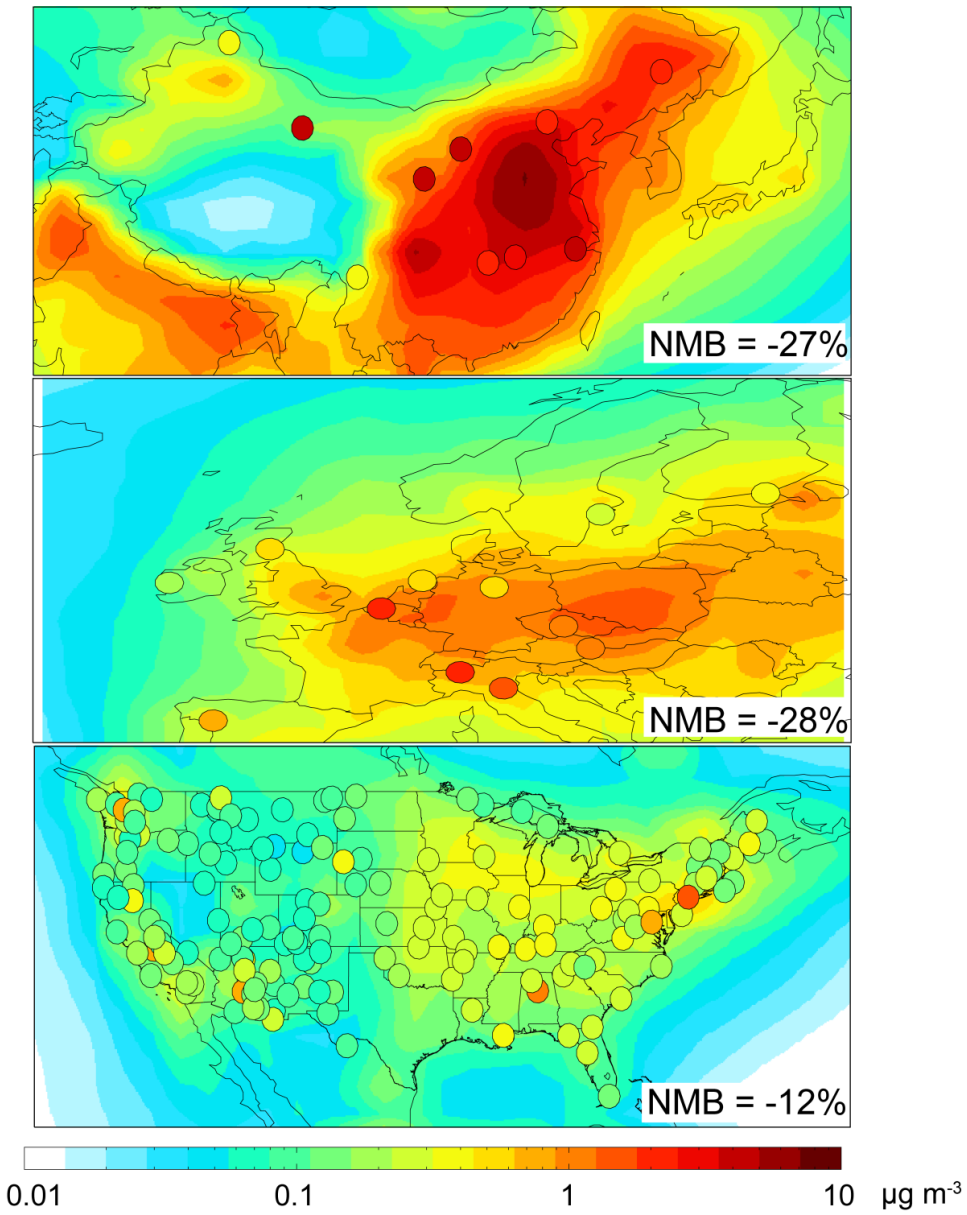

Figure 3.2: Annual mean surface air concentrations of BC in China, Europe, and the US. Model results for 2009 (solid contours) are compared to observations (circles). Observations are from *X.Y. Zhang et al.* [2008] in China for 2006, from the EMEP network in Europe for 2002–2003 (http://tarantula.nilu.no/projects/ccc/emepdata.html), and from the IMPROVE network in the US for 2009 (http://vista.cira.colostate.edu/improve/Data/IMPROVE/AsciiData.aspx). Normalized mean bias (NMB) statistics for each region are shown inset.

We diagnose for each source region the normalized mean bias$NMB = \sum(M_i - O_i)/\sum O_i$, where sums are over the ensemble of sites *i*, and M_i and O_i are the modeled and observed values. NMB values are −27% for China, −28% for Europe, and −12% for the US. Underestimation in China mainly occurs in western China, likely associated with the use of low-quality fuels for heating [*Fu et al.*, 2012]. For eastern China the NMB is −13%. This is consistent with previous top-down estimates of China's BC emissions [*Kondo et al.*, 2011a; *X. Wang et al.*, 2013], which implied no significant bias in the [*Zhang et al.*, 2009] inventory. Underestimation in Europe is mainly due to three (out of twelve) sites in northern Italy and Belgium. Without these three sites the NMB would be +7%.

Figure 3.3 evaluates the model simulation of continental outflow with aircraft observations through the depth of the troposphere over the US, the Pacific Rim, and the Arctic. Observations over the US are from the ensemble of HIPPO data (green lines in Figure 3.4). Observations for Asian outflow are from the A-FORCE aircraft campaign conducted over the Yellow Sea, the East China Sea, and the western Pacific in March-April 2009 [*Oshima et al.*, 2012]. Observations in the Arctic are from the ARCTAS aircraft campaign in April 2008 [*Jacob et al.*, 2010; *Q. Wang et al.*, 2011]. Model results are sampled along the flight tracks at the same time and location as the observations, and the aircraft data are averaged in time over their transit through a GEOS-Chem gridbox or the GEOS-Chem time-step of 15 min, whichever is less. We then use median of the observed and simulated data in 1 km altitude bins to generate the vertical profiles. We exclude observations in the stratosphere ($[O_3]/[CO] > 1.25$ mol mol^{-1}) [*Hudman et al.*, 2007] and in fire plumes ($[CH_3CN] > 200$ ppt) for ARCTAS.

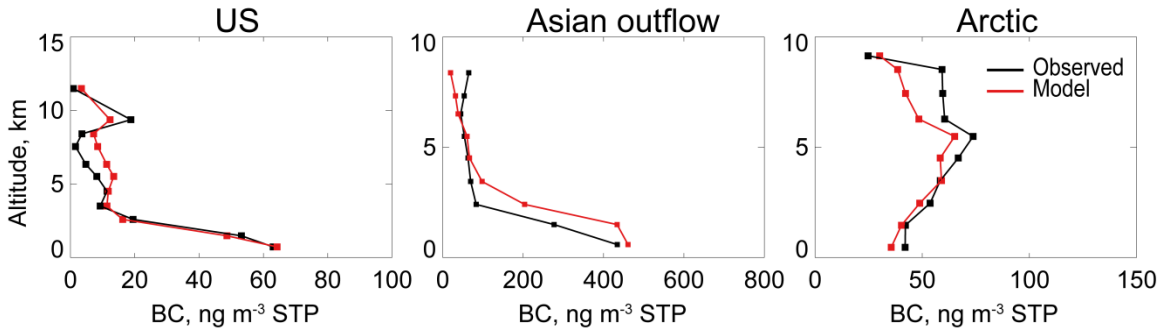

Figure 3.3: Median vertical profiles of BC concentrations in continental outflow regions. Aircraft observations in 1-km altitude bins (black) are compared to GEOS-Chem model values sampled along the flight tracks (red). The US profile is for the ensemble of HIPPO observations shown as green lines in Fig. 3.4. The Asian outflow profile is from the A-FORCE campaign conducted over the Yellow Sea, the East China Sea, and the western Pacific Ocean in March-April 2009 [*Oshima et al.*, 2012]. Observations in the Arctic are from the ARCTAS campaign in April 2008 as described by *Q. Wang et al.* [201 1]. Note differences in linear scales between panels.

Figure 3.3 indicates order-of-magnitude decreases of observed BC concentrations from the boundary layer to the free troposphere over the US and in Asian outflow, reflecting scavenging and dilution during continental ventilation [*Oshima et al.*, 2012]. The model successfully reproduces these decreases. Observations over the Arctic in spring show a mid-troposphere maximum driven by Russian fire effluents and Asian ouflow in warm conveyor belts [*Matsui et al.*, 2011]. The model again provides a successful simulation, comparable to that shown in *Q. Wang et al.* [2011] where further analysis of model results for the Arctic is presented. Overall, any biases shown in Fig. 3.3 are relatively small compared the literature range of model errors for the remote troposphere [*Shindell et al.*, 2008; *Koch et al.*, 2009b].

3.4 BC distributions over the Central Pacific

Figure 3.4 shows latitude-altitude curtains of BC concentrations for the five HIPPO deployments across the Central Pacific. The SP2 instrument detects particles in the 90-600 nm size range, estimated to represent ~90% of total BC mass. An upwards correction of 10% is applied to the observations to account for BC mass contained in particles below the SP2 limit of detection [*Schwarz et al.*, 2010]. The model is sampled along the flight tracks at the time and location of the observations, and the aircraft data are averaged in time over their transit through a GEOS-Chem gridbox or the GEOS-Chem time-step of 15 min, whichever is less. We focus here on the Central Pacific (red lines in Fig. 3.4) and exclude observations in the stratosphere as diagnosed by $[O_3]/[CO] > 1.25$ mol mol^{-1}.

The SP2 instrument detects individual particles and so its effective detection limit (EDL) varies with collection time and instrument flow rate. The statistical analysis is presented by *Schwarz et al.* [2013]. The EDLs (at the two-sigma level) are 0.01 and 0.1 ng m^{-3} STP for sampling times of 15 min and 1 min respectively near the ground and increase to 0.05 and 0.5 ng m^{-3} STP at 200 hPa. All concentrations henceforth are given for standard conditions of temperature and pressure (STP), so that ng m^{-3} STP is a mixing ratio unit.

The most prominent feature of the observations in Fig. 3.4 is the strong latitudinal gradient of BC concentrations, with minimum values around the intertropical convergence zone (ITCZ). The model reproduces this feature and attributes the equatorial minimum to scavenging by deep convection. Half of observed concentrations there are

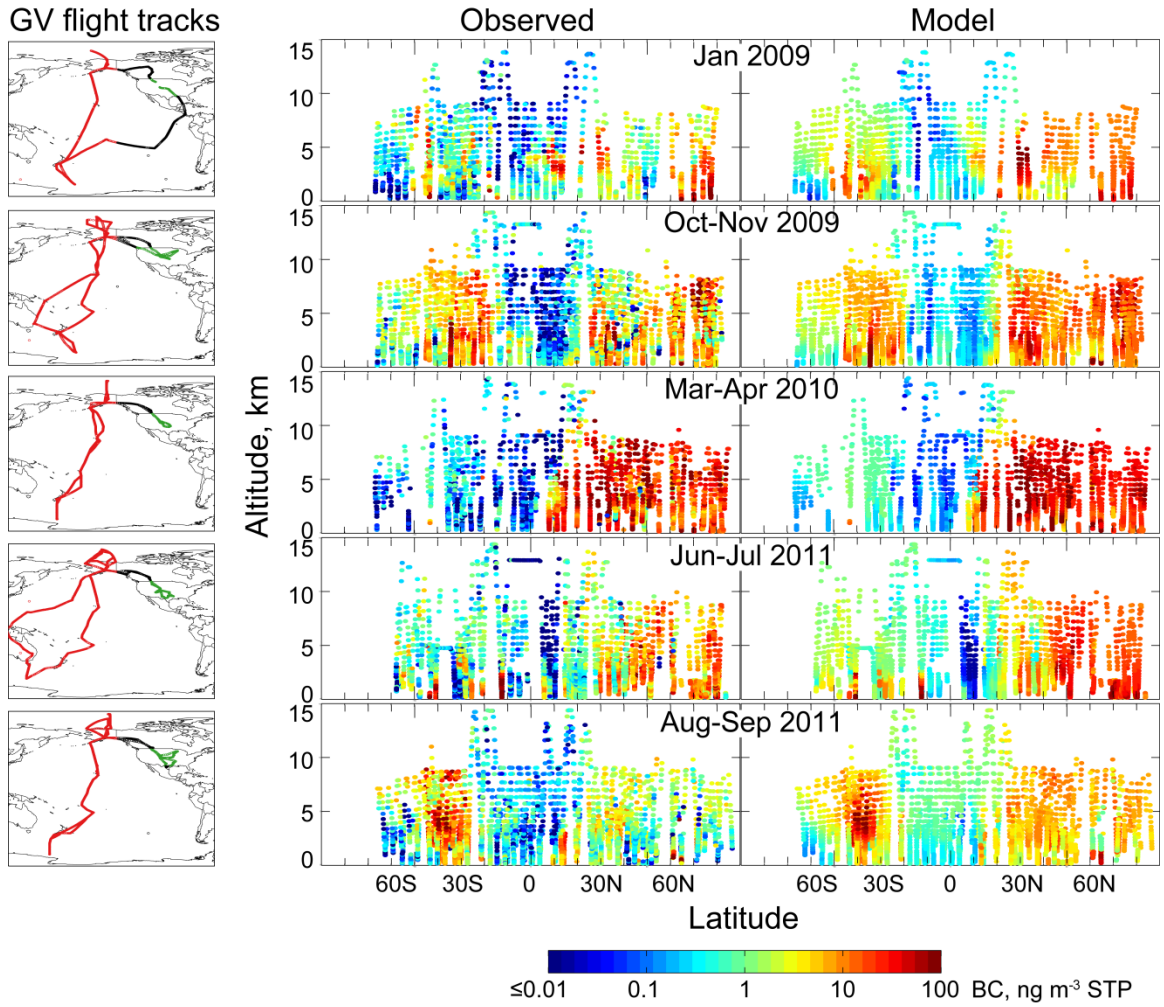

Figure 3.4: BC concentrations over the central Pacific (west of 140°W) as a function of altitude and latitude for the five HIPPO deployments (red lines on the maps). Observations are compared to GEOS-Chem model results sampled along the flight tracks. Flight tracks over the US (green lines) are not included here but are used for model comparison to observations in Figure 3.3. The observations are averaged over the GEOS-Chem grid and time-step of 15 min.

below the corresponding EDLs. We see spring maxima of BC concentrations in both the northern and southern extratropics, which the model attributes to efficient continental outflow in the north and to the biomass burning season in the south. Vertical gradients

through the troposphere are not systematic and often weak, both in the model and in the observations. Model results are too high in the northern extratropics. More quantitative model evaluation and interpretation is presented below.

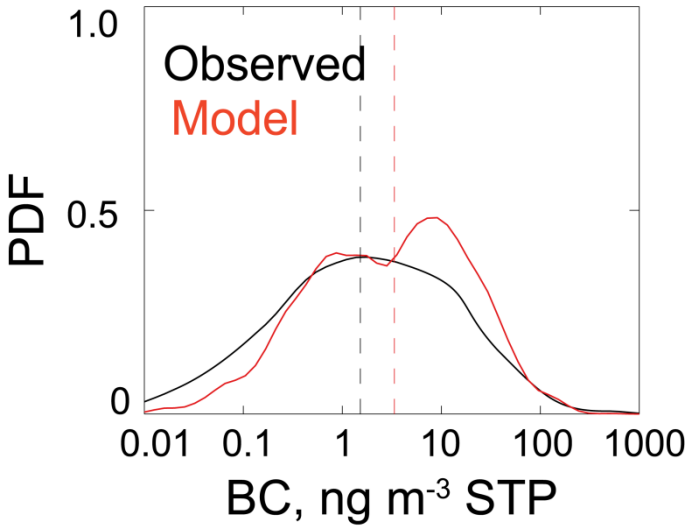

Figure 3.5: Probability density functions of observed and simulated BC concentrations for the ensemble of HIPPO Central Pacific flight tracks (Figure 3.4). Dashed lines show the medians.

Figure 3.5 shows the probability density function (PDF) of simulated and observed BC concentrations for the ensemble of the data. The observed PDF is approximately log-normal, and this holds also for different HIPPO data subsets. 5% of observations are below 0.01 ng m^{-3} STP, including 0 values indicating that the SP2 did not see a single BC particle during the integration time. We find a median of 1.5 ng m^{-3} STP for the observations and 3.4 ng m^{-3} STP in the model for the ensemble of the data. The bump in the model distribution at 10 ng m^{-3} STP corresponds to the extratropical northern

hemisphere. Latitudinally binned medians in the observations are 8.3 ng m^{-3} STP at > 60°N, 3.1 at 20 - 60°N, 0.29 at 20°S - 20°N, and 1.3 at 20-60°S, all with 30% systematic uncertainty; corresponding model values are 16, 8.8, 0.44 and 2.1 ng m^{-3} STP. The model captures the high end of the observed distribution (>100 ng m^{-3} STP) but not the low end (<0.1 ng m^{-3} STP). This low end includes many individual observations below the EDLs, but the statistical distribution should still be robust. Such extremely low observed values, mainly in the tropics (Fig. 3.4) are a remarkable feature of the HIPPO data and must reflect extremely efficient and repeated scavenging that the model cannot reproduce. We find that they are mostly associated with a C_2H_2/CO ratio less than 0.5 ppt ppb^{-1}, indicative of air very remote from combustion influence [*Xiao et al.*, 2007].

We searched for correlations between BC and CO concentrations in the HIPPO data to explain variability in BC concentrations, but found these to be in general insignificant due to the dominant role of scavenging in determining BC variability. Fire plumes were the exception. This is illustrated in Figure 3.6 with scatterplots of observed and model BC vs. CO concentrations for 20^oS-20^oN and 20^o-60^oN during the Mar-Apr 2010 deployment. The tropics show significant correlation in both the model and observations, with consistent slopes, reflecting transport of fire effluents from South Asia. By contrast there is no correlation at northern mid-latitudes, either in the observations or the model.

Figure 3.7 compares simulated and observed BC columns as a function of latitude for different seasons. The columns were computed by integrating vertical profiles from the surface to 10 km in 10-degree latitude bands. The latitudinal structure was previously

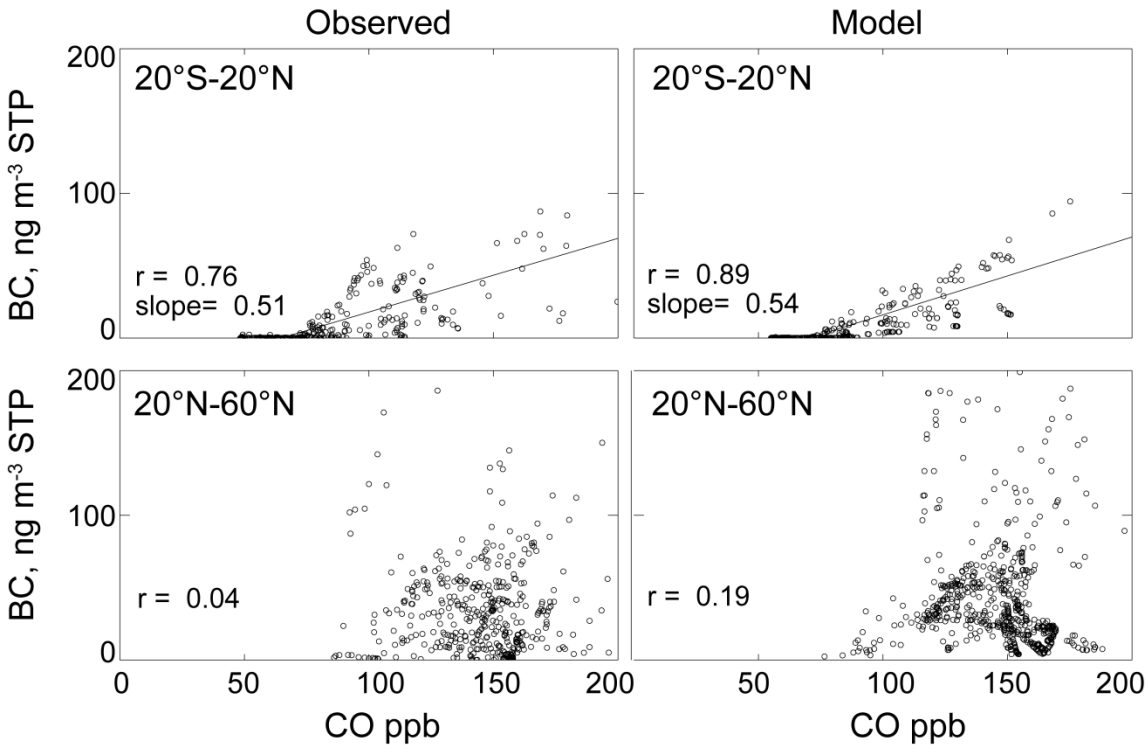

Figure 3.6: Relationships of BC and CO concentrations in HIPPO from the Mar-Apr 2010 deployment in the tropics and northern mid-latitudes. Model results (right panels) are compared to observations (left panels). Correlation coefficients and slopes of reduced-major-axis (RMA) regressions are shown for the tropics.

discussed in the context of Figure 3.4. Maximum and minimum columns span three orders of magnitude. Northern hemisphere columns are highest in March-April when Asian outflow is strongest [*Liu et al.*, 2003], and that is also when southern hemisphere columns are lowest (wet season in southern tropics). The model reproduces the observed latitudinal and seasonal variation in Fig. 3.7 with $r = 0.92$ and a mean positive bias of 48%. The column bias is relatively smaller than the bias in median concentrations (Fig. 3.5) because the columns are weighted more by high concentrations where the model performs better. Note that radiative forcing due to BC does not scale linearly with

columns because of the vertical dependence of radiative forcing efficiency [*Samset and Myhre*, 2011; *Samset et al.*, 2013].

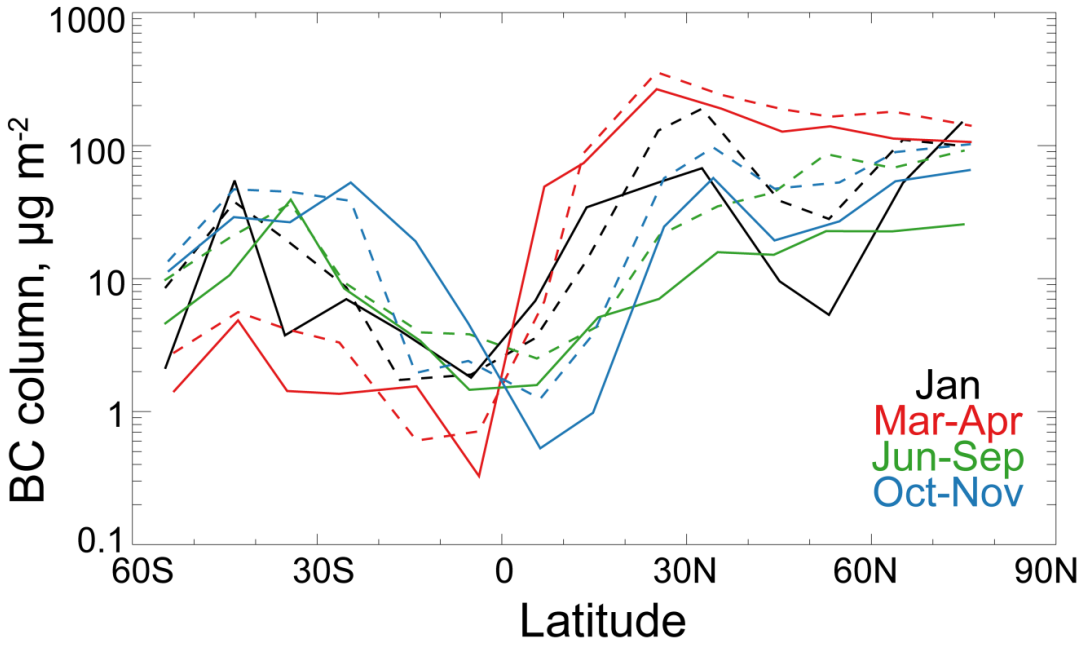

Figure 3.7: Latitudinal and seasonal variation of BC columns (0-10 km) across the central Pacific during HIPPO for different seasons. The Jun-Sep data are for the last two HIPPO deployments (Figure 3.4). Model results (dashed) are compared to observations (solid).

Figure 3.8 shows median vertical profiles of observed and model BC concentrations for different latitudes and seasons. In the Arctic, BC concentrations tend to increase with altitude in spring and fall, reflecting WCB transport from mid-latitudes, but peak near the surface in winter when transport from mid-latitudes takes place at low altitudes. At northern and southern mid-latitudes, peak concentrations are generally in the free troposphere because of WCB lifting. Tropical concentrations are generally highest near

the surface because of scavenging by deep convection. The model fails to reproduce the steep vertical gradient observed in the tropics, suggestive of insufficient scavenging.

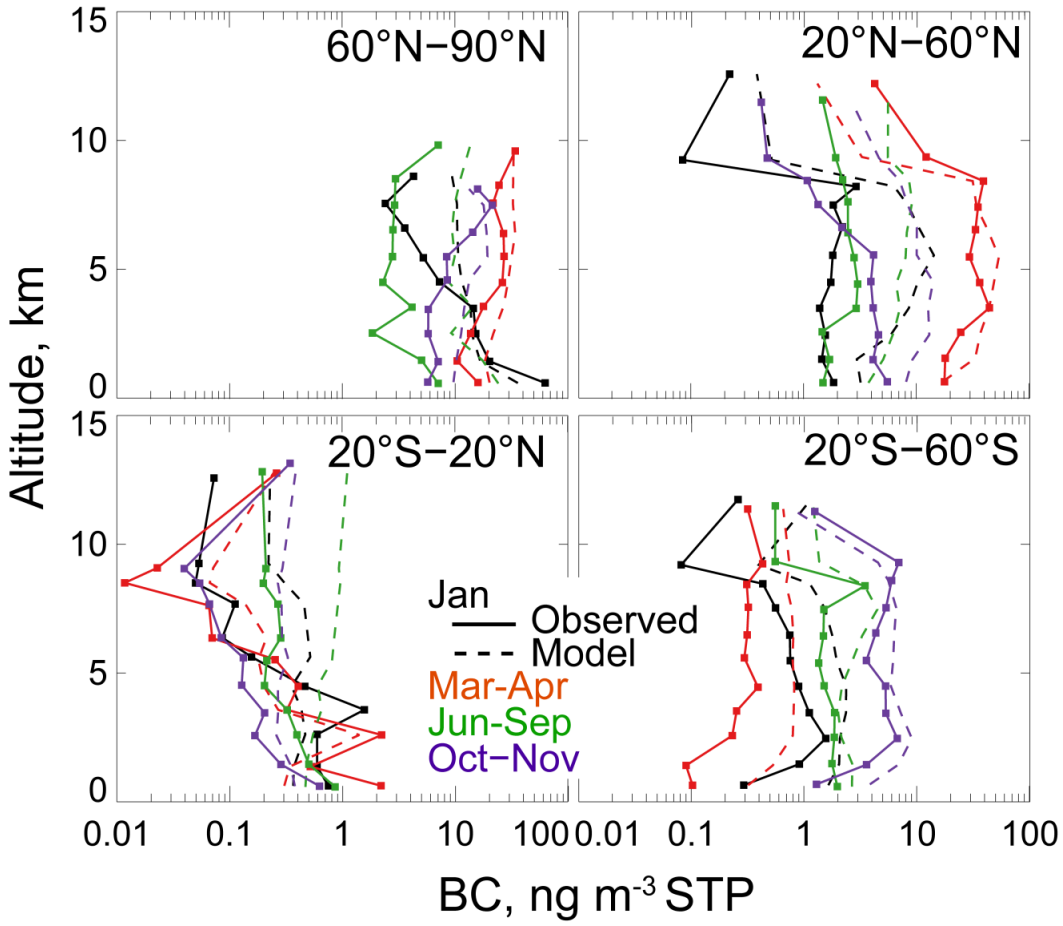

Figure 3.8: Median profiles of observed and model BC concentrations in different latitude bands and seasons across the central Pacific along HIPPO flight tracks.

We find that the overall high model bias in simulating the HIPPO BC data cannot be readily corrected. It is not due to sources or transport, as discussed above, and presumably reflects errors in scavenging. We can increase the scavenging efficiency in the model by adjustment of related parameters but there is no simple adjustment that

improves the ensemble of the HIPPO data, as described in the Appendix A, and that does not also compromise other aspects of the model aerosol simulation. It is possible that the model underestimates the frequency of precipitation events in the free troposphere, which would cumulatively affect observations in very remote air. This would be an issue with the GEOS-5 precipitation fields rather than the scavenging parameterization. In any case, our model performs better in simulating the HIPPO BC data than the ensemble of AeroCom models [*Schwarz et al.*, 2010; *Schwarz et al.*, 2013]. Combined with our successful simulation of BC in source regions and continental outflow (section 3.3), this provides a basis to use the model for BC source attribution and radiative forcing estimates.

3.5 Global BC Distribution and Source Attribution

Figure 3.9 shows the zonal annual mean distribution of BC in GEOS-Chem and the contributions from different sources in the year 2009. The ITCZ minimum along the HIPPO flight tracks is not seen in the zonal mean due to the influence of tropical continents. Minima in the zonal mean are instead at high southern latitudes and in the tropical upper troposphere. Fuel combustion dominates in the northern hemisphere while open fires are more important in the southern hemisphere. Aircraft are important only in the northern stratosphere. We find BC concentrations of 0.4-6 ng m^{-3} STP at 200-100 hPa, consistent with HIPPO observations in the stratosphere [*Schwarz et al.*, 2013].

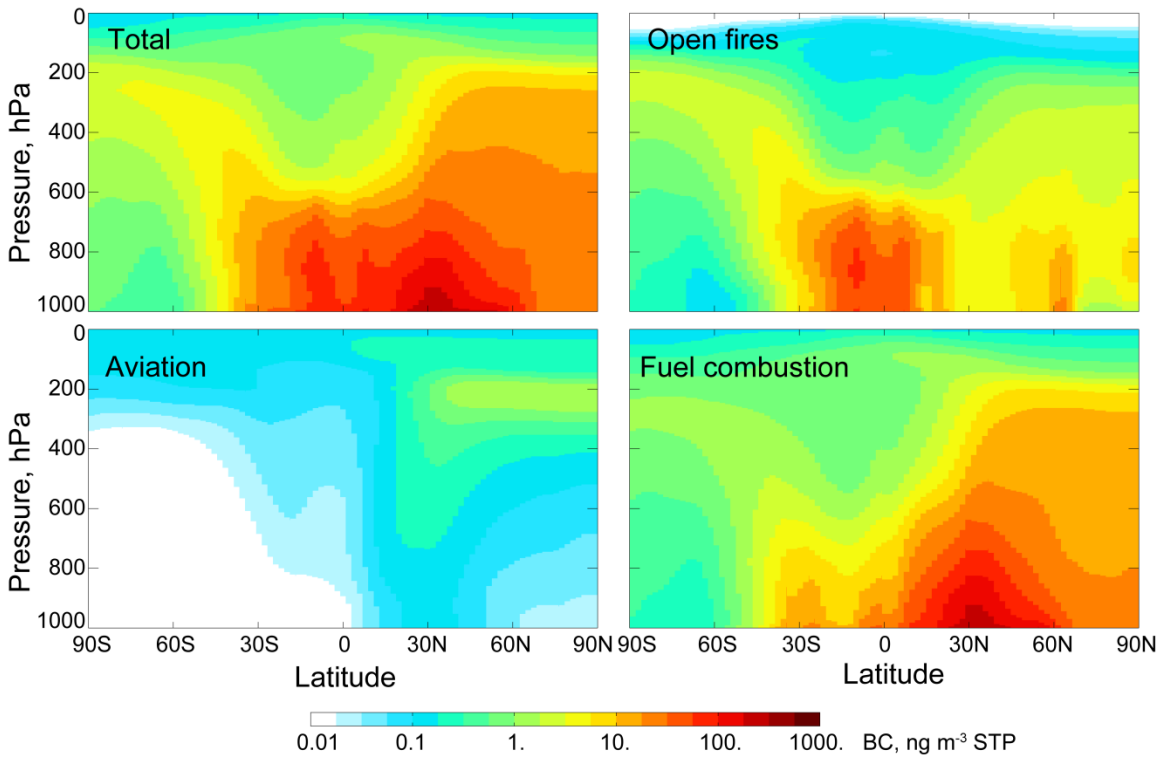

Figure 3.9: Annual zonal mean concentrations of BC simulated by GEOS-Chem for 2009 as a function of latitude and pressure, with contributions from different source types.

We compute in the model a global atmospheric BC burden of 77 Gg for 2009, of which 0.9 Gg is in the stratosphere. Open fires contribute 31% of the tropospheric burden. The tropospheric lifetime of BC against deposition is 4.2 d. Wet deposition accounts for 77% of the global sink and the rest is from dry deposition. Our lifetime is shorter than the range of 4.9-11.4 d in the AeroCom models [*Schulz et al.*, 2006; *Koch et al.*, 2009b], consistent with our better performance in the simulation of HIPPO and other remote data. The global lifetime of BC is closely related to the efficiency of transport to the free troposphere, where the lifetime is long because of infrequent precipitation. We find in GEOS-Chem that 33% of the BC burden is in the free troposphere above 2 km and 8.7%

is above 5 km. In comparison, the AeroCom models have 21 ± 11% of BC above 5 km [*Schulz et al.*, 2006]. This has important implications for radiative forcing because BC in the free troposphere is more likely to be above clouds and thus have a large radiative forcing efficiency [*Samset and Myhre*, 2011; *Samset et al.*, 2013].

3.6 Global BC AAOD and Radiative Forcing

Figure 3.10 shows the global annual mean distribution of BC AAOD (here and after, AAOD is for a wavelength of 550 nm) in the model, and compares with observations from the AERONET network. We compute the AAOD in the model as a product of the BC column and a constant mass absorption coefficient (MAC) of 11.3 m^2 g^{-1} accounting for enhancement in absorption due to coating [*Bond and Bergstrom*, 2006]. The model results are for 2009. The observed BC AAOD are 1996-2011 averages from AERONET level 2.0 data together with level 1.5 data for low-AOD conditions so as to minimize sampling bias (ftp://ftp-projects.zmaw.de/aerocom/aeronet/STATISTICS/grd_1203/). BC AAOD is retrieved by applying the refractive index for total aerosol to fine-mode aerosol (particles with diameter < 1 μm) and assuming all fine-mode AAOD to be from BC.

The model gives a global mean BC AAOD of 0.0017. Comparison to the AERONET sites in Fig. 3.10 indicates a global normalized mean bias (NMB) of -32% relative to the AERONET data. The bias is less in extratropical northern latitudes (-22%) than in the tropics (-65%). Part of the tropical bias could reflect interannual variability of fires, as

GFED3 BC emissions from fires are 1.6 Tg a^{-1} for 2009 but 2.1 ± 0.40 Tg a^{-1} for the 1996-2011 average. *Randerson et al.* [2012] argued that the GFED3 inventory is globally too low by 26% because it underestimates small fires. The oceans account for 41% of global BC AAOD in the model. The AERONET data are almost exclusively over continents, but there are a few island sites (Fig. 3.10). Comparison to these sites shows a high model bias over the northern Pacific, consistent with HIPPO, but a low bias over the tropical oceans that is inconsistent with HIPPO.

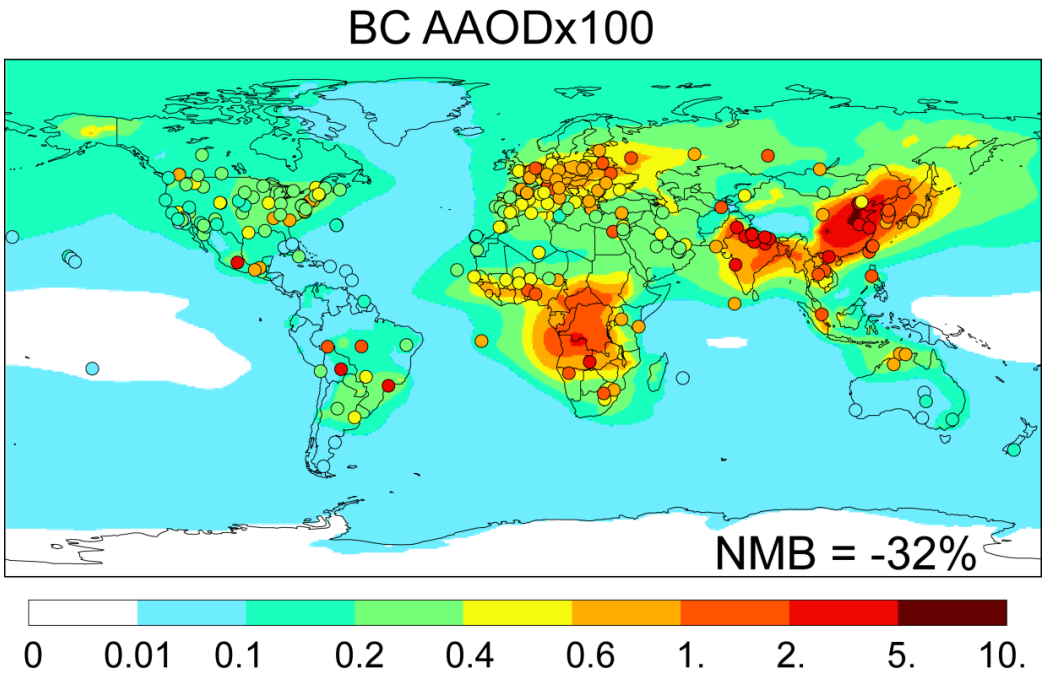

Figure 3.10: Global distribution of BC absorbing aerosol optical depth (AAOD) at 550 nm. Annual mean model values for 2009 (background) are compared to AERONET observations for 1996-2011 (circles). The AERONET data were obtained from ftp://ftp-projects.zmaw.de/aerocom/aeronet/STATISTICS/grd_1203/.

There are large uncertainties associated with the AERONET BC AAOD data. *Bond et al.* [2013] argued that values should be increased by 75% through better coarse-mode refractive index assumptions. On the other hand, *C.E. Chung et al.* [2012] argued that organic carbon (OC) aerosol accounts for 20% of fine-mode absorption. The use of the same refractive index for all aerosol sizes would also cause a large overestimate in dusty regions. Combining factors in *C.E. Chung et al.* [2012] and *Bond et al.* [2013] would imply a multiplicative factor of 1.4 to the AERONET data in Fig. 3.10 and a model NMB of -51% (a factor of 2). AERONET observes only under clear skies but comparison of clear-sky to all-sky conditions in our model suggests that the resulting bias is insignificant (3%), consistent with the results of *Bond et al.* [2013].

Figure 3.11 shows the global distribution of annual TOA DRF based on 3-D monthly mean fields of BC concentrations in GEOS-Chem. The global mean TOA DRF is 0.19 W m^{-2}. The forcing calculation follows *J. Wang et al.* [2008] but with improvement in the treatment of cloud effects *J. Wang et al.* [2013]. A four-stream broadband radiative transfer model (RTM), using monthly mean surface reflectance data [*Koelemeijer et al.*, 2003] is employed for the forcing calculation. The RTM is applied to the solar spectrum for six bands ranging from 0.2 to 4 μm. It assumes with a MAC for BC of 11.3 m^2 g^{-1} at 550 nm, consistent with our AAOD calculation. The global distribution of TOA DRF generally follows the AAOD pattern in Fig. 3.10 but with elevated forcing in polar regions. This reflects higher aerosol forcing efficiency (AFE, defined as the TOA DRF normalized by BC AAOD) associated with high surface albedo and high solar zenith angle [*Samset and Myhre*, 2011]. The oceans account for 41% of the global AAOD and

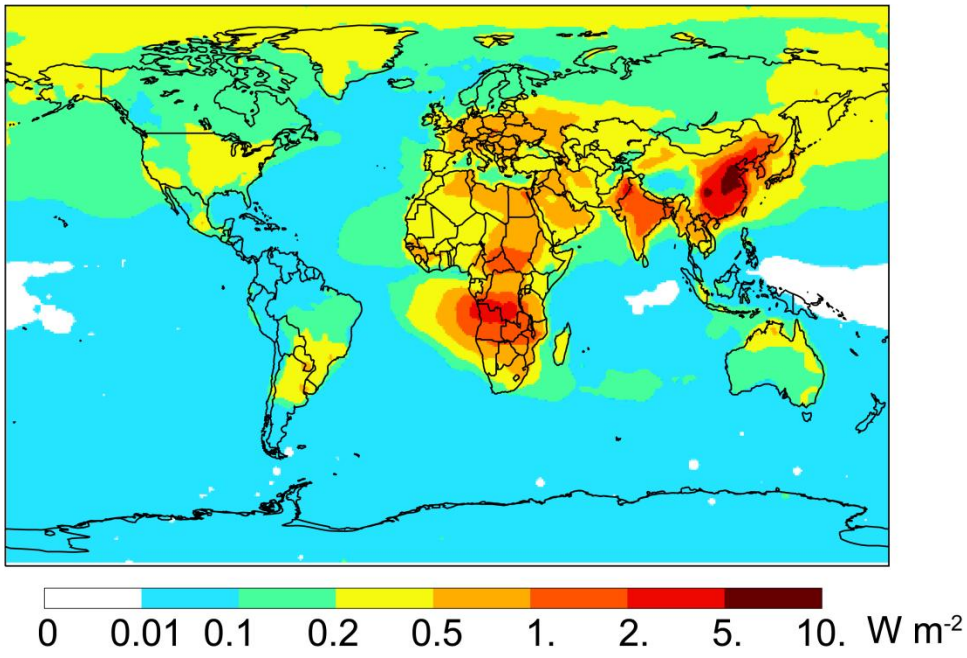

Figure 3.11: Global annual mean distribution of BC direct radiative forcing (DRF) at the top of the atmosphere (TOA). The radiative transfer model of *J. Wang et al.* [2008, 2013] is applied to the 3-D distribution of BC mass concentrations from GEOS-Chem.

36% of the TOA DRF. The AFE tends to be lower than average over the oceans because the surface is dark.

We can estimate the uncertainty in our TOA DRF estimate associated with the global BC distribution. The model shows little bias relative to in situ observations in source regions and continental outflow. It is however too high relative to the HIPPO data (+48% column mean bias) and too low relative to the AERONET AAOD data (possibly a factor of 2 as discussed above). We cannot reconcile these opposite biases with our model. If we discount the AERONET data and decrease the model AAOD over the oceans by 32% to correct the HIPPO overestimate, we obtain as lower bound a global BC AAOD of 0.0014

and TOA DRF of 0.17 W m^{-2}. If we discount the in situ continental data and increase the model AAOD over land by a factor of 2 to match the AERONET data with corrections from *Bond et al.* [2013] and *C.E. Chung et al.* [2012], we obtain as upper bound a global BC AAOD of 0.0026 and TOA DRF of 0.31 W m^{-2}. There are additional uncertainties related to the mixing state of BC and the radiative transfer model. Comparisons to previous studies are presented in the next section.

3.7 Comparison with previous studies

Previous studies of BC radiative forcing have used various CTMs to simulate the global distribution of BC, sometimes in combination with constraints from AERONET and satellite observations. Table 3.2 compiles results from recent studies and from the AeroCom activity Phase I [*Schulz et al.*, 2006], which intercompared results from eight CTMs. AeroCom Phase II [*Myhre et al.*, 2013] has results similar to Phase I but only reports forcing for fuel BC (not including open fires) and so is not included in the Table.

We see from Table 3.2 that our best estimate of 0.19 W m^{-2} for BC radiative forcing is below the range of previous studies. To understand the differences, we can express the DRF as the product of four driving variables [*Bond et al.*, 2013]:

$$\text{DRF} = \text{Emission} \times \text{Lifetime} \times \text{MAC} \times \text{AFE} \qquad (3.1)$$

Our global emission of BC (6.5 Tg a^{-1}) is similar to the AeroCom value of 6.3 Tg a^{-1}, and much lower than the *Bond et al.* [2013] value of 17 Tg a^{-1} which was scaled to match

AERONET AAOD observations. Such a large emission cannot be reconciled with the ensemble of in situ observations presented here, at least in the context of GEOS-Chem. It would produce a large positive bias in source regions, in continental outflow, and in the HIPPO data. Correcting for this bias would require an unrealistically short aerosol lifetime.

We compute a global tropospheric lifetime of 4.2 days for BC in GEOS-Chem, much lower than 6.8 ±1.8 days in AeroCom and 6.1 days in *Bond et al.* [2013]. This reflects our modifications to the GEOS-Chem wet scavenging scheme to better match the HIPPO observations while retaining consistency with other observations. Prior to these modifications, the tropospheric lifetime of BC in GEOS-Chem was 5.9 days [*Q. Wang et al.*, 2011]. The longer lifetime in the AeroCom models is likely responsible for their order-of-magnitude overestimates of the HIPPO data [*Schwarz et al.*, 2010; *Schwarz et al.*, 2013]. This has important implications because a longer BC lifetime allows for a greater load at high altitude where the BC radiative forcing efficiency is high.

We thus obtain an atmospheric load for BC of 0.15 mg m^{-2}, much lower than the AeroCom value of 0.23 ±0.07 mg m^{-2} and the *Bond et al.* [2013] value of 0.55 mg m^{-2}. Our estimate of the atmospheric load is most consistent with the ensemble of in situ observations presented in this paper. It underestimates the AERONET observations by as much as a factor 2 but there is large uncertainty in these observations as discussed above. The AERONET data provide little information over the oceans and no information on the

Table 3.2: BC direct radiative forcing (DRF) at top-of-atmosphere and global driving variables[a]

Reference	Emission ($Tg\ a^{-1}$)	Lifetime (d)	Load ($mg\ m^{-2}$)	Load above 5 km (%)	MAC ($m^2\ g^{-1}$)	AAOD x100	AFE ($W\ m^{-2}$ /AAOD)	DRF ($W\ m^{-2}$)
This work[b]	6.5	4.2	0.15	8.7	11	0.17(0.14-0.26)	114	0.19(0.17-0.31)
Schulz et al. [2006][c]	6.3	6.8±1.8	0.23±0.07	21±11	7.9±1.9	0.18±0.08	168±53	0.27±0.06
Ramanathan and Carmichael [2008][d]						0.67	134	0.9
C.E. Chung et al. [2012][e]						0.77	84	0.65
Bond et al. [2013][f]	17	6.1	0.55		11	0.60	147	0.88

[a]Results are for BC from all sources. Lifetime is tropospheric lifetime against deposition, MAC is the mass absorption coefficient and AFE is the aerosol forcing efficiency.
[b]Ranges given for AAOD and DRF reflect model adjustments to match either the HIPPO or AERONET data (see text).
[c]Averages and standard deviations for 8 models from AeroCom Phase I simulations (the ULAQ model is not included as it only reports clear-sky forcing). All AeroCom models use the same emissions. Results from AeroCom Phase II simulations [*Myhre et al.*, 2013] are not presented here because they report BC forcings from fuel sources only.
[d]AAODs derived from a combination of AERONET observations, MODIS satellite observations, and the GOCART model.
[e]AAODs derived from a combination of AERONET observations, MODIS and MISR satellite observations, and the GOCART model.
[f]results are from AeroCom Phase I simulations with scaling factors to match AERONET AAODs.

vertical distribution of BC, which is critical for the DRF calculation. The AeroCom models have 21±11% of the global BC load residing above 5 km, whereas that fraction is 8.7% in GEOS-Chem.

Our global BC AAOD estimate (0.0017) is consistent with AeroCom (0.0018±0.0008) but this simply reflects their assumption of a small MAC (7.9 m^2 g^{-1}). It is now considered that 11 m^2 g^{-1} (as used in our work) is more appropriate [*Bond and Bergstrom*, 2006; *Bond et al.*, 2013]. Other studies in Table 3.2 give much higher values for BC AAOD (0.0067-0.0077), reflecting their use of AERONET constraints over land but also assumptions over the oceans that would vastly overestimate the HIPPO data.

Our AFE of 114 W m^{-2} reflects application of the *J. Wang et al.* [2008. 2013] RTM to our global 3-D BC concentration fields. It is higher than the value of *C.E. Chung et.* [2012] (84 W m^{-2}) but lower than other reported values in Table 3.2 (134-168 W m^{-2}). Differences in AFE may reflect in part RTM but also the vertical distribution of BC [*Samset et al.*, 2013; *Stier et al.*, 2013]. Our lower AFE relative to AeroCom is consistent with our lower fraction of BC in the upper troposphere, supported by the aircraft data.

3.8 Conclusions

We used the GOES-Chem chemical transport model (CTM) to interpret extensive vertical profiles of black carbon (BC) concentrations from the HIPPO campaign in five deployments across the central Pacific from 85°N to 67°S during 2009-2011. Our goal

was to better understand the factors controlling BC concentrations in the remote troposphere and the implications for BC radiative forcing.

The HIPPO observations indicate very low BC concentrations over the Pacific, particularly in the tropics where values are often less than 0.1 ng m^{-3} STP through the depth of the troposphere. Reproducing these observations requires more efficient wet scavenging of BC than is usually implemented in models. We find that a GEOS-Chem simulation with global BC source of 6.5 Tg a^{-1}, and an improved representation of scavenging leading to a tropospheric BC lifetime of 4.2 days, reproduces the general features of the HIPPO data although it is biased high by a factor of 2 in median concentrations and 1.48 in column load. It also provides a successful simulation of BC concentrations in northern mid-latitudes source regions and continental outflow. Comparison to global AERONET absorbing aerosol optical depth (AAOD) data indicates a mean underestimate of 32%, although the magnitude of this bias depends on the assumptions in the AERONET product.

It appears from the HIPPO data that BC concentrations over the remote oceans, and in particular in the upper troposphere, are considerably lower than in the AeroCom CTMs commonly used for BC radiative forcing estimates. The AeroCom CTMs have a BC lifetime of 6.8 $\pm$1.8 days. Longer BC lifetimes allow more BC to reach the free troposphere where its radiation forcing efficiency is larger. We find in GEOS-Chem that 8.7% of the BC load is in the free troposphere above 5 km, compared to 21 $\pm$11% in the AeroCom models.

We combined our global 3-D distribution of BC concentrations with a radiative transfer model to infer a global top-of-atmosphere DRF for BC of 0.19 W m^{-2}, with an uncertainty range of 0.17-0.31 W m^{-2} based on uncertainty in the BC atmospheric distribution. This is much lower than the estimate of 0.27 ± 0.06 W m^{-2} from the AeroCom models [*Schulz et al.*, 2006] and more recent estimates of 0.7-0.9 W m^{-2} [*C.E. Chung et al.*, 2012; *Bond et al.*, 2013]. We find that the difference is largely driven by the estimates of BC concentrations over the oceans and in the free troposphere. Based on the constraints offered by the HIPPO observations and consistent also with other BC data, it appears that the radiative forcing from BC is much less than previously thought.

Appendices

Appendix A. Scavenging of BC in GEOS-Chem

A1. Updates to GEOS-Chem wet deposition

The standard wet deposition scheme in GEOS-Chem [*Liu et al.*, 2001; *Q. Wang et al.*, 2011] includes scavenging from convective updrafts as well as rainout/washout from anvil and large-scale (grid-resolved) precipitation. The GEOS-5 meteorological archive provides 3-D entrainment/detrainment convective mass fluxes with 6-h temporal resolution. These are treated in GEOS-Chem as a single convective updraft for each model grid square. As air rises in the updraft over a distance Δz between two successive model layers, aerosol incorporated in the cloud water is scavenged down to the bottom of the updraft. In the original scheme of *Liu et al*. [2001] and *Q. Wang et al.* [2011], the fraction f of aerosol mass scavenged from the updraft is given by

$$f = 1 - e^{-\alpha k \Delta z} \qquad \text{(A1)}$$

where k is a coefficient for conversion of cloud water to precipitation with values of 5×10^{-4} m^{-1} over land and 10^{-3} m^{-1} over ocean, and α is the fraction of aerosol mass incorporated in cloud water. α is set to 1 for water-soluble aerosols (excluding hydrophobic BC) at $T \geq 258$ K, and for ice nuclei (IN, including hydrophobic BC and dust aerosols) at $T < 258$ K. It is set to 0 in other cases.

In the model simulation presented in chapter 3 we set a minimum value of 0.5 for α to account for impaction scavenging. While nucleation scavenging dominates the removal of water-soluble aerosols, impaction scavenging still provides an important mechanism for the removal of hydrophobic aerosols during convective updrafts as indicated by a cloud-resolving model study [*Ekman et al.*, 2004]. Similar treatment (in-cloud scavenging ratio of 0.4 for accumulation-mode insoluble aerosols) is used in the ECHAMS-HAM model [*Croft et al.*, 2010].

We now further distinguish between homogeneous and heterogeneous freezing nucleation for cold clouds ($T < 258$ K). At $258\ \text{K} > T \geq 237$ K, we assume that heterogeneous nucleation dominates ice formation and thus $\alpha = 1$ only for IN ($\alpha = 0.5$ for other aerosols). At $T < 237$ K, we assume that homogeneous nucleation takes place with $\alpha = 1$ for all aerosols.

Aerosol scavenging by anvil and large-scale precipitation takes place both in cloud (rainout) and below cloud (washout) in the fraction of the grid box experiencing precipitation. For in-cloud scavenging, the original scheme incorporates all water-soluble aerosols at $T \geq 258$ K or all IN at $T < 258$ K into clouds followed by efficient scavenging when cloud water is converted to precipitation. Now we introduce homogeneous freezing nucleation for in-cloud removal and incorporate 100% of all aerosols into clouds at $T <$ 237 K, same as for convective updrafts. Below-cloud scavenging remains as described by *Q. Wang et al.* [2011].

A2. Sensitivity to scavenging parameterization

Figure A1 shows mean vertical profiles of BC from HIPPO averaged over four latitudinal bands and over all seasons. Observations (in black) and model results used in chapter 3

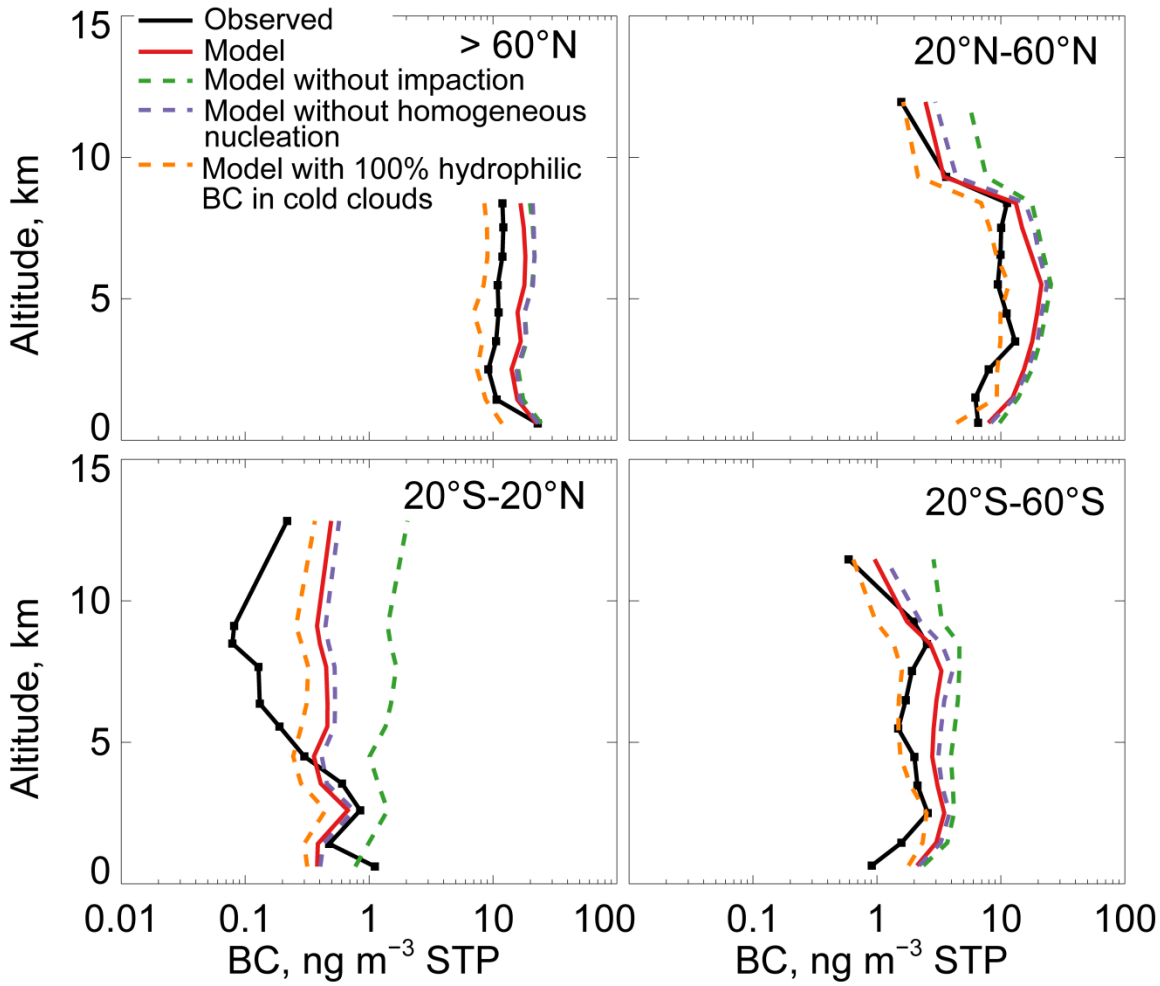

Figure A1: Mean vertical profiles of BC concentrations from HIPPO in four latitudinal ranges and averaged over all four seasons (Figure 3.8). Observations are compared with model results using different scavenging parameterizations. Results presented in Chapter 3 use the model as shown by the red solid line.

(in red) represent averages across seasons of the data in Figure 3.8. The effects of the above updates to the GEOS-Chem wet deposition scheme are shown in sensitivity simulations with these updates removed.

The scavenging of hydrophobic BC in convective updrafts has the largest effect over the tropics, where it decreases BC concentrations by a factor of 2 in the boundary layer and a factor of 4 in the upper troposphere. It also has significant effects in the upper troposphere at mid-latitudes. Even though hydrophobic BC in the model has a lifetime of only one day against conversion to hydrophilic, it still accounts for 10-40% of total BC in source regions and thus provides a large reservoir for deep convective transport to the upper troposphere. The more efficient scavenging of this BC in the tropics corrects the shape of the GEOS-Chem vertical profile from an increase with altitude to a weak decrease with altitude. It also corrects the model bias in the upper troposphere at mid-latitudes. However, it still cannot reproduce the sharp decrease with altitude in the HIPPO observations in the tropics. A larger value of α for impaction scavenging in Equation A1 would decrease BC concentrations in the upper troposphere but causes underestimate of concentrations in the lower troposphere. Homogeneous ice nucleation at temperatures cooler than 237 K decreases BC concentrations by 20% in the upper troposphere and 10% for the column (Fig. A1). The effect is relatively small because most precipitation occurs at $T > 237$ K.

The above two updates in GEOS-Chem result in a tropospheric lifetime of 4.2 days for BC (3.9 days for fuel BC and 5.4 days for open fire BC). The tropospheric lifetime of

^{210}Pb aerosol is 8.6 days, consistent with the best estimate of 9 days constrained by observations [*Liu et al.*, 2001].

Even with the updates in wet deposition, the model still has a high bias relative to HIPPO observations (48% in column average). The updates have little effect in the Arctic and we explored further the sensitivity to scavenging from cold clouds in the temperature range where ice crystal activation takes place by heterogeneous freezing ($237 < T < 258$ K). Although hydrophilic BC is not an effective IN, it could be incorporated in precipitation by riming. We conducted a sensitivity simulation with 100% hydrophilic BC incorporated into clouds at $T < 258$ K. Figure A1 shows improved model comparison over mid-latitudes and in the upper troposphere, but we find that concentrations in source regions are negatively affected, and so is the Arctic in winter-spring when observed concentrations are relatively high (Figure A2). The lifetime of ^{210}Pb decreases to 7.4 days.

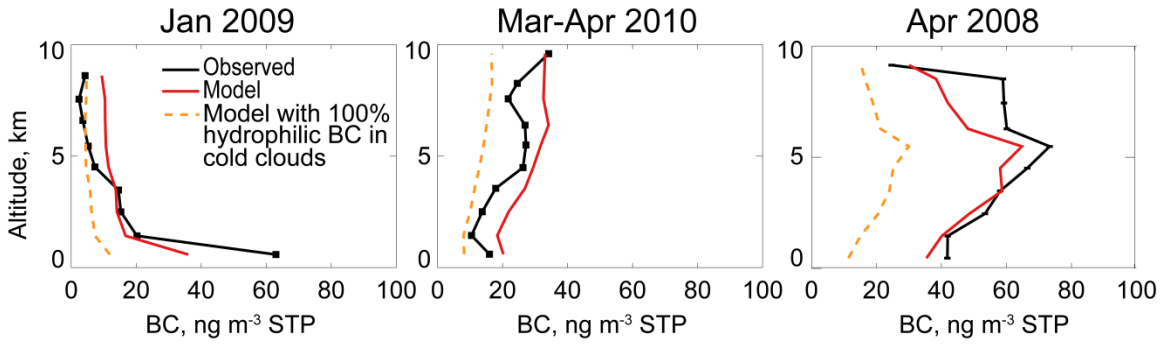

Figure A2: Median vertical profiles of BC concentrations in the Arctic in winter-spring. Observations are compared with results from GEOS-Chem as used in Chapter 3 (red solid line) and including 100% scavenging of hydrophilic BC in cold clouds (dashed line). Observations are from the ARCTAS campaign in 2008 and from HIPPO for the rest.

References

Aiken, A. C., et al. (2008), O/C and OM/OC Ratios of Primary, Secondary, and Ambient Organic Aerosols with High-Resolution Time-of-Flight Aerosol Mass Spectrometry, *Environ. Sci. Technol.*, *42*(12), 4478-4485, doi:10.1021/es703009q.

Akagi, S. K., R. J. Yokelson, C. Wiedinmyer, M. J. Alvarado, J. S. Reid, T. Karl, J. D. Crounse, and P. O. Wennberg (2011), Emission factors for open and domestic biomass burning for use in atmospheric models, *Atmos. Chem. Phys.*, *11*(9), 4039-4072, doi:10.5194/acp-11-4039-2011.

Amos, H. M., et al. (2012), Gas-particle partitioning of atmospheric Hg(II) and its effect on global mercury deposition, *Atmos. Chem. Phys.*, *12*(1), 591-603, doi:10.5194/acp-12-591-2012.

Andreae, M. O., and P. Merlet (2001), Emission of trace gases and aerosols from biomass burning, *Global Biogeochem. Cycles*, *15*(4), 955-966.

Andreae, M. O., and D. Rosenfeld (2008), Aerosol-cloud-precipitation interactions. Part 1. The nature and sources of cloud-active aerosols, *Eearth-Sci. Rev.*, *89*(1-2), 13-41, doi:10.1016/j.earscirev.2008.03.001.

Balkanski, Y. J., D. J. Jacob, G. M. Gardner, W. C. Graustein, and K. K. Turekian (1993), Transport and residence times of tropospheric aerosols inferred from a global three-dimensional simulation of 210Pb, *J. Geophys. Res.*, *98*(D11), 20573-20586, doi:10.1029/93jd02456.

Barrie, L. A., R. M. Hoff, and S. M. Daggupaty (1981), THE INFLUENCE OF MID-LATITUDINAL POLLUTION SOURCES ON HAZE IN THE CANADIAN ARCTIC, *Atmos. Environ.*, *15*(8), 1407-1419.

Baumgardner, D., R. Subramanian, C. Twohy, J. Stith, and G. Kok (2008), Scavenging of black carbon by ice crystals over the northern Pacific, *Geophys. Res. Lett.*, *35*(22), L22815, doi:10.1029/2008gl035764.

Bey, I., D. J. Jacob, J. A. Logan, and R. M. Yantosca (2001), Asian chemical outflow to the Pacific in spring: Origins, pathways, and budgets, *J. Geophys. Res.*, *106*(D19), 23097-23113, doi:10.1029/2001jd000806.

Bond, T. C. (2007), Can warming particles enter global climate discussions?, *Environmental Research Letters*, *2*(4), 045030, doi:10.1088/1748-9326/2/4/045030.

Bond, T. C., and R. W. Bergstrom (2006), Light absorption by carbonaceous particles: An investigative review, *Aerosol Sci. Technol.*, *40*(1), 27-67, doi:10.1080/02786820500421521.

Bond, T. C., E. Bhardwaj, R. Dong, R. Jogani, S. K. Jung, C. Roden, D. G. Streets, and N. M. Trautmann (2007), Historical emissions of black and organic carbon aerosol from energy-related combustion, 1850-2000, *Global Biogeochem. Cycles*, *21*(2), Gb2018, doi:10.1029/2006gb002840.

Bond, T. C., et al. (2013), Bounding the role of black carbon in the climate system: A scientific assessment, *J. Geophys. Res.*, *118*(11), 5380-5552, doi:10.1002/jgrd.50171.

Brock, C. A., et al. (2011), Characteristics, sources, and transport of aerosols measured in spring 2008 during the aerosol, radiation, and cloud processes affecting Arctic Climate (ARCPAC) Project, *Atmos. Chem. Phys.*, *11*(6), 2423-2453, doi:10.5194/acp-11-2423-2011.

Chen, Y., S. M. Kreidenweis, L. M. McInnes, D. C. Rogers, and P. J. DeMott (1998), Single particle analyses of ice nucleating aerosols in the upper troposphere and lower stratosphere, *Geophys. Res. Lett.*, *25*(9), 1391-1394, doi:10.1029/97gl03261.

Chung, C. E., V. Ramanathan, and D. Decremer (2012), Observationally constrained estimates of carbonaceous aerosol radiative forcing, *P. Natl. Acad. Sci. USA*, *109*(29), 11624-11629, doi:10.1073/pnas.1203707109.

Chung, C. E., V. Ramanathan, D. Kim, and I. A. Podgorny (2005), Global anthropogenic aerosol direct forcing derived from satellite and ground-based observations, *J. Geophys. Res.*, *110*(D24), D24207, doi:10.1029/2005jd006356.

Chung, S. H., and J. H. Seinfeld (2002), Global distribution and climate forcing of carbonaceous aerosols, *J. Geophys. Res.*, *107*(D19), 4407, doi:10.1029/2001jd001397.

Cooke, W. F., C. Liousse, H. Cachier, and J. Feichter (1999), Construction of a 1 degrees x 1 degrees fossil fuel emission data set for carbonaceous aerosol and implementation and radiative impact in the ECHAM4 model, *J. Geophys. Res.*, *104*(D18), 22137-22162.

Cozic, J., B. Verheggen, S. Mertes, P. Connolly, K. Bower, A. Petzold, U. Baltensperger, and E. Weingartner (2007), Scavenging of black carbon in mixed phase clouds at the high alpine site Jungfraujoch, *Atmos. Chem. Phys.*, *7*(7), 1797-1807.

Cozic, J., S. Mertes, B. Verheggen, D. J. Cziczo, S. J. Gallavardin, S. Walter, U. Baltensperger, and E. Weingartner (2008), Black carbon enrichment in atmospheric ice particle residuals observed in lower tropospheric mixed phase clouds, *J. Geophys. Res.*, *113*(D15), D15209, doi:10.1029/2007jd009266.

Croft, B., U. Lohmann, R. V. Martin, P. Stier, S. Wurzler, J. Feichter, R. Posselt, and S. Ferrachat (2009), Aerosol size-dependent below-cloud scavenging by rain and snow in the ECHAM5-HAM, *Atmos. Chem. Phys.*, *9*(14), 4653-4675.

Croft, B., U. Lohmann, R. V. Martin, P. Stier, S. Wurzler, J. Feichter, C. Hoose, U. Heikkila, A. van Donkelaar, and S. Ferrachat (2010), Influences of in-cloud aerosol scavenging parameterizations on aerosol concentrations and wet deposition in ECHAM5-HAM, *Atmos. Chem. Phys.*, *10*(4), 1511-1543.

Dana, M. T., and J. M. Hales (1976), STATISTICAL ASPECTS OF WASHOUT OF POLYDISPERSE AEROSOLS, *Atmos. Environ.*, *10*(1), 45-50.

DelGenio, A. D., M. S. Yao, W. Kovari, and K. K. W. Lo (1996), A prognostic cloud water parameterization for global climate models, *J. Climate.*, *9*(2), 270-304.

Djupstrom, M., J. M. Pacyna, W. Maenhaut, J. W. Winchester, S. M. Li, and G. E. Shaw (1993), CONTAMINATION OF ARCTIC AIR AT 3 SITES DURING A HAZE EVENT IN LATE WINTER 1986, *Atmos. Environ. Part A-General Topics*, *27*(17-18), 2999-3010, doi:10.1016/0960-1686(93)90332-s.

Doherty, S. J., S. G. Warren, T. C. Grenfell, A. D. Clarke, and R. E. Brandt (2010), Light-absorbing impurities in Arctic snow, *Atmos. Chem. Phys.*, *10*(23), 11647-11680, doi:10.5194/acp-10-11647-2010.

Drury, E., D. J. Jacob, R. J. D. Spurr, J. Wang, Y. Shinozuka, B. E. Anderson, A. D. Clarke, J. Dibb, C. McNaughton, and R. Weber (2010), Synthesis of satellite (MODIS), aircraft (ICARTT), and surface (IMPROVE, EPA-AQS, AERONET) aerosol observations over eastern North America to improve MODIS aerosol retrievals and constrain surface aerosol concentrations and sources, *J. Geophys. Res.*, *115*, D14204, doi:10.1029/2009jd012629.

Dubovik, O., B. Holben, T. F. Eck, A. Smirnov, Y. J. Kaufman, M. D. King, D. Tanre, and I. Slutsker (2002), Variability of absorption and optical properties of key aerosol types observed in worldwide locations, *J. Atmos. Sci.*, *59*(3), 590-608, doi:10.1175/1520-0469(2002)059<0590:voaaop>2.0.co;2.

Dunlea, E. J., et al. (2009), Evolution of Asian aerosols during transpacific transport in INTEX-B, *Atmos. Chem. Phys.*, *9*(19), 7257-7287.

Ekman, A. M. L., C. Wang, J. Wilson, and J. Strom (2004), Explicit simulations of aerosol physics in a cloud-resolving model: a sensitivity study based on an observed convective cloud, *Atmos. Chem. Phys.*, *4*, 773-791.

Eleftheriadis, K., S. Vratolis, and S. Nyeki (2009), Aerosol black carbon in the European Arctic: Measurements at Zeppelin station, Ny-Alesund, Svalbard from 1998-2007, *Geophys. Res. Lett.*, *36*, L02809, doi:10.1029/2008gl035741.

Feng, J. (2007), A 3-mode parameterization of below-cloud scavenging of aerosols for use in atmospheric dispersion models, *Atmos. Environ.*, *41*(32), 6808-6822, doi:10.1016/j.atmosenv.2007.04.046.

Feng, J. (2009), A size-resolved model for below-cloud scavenging of aerosols by snowfall, *J. Geophys. Res.*, *114*, D08203, doi:10.1029/2008jd011012.

Fisher, J. A., et al. (2011), Sources, distribution, and acidity of sulfate-ammonium aerosol in the Arctic in winter-spring, *Atmos. Environ.*, *45*(39), 7301-7318.

Fisher, J. A., et al. (2010), Source attribution and interannual variability of Arctic pollution in spring constrained by aircraft (ARCTAS, ARCPAC) and satellite (AIRS) observations of carbon monoxide, *Atmos. Chem. Phys.*, *10*(3), 977-996.

Flanner, M. G., C. S. Zender, J. T. Randerson, and P. J. Rasch (2007), Present-day climate forcing and response from black carbon in snow, *J. Geophys. Res.*, *112*(D11), D11202, doi:10.1029/2006jd008003.

Forster, P., et al. (2007), Changes in Atmospheric Constituents and in Radiative Forcing. In: Climate Change 2007: The Physical Science Basis. Contribution of Working Group I to the Fourth Assessment Report of the Intergovernmental Panel on Climate Change [Solomon, S., D. Qin, M. Manning, Z. Chen, M. Marquis, K.B. Averyt, M.Tignor and H.L. Miller (eds.)]. Cambridge University Press, Cambridge, United Kingdom and New York, NY, USA.

Frossard, A. A., P. M. Shaw, L. M. Russell, J. H. Kroll, M. R. Canagaratna, D. R. Worsnop, P. K. Quinn, and T. S. Bates (2011), Springtime Arctic haze contributions of submicron organic particles from European and Asian combustion sources, *J. Geophys. Res.*, *116*(D5), D05205, doi:10.1029/2010jd015178.

Fu, T. M., D. J. Jacob, and C. L. Heald (2009), Aqueous-phase reactive uptake of dicarbonyls as a source of organic aerosol over eastern North America, *Atmos. Environ.*, *43*(10), 1814-1822, doi:10.1016/j.atmosenv.2008.12.029.

Fu, T. M., D. J. Jacob, F. Wittrock, J. P. Burrows, M. Vrekoussis, and D. K. Henze (2008), Global budgets of atmospheric glyoxal and methylglyoxal, and implications for formation of secondary organic aerosols, *J. Geophys. Res.*, *113*(D15), D15303, doi:10.1029/2007jd009505.

Fu, T. M., et al. (2012), Carbonaceous aerosols in China: top-down constraints on primary sources and estimation of secondary contribution, *Atmos. Chem. Phys.*, *12*(5), 2725-2746, doi:10.5194/acp-12-2725-2012.

Giorgi, F., and W. L. Chameides (1986), Rainout lifetimes of highly soluble aerosols and gases as inferred from simulations with a general-circulation model, *J. Geophys. Res.*, *91*(D13), 14367-14376.

Gong, S. L., T. L. Zhao, S. Sharma, D. Toom-Sauntry, D. Lavoue, X. B. Zhang, W. R. Leaitch, and L. A. Barrie (2010), Identification of trends and interannual variability of sulfate and black carbon in the Canadian High Arctic: 1981-2007, *J. Geophys. Res.*, *115*, D07305, doi:10.1029/2009jd012943.

Hansen, A. D. A., and H. Rosen (1984), Vertical distributions of particulate carbon, sulfur, and bromine in the Arctic haze and comparison with ground-level measurements at Barrow, Alaska, *Geophys. Res. Lett.*, *11*(5), 381-384, doi:10.1029/GL011i005p00381.

Hansen, A. D. A., and T. Novakov (1989), Aerosol black carbon measurements in the Arctic haze during AGASP-II, *J. Atmos. Chem.*, *9*(1), 347-361, doi:10.1007/bf00052842.

Hansen, A. D. A., T. J. Conway, L. P. Strele, B. A. Bodhaine, K. W. Thoning, P. Tans, and T. Novakov (1989), Correlations among combustion effluent species at Barrow, Alaska: Aerosol black carbon, carbon dioxide, and methane, *J. Atmos. Chem.*, *9*(1), 283-299, doi:10.1007/bf00052838.

Heald, C. L., D. J. Jacob, R. J. Park, L. M. Russell, B. J. Huebert, J. H. Seinfeld, H. Liao, and R. J. Weber (2005), A large organic aerosol source in the free troposphere missing from current models, *Geophys. Res. Lett.*, *32*(18), L18809, doi:10.1029/2005gl023831.

Heald, C. L., et al. (2011), Exploring the vertical profile of atmospheric organic aerosol: comparing 17 aircraft field campaigns with a global model, *Atmos. Chem. Phys. Discuss.*, *11*(9), 25371-25425, doi:10.5194/acpd-11-25371-2011.

Hegg, D. A., S. G. Warren, T. C. Grenfell, S. J. Doherty, and A. D. Clarke (2010), Sources of light-absorbing aerosol in arctic snow and their seasonal variation, *Atmos. Chem. Phys.*, *10*(22), 10923-10938, doi:10.5194/acp-10-10923-2010.

Hegg, D. A., S. G. Warren, T. C. Grenfell, S. J. Doherty, T. V. Larson, and A. D. Clarke (2009), Source Attribution of Black Carbon in Arctic Snow, *Environ. Sci. Technol.*, *43*(11), 4016-4021, doi:10.1021/es803623f.

Held, A., D. A. Orsini, P. Vaattovaara, M. Tjernström, and C. Leck (2011), Near-surface profiles of aerosol number concentration and temperature over the Arctic Ocean, *Atmos. Meas. Tech. Discuss.*, *4*(3), 3017-3053, doi:10.5194/amtd-4-3017-2011.

Henze, D. K., and J. H. Seinfeld (2006), Global secondary organic aerosol from isoprene oxidation, *Geophys. Res. Lett.*, *33*(9), L09812, doi:10.1029/2006gl025976.

Henze, D. K., J. H. Seinfeld, N. L. Ng, J. H. Kroll, T. M. Fu, D. J. Jacob, and C. L. Heald (2008), Global modeling of secondary organic aerosol formation from aromatic hydrocarbons: high- vs. low-yield pathways, *Atmos. Chem. Phys.*, *8*(9), 2405-2420.

Hirdman, D., J. F. Burkhart, H. Sodemann, S. Eckhardt, A. Jefferson, P. K. Quinn, S. Sharma, J. Strom, and A. Stohl (2010), Long-term trends of black carbon and sulphate aerosol in the Arctic: changes in atmospheric transport and source region emissions, *Atmos. Chem. Phys.*, *10*(19), 9351-9368, doi:10.5194/acp-10-9351-2010.

Hodzic, A., J. L. Jimenez, S. Madronich, M. R. Canagaratna, P. F. DeCarlo, L. Kleinman, and J. Fast (2010), Modeling organic aerosols in a megacity: potential contribution of semi-volatile and intermediate volatility primary organic compounds to secondary organic aerosol formation, *Atmos. Chem. Phys.*, *10*(12), 5491-5514, doi:10.5194/acp-10-5491-2010.

Holmes, C. D., D. J. Jacob, E. S. Corbitt, J. Mao, X. Yang, R. Talbot, and F. Slemr (2010), Global atmospheric model for mercury including oxidation by bromine atoms, *Atmos. Chem. Phys.*, *10*(24), 12037-12057, doi:10.5194/acp-10-12037-2010.

Huang, L., S. L. Gong, C. Q. Jia, and D. Lavoue (2010), Importance of deposition processes in simulating the seasonality of the Arctic black carbon aerosol, *J. Geophys. Res.*, *115*, D17207, doi:10.1029/2009jd013478.

Hudman, R. C., et al. (2007), Surface and lightning sources of nitrogen oxides over the United States: Magnitudes, chemical evolution, and outflow, *J. Geophys. Res.*, *112*(D12), D12s05, doi:10.1029/2006jd007912.

IEA (2010), *Energy Statistics of Non-OECD Countries 2010*, OECD Publishing, Paris, France.

Jacob, D. J., et al. (2010), The Arctic Research of the Composition of the Troposphere from Aircraft and Satellites (ARCTAS) mission: design, execution, and first results, *Atmos. Chem. Phys.*, *10*(11), 5191-5212, doi:10.5194/acp-10-5191-2010.

Jacob, D. J., et al. (1997), Evaluation and intercomparison of global atmospheric transport models using 222Rn and other short-lived tracers, *J. Geophys. Res.*, *102*(D5), 5953-5970, doi:10.1029/96jd02955.

Jacobson, M. Z. (2001), Strong radiative heating due to the mixing state of black carbon in atmospheric aerosols, *Nature*, *409*(6821), 695-697.

Jacobson, M. Z. (2002), Control of fossil-fuel particulate black carbon and organic matter, possibly the most effective method of slowing global warming, *J. Geophys. Res.*, *107*(D19), 4410, doi:10.1029/2001jd001376.

Jacobson, M. Z. (2004), Climate response of fossil fuel and biofuel soot, accounting for soot's feedback to snow and sea ice albedo and emissivity, *J. Geophys. Res.*, *109*(D21), D21201, doi:10.1029/2004jd004945.

Jimenez, J. L., et al. (2003), Ambient aerosol sampling using the Aerodyne Aerosol Mass Spectrometer, *J. Geophys. Res.*, *108*(D7), 8425, doi:10.1029/2001jd001213.

Karcher, B., O. Mohler, P. J. DeMott, S. Pechtl, and F. Yu (2007), Insights into the role of soot aerosols in cirrus cloud formation, *Atmos. Chem. Phys.*, *7*(16), 4203-4227.

Kipling, Z., P. Stier, J. P. Schwarz, A. E. Perring, J. R. Spackman, G. W. Mann, C. E. Johnson, and P. J. Telford (2013), Constraints on aerosol processes in climate models from vertically-resolved aircraft observations of black carbon, *Atmos. Chem. Phys.*, *13*(12), 5969-5986, doi:10.5194/acp-13-5969-2013.

Klonecki, A., P. Hess, L. Emmons, L. Smith, J. Orlando, and D. Blake (2003), Seasonal changes in the transport of pollutants into the Arctic troposphere-model study, *J. Geophys. Res.*, *108*(D4), doi:8367

10.1029/2002jd002199.

Koch, D. (2001), Transport and direct radiative forcing of carbonaceous and sulfate aerosols in the GISS GCM, *J. Geophys. Res.*, *106*(D17), 20311-20332, doi:10.1029/2001jd900038.

Koch, D., and J. Hansen (2005), Distant origins of Arctic black carbon: A Goddard Institute for Space Studies ModelE experiment, *J. Geophys. Res.*, *110*(D4), D04204, doi:10.1029/2004jd005296.

Koch, D., T. C. Bond, D. Streets, N. Unger, and G. R. van der Werf (2007), Global impacts of aerosols from particular source regions and sectors, *J. Geophys. Res.*, *112*(D2), D02205, doi:10.1029/2005jd007024.

Koch, D., S. Menon, A. Del Genio, R. Ruedy, I. Alienov, and G. A. Schmidt (2009a), Distinguishing Aerosol Impacts on Climate over the Past Century, *J. Climate.*, *22*(10), 2659-2677, doi:10.1175/2008jcli2573.1.

Koch, D., et al. (2009b), Evaluation of black carbon estimations in global aerosol models, *Atmos. Chem. Phys.*, *9*(22), 9001-9026.

Koelemeijer, R. B. A., J. F. de Haan, and P. Stammes (2003), A database of spectral surface reflectivity in the range 335-772 nm derived from 5.5 years of GOME observations, *J. Geophys. Res.*, *108*(D2), 4070, doi:10.1029/2002jd002429.

Kondo, Y., N. Oshima, M. Kajino, R. Mikami, N. Moteki, N. Takegawa, R. L. Verma, Y. Kajii, S. Kato, and A. Takami (2011a), Emissions of black carbon in East Asia estimated from observations at a remote site in the East China Sea, *J. Geophys. Res.*, *116*, D16201, doi:10.1029/2011jd015637.

Kondo, Y., et al. (2011b), Emissions of black carbon, organic, and inorganic aerosols from biomass burning in North America and Asia in 2008, *J. Geophys. Res.*, *116*, D08204, doi:10.1029/2010jd015152.

Kristjansson, J. E., T. Iversen, A. Kirkevag, O. Seland, and J. Debernard (2005), Response of the climate system to aerosol direct and indirect forcing: Role of cloud feedbacks, *J. Geophys. Res.*, *110*(D24), doi:D24206

10.1029/2005jd006299.

Law, K. S., and A. Stohl (2007), Arctic air pollution: Origins and impacts, *Science*, *315*(5818), 1537-1540, doi:10.1126/science.1137695.

Leibensperger, E. M., L. J. Mickley, D. J. Jacob, W. T. Chen, J. H. Seinfeld, A. Nenes, P. J. Adams, D. G. Streets, N. Kumar, and D. Rind (2012), Climatic effects of 1950-2050 changes in US anthropogenic aerosols- Part 1: Aerosol trends and radiative forcing, *Atmos. Chem. Phys.*, *12*(7), 3333-3348, doi:10.5194/acp-12-3333-2012.

Liu, H. Y., D. J. Jacob, I. Bey, and R. M. Yantosca (2001), Constraints from Pb-210 and Be-7 on wet deposition and transport in a global three-dimensional chemical tracer model driven by assimilated meteorological fields, *J. Geophys. Res.*, *106*(D11), 12109-12128.

Liu, H. Y., D. J. Jacob, I. Bey, R. M. Yantosca, B. N. Duncan, and G. W. Sachse (2003), Transport pathways for Asian pollution outflow over the Pacific: Interannual and seasonal variations, *J. Geophys. Res.*, *108*(D20), 8786, doi:10.1029/2002jd003102.

Liu, J., S. Fan, L. W. Horowitz, and H. Levy, II (2011), Evaluation of factors controlling long-range transport of black carbon to the Arctic, *Journal of Geophysical Research-Atmospheres*, *116*, D04307, doi:10.1029/2010jd015145.

Liu, J. F., S. M. Fan, L. W. Horowitz, and H. Levy (2011), Evaluation of factors controlling long-range transport of black carbon to the Arctic, *J. Geophys. Res.*, *116*, D04307, doi:10.1029/2010jd015145.

Lu, Z., D. G. Streets, Q. Zhang, S. Wang, G. R. Carmichael, Y. F. Cheng, C. Wei, M. Chin, T. Diehl, and Q. Tan (2010), Sulfur dioxide emissions in China and sulfur trends in East Asia since 2000, *Atmos. Chem. Phys.*, *10*(13), 6311-6331, doi:10.5194/acp-10-6311-2010.

Mao, J., et al. (2010), Chemistry of hydrogen oxide radicals (HOx) in the Arctic troposphere in spring, *Atmos. Chem. Phys.*, *10*(13), 5823-5838, doi:10.5194/acp-10-5823-2010.

Mao, Y. H., Q. B. Li, L. Zhang, Y. Chen, J. T. Randerson, D. Chen, and K. N. Liou (2011), Biomass burning contribution to black carbon in the Western United States Mountain Ranges, *Atmos. Chem. Phys.*, *11*(21), 11253-11266, doi:10.5194/acp-11-11253-2011.

Matsui, H., et al. (2011), Seasonal variation of the transport of black carbon aerosol from the Asian continent to the Arctic during the ARCTAS aircraft campaign, *J. Geophys. Res.*, *116*, D05202, doi:10.1029/2010jd015067.

McConnell, J. R., R. Edwards, G. L. Kok, M. G. Flanner, C. S. Zender, E. S. Saltzman, J. R. Banta, D. R. Pasteris, M. M. Carter, and J. D. W. Kahl (2007), 20th-century industrial black carbon emissions altered arctic climate forcing, *Science*, *317*(5843), 1381-1384, doi:10.1126/science.1144856.

McNaughton, C. S., et al. (2011), Absorbing aerosol in the troposphere of the Western Arctic during the 2008 ARCTAS/ARCPAC airborne field campaigns, *Atmos. Chem. Phys.*, *11*(15), 7561-7582, doi:10.5194/acp-11-7561-2011.

Murakami, M., T. Kimura, C. Magono, and K. Kikuchi (1983), OBSERVATIONS OF PRECIPITATION SCAVENGING FOR WATER-SOLUBLE PARTICLES, *J. Meteorol. Soc. Jap.*, *61*(3), 346-358.

Myhre, G., et al. (2013), Radiative forcing of the direct aerosol effect from AeroCom Phase II simulations, *Atmos. Chem. Phys.*, *13*(4), 1853-1877, doi:10.5194/acp-13-1853-2013.

Nilsson, E. D., and U. Rannik (2001), Turbulent aerosol fluxes over the Arctic Ocean 1. Dry deposition over sea and pack ice, *J. Geophys. Res.*, *106*(D23), 32125-32137.

Oshima, N., et al. (2012), Wet removal of black carbon in Asian outflow: Aerosol Radiative Forcing in East Asia (A-FORCE) aircraft campaign, *J. Geophys. Res.*, *117*(D3), D03204, doi:10.1029/2011jd016552.

Park, R. J., D. J. Jacob, M. Chin, and R. V. Martin (2003), Sources of carbonaceous aerosols over the United States and implications for natural visibility, *J. Geophys. Res.*, *108*(D12), 4355, doi:10.1029/2002jd003190.

Park, R. J., D. J. Jacob, N. Kumar, and R. M. Yantosca (2006), Regional visibility statistics in the United States: Natural and transboundary pollution influences, and implications for the Regional Haze Rule, *Atmos. Environ.*, *40*(28), 5405-5423, doi:10.1016/j.atmosenv.2006.04.059.

Park, R. J., et al. (2005), Export efficiency of black carbon aerosol in continental outflow: Global implications, *J. Geophys. Res.*, *110*(D11), D11205, doi:10.1029/2004jd005432.

Quinn, P. K., T. L. Miller, T. S. Bates, J. A. Ogren, E. Andrews, and G. E. Shaw (2002), A 3-year record of simultaneously measured aerosol chemical and optical properties at Barrow, Alaska, *J. Geophys. Res.*, *107*(D11), 4130, doi:10.1029/2001jd001248.

Quinn, P. K., G. Shaw, E. Andrews, E. G. Dutton, T. Ruoho-Airola, and S. L. Gong (2007), Arctic haze: current trends and knowledge gaps, *Tellus Ser. B-Chem. Phys. Meteorol.*, *59*(1), 99-114, doi:10.1111/j.1600-0889.2006.00238.x.

Quinn, P. K., et al. (2008), Short-lived pollutants in the Arctic: their climate impact and possible mitigation strategies, *Atmos. Chem. Phys.*, *8*(6), 1723-1735.

Ramanathan, V., and G. Carmichael (2008), Global and regional climate changes due to black carbon, *Nature Geoscience*, *1*(4), 221-227, doi:10.1038/ngeo156.

Randerson, J. T., Y. Chen, G. R. van der Werf, B. M. Rogers, and D. C. Morton (2012), Global burned area and biomass burning emissions from small fires, *Journal of Geophysical Research-Biogeosciences*, *117*, G04012, doi:10.1029/2012jg002128.

Rasch, P. J., et al. (2000), A comparison of scavenging and deposition processes in global models: results from the WCRP Cambridge Workshop of 1995, *Tellus B*, *52*(4), 1025-1056, doi:10.1034/j.1600-0889.2000.00980.x.

Reddy, M. S., and O. Boucher (2004), A study of the global cycle of carbonaceous aerosols in the LMDZT general circulation model, *J. Geophys. Res.*, *109*(D14), D14202, doi:10.1029/2003jd004048.

Reid, J. S., R. Koppmann, T. F. Eck, and D. P. Eleuterio (2005), A review of biomass burning emissions part II: intensive physical properties of biomass burning particles, *Atmos. Chem. Phys.*, *5*, 799-825.

Reid, J. S., et al. (2009), Global Monitoring and Forecasting of Biomass-Burning Smoke: Description of and Lessons From the Fire Locating and Modeling of Burning Emissions (FLAMBE) Program, *Ieee Journal of Selected Topics in Applied Earth Observations and Remote Sensing*, *2*(3), 144-162, doi:10.1109/jstars.2009.2027443.

Remer, L. A., et al. (2005), The MODIS Aerosol Algorithm, Products, and Validation, *J. Atmos. Sci.*, *62*(4), 947-973, doi:10.1175/jas3385.1.

Ricard, V., J. L. Jaffrezo, V. M. Kerminen, R. E. Hillamo, M. Sillanpaa, S. Ruellan, C. Liousse, and H. Cachier (2002), Two years of continuous aerosol measurements in northern Finland, *J. Geophys. Res.*, *107*(D11), 4129, doi:10.1029/2001jd000952.

Riemer, N., M. West, R. Zaveri, and R. Easter (2010), Estimating black carbon aging time-scales with a particle-resolved aerosol model, *J. Aerosol Sci.*, *41*(1), 143-158, doi:10.1016/j.jaerosci.2009.08.009.

Rosen, H., T. Novakov, and B. A. Bodhaine (1981), SOOT IN THE ARCTIC, *Atmos. Environ.*, *15*(8), 1371-1374, doi:10.1016/0004-6981(81)90343-7.

Samset, B. H., and G. Myhre (2011), Vertical dependence of black carbon, sulphate and biomass burning aerosol radiative forcing, *Geophys. Res. Lett.*, *38*, L24802, doi:10.1029/2011gl049697.

Samset, B. H., et al. (2013), Black carbon vertical profiles strongly affect its radiative forcing uncertainty, *Atmos. Chem. Phys.*, *13*(5), 2423-2434, doi:10.5194/acp-13-2423-2013.

Sato, M., J. Hansen, D. Koch, A. Lacis, R. Ruedy, O. Dubovik, B. Holben, M. Chin, and T. Novakov (2003), Global atmospheric black carbon inferred from AERONET, *P. Natl. Acad. Sci. USA*, *100*(11), 6319-6324, doi:10.1073/pnas.0731897100.

Schnell, R. C. (1984), Arctic Haze and the Arctic Gas and Aerosol Sampling Program (Agasp), *Geophys. Res. Lett.*, *11*(5), 361-364.

Schnell, R. C., and W. E. Raatz (1984), Vertical and Horizontal Characteristics of Arctic Haze during Agasp - Alaskan Arctic, *Geophys. Res. Lett.*, *11*(5), 369-372.

Schnell, R. C., T. B. Watson, and B. A. Bodhaine (1989), NOAA WP-3D INSTRUMENTATION AND FLIGHT OPERATIONS ON AGASP-II, *J. Atmos. Chem.*, *9*(1-3), 3-16, doi:10.1007/bf00052822.

Schulz, M., et al. (2006), Radiative forcing by aerosols as derived from the AeroCom present-day and pre-industrial simulations, *Atmos. Chem. Phys.*, *6*, 5225-5246.

Schwarz, J. P., J. R. Spackman, R. S. Gao, L. A. Watts, P. Stier, M. Schulz, S. M. Davis, S. C. Wofsy, and D. W. Fahey (2010), Global-scale black carbon profiles observed in the remote atmosphere and compared to models, *Geophys. Res. Lett.*, *37*(18), L18812, doi:10.1029/2010gl044372.

Schwarz, J. P., B. H. Samset, A. E. Perring, J. R. Spackman, R. S. Gao, P. Stier, M. Schulz, F. L. Moore, E. A. Ray, and D. W. Fahey (2013), Global-scale seasonally resolved black carbon vertical profiles over the Pacific, *Geophys. Res. Lett.*, n/a-n/a, doi:10.1002/2013gl057775.

Sharma, S., E. Andrews, L. A. Barrie, J. A. Ogren, and D. Lavoue (2006), Variations and sources of the equivalent black carbon in the high Arctic revealed by long-term observations at Alert and Barrow: 1989-2003, *J. Geophys. Res.*, *111*(D14), doi:D14208

10.1029/2005jd006581.

Shaw, G. E. (1982), EVIDENCE FOR A CENTRAL EURASIAN SOURCE AREA OF ARCTIC HAZE IN ALASKA, *Nature*, *299*(5886), 815-818.

Shaw, P. M., L. M. Russell, A. Jefferson, and P. K. Quinn (2010), Arctic organic aerosol measurements show particles from mixed combustion in spring haze and from frost flowers in winter, *Geophys. Res. Lett.*, *37*, L10803, doi:10.1029/2010gl042831.

Shindell, D. T., et al. (2008), A multi-model assessment of pollution transport to the Arctic, *Atmos. Chem. Phys.*, *8*(17), 5353-5372.

Simone, N. W., M. E. J. Stettler, and S. R. H. Barrett (2013), Rapid estimation of global civil aviation emissions with uncertainty quantification, *Transportation Research Part D*, in press, doi:10.1016/j.trd.2013.07.001, 2013.

Spackman, J. R., R. S. Gao, W. D. Neff, J. P. Schwarz, L. A. Watts, D. W. Fahey, J. S. Holloway, T. B. Ryerson, J. Peischl, and C. A. Brock (2010), Aircraft observations of enhancement and depletion of black carbon mass in the springtime Arctic, *Atmos. Chem. Phys.*, *10*(19), 9667-9680, doi:10.5194/acp-10-9667-2010.

Stier, P., et al. (2013), Host model uncertainties in aerosol radiative forcing estimates: results from the AeroCom Prescribed intercomparison study, *Atmos. Chem. Phys.*, *13*(6), 3245-3270, doi:10.5194/acp-13-3245-2013.

Stith, J. L., C. H. Twohy, P. J. DeMott, D. Baumgardner, T. Campos, R. Gao, and J. Anderson (2011), Observations of ice nuclei and heterogeneous freezing in a Western Pacific extratropical storm, *Atmos. Chem. Phys.*, *11*(13), 6229-6243, doi:10.5194/acp-11-6229-2011.

Stohl, A. (2006), Characteristics of atmospheric transport into the Arctic troposphere, *J. Geophys. Res.*, *111*(D11), D11306, doi:10.1029/2005jd006888.

Stohl, A., et al. (2007), Arctic smoke - record high air pollution levels in the European Arctic due to agricultural fires in Eastern Europe in spring 2006, *Atmos. Chem. Phys.*, *7*, 511-534.

Stone, R. S., et al. (2010), A three-dimensional characterization of Arctic aerosols from airborne Sun photometer observations: PAM-ARCMIP, April 2009, *J. Geophys. Res.*, *115*, D13203, doi:10.1029/2009jd013605.

Targino, A. C., et al. (2009), Influence of particle chemical composition on the phase of cold clouds at a high-alpine site in Switzerland, *J. Geophys. Res.*, *114*, D18206, doi:10.1029/2008jd011365.

Textor, C., et al. (2006), Analysis and quantification of the diversities of aerosol life cycles within AeroCom, *Atmos. Chem. Phys.*, *6*, 1777-1813.

Tilmes, S., et al. (2011), Source contributions to Northern Hemisphere CO and black carbon during spring and summer 2008 from POLARCAT and START08/preHIPPO observations and MOZART-4, *Atmos. Chem. Phys. Discuss.*, *11*(2), 5935-5983, doi:10.5194/acpd-11-5935-2011.

Torres, O., A. Tanskanen, B. Veihelmann, C. Ahn, R. Braak, P. K. Bhartia, P. Veefkind, and P. Levelt (2007), Aerosols and surface UV products from Ozone Monitoring Instrument observations: An overview, *J. Geophys. Res.*, *112*(D24), D24s47, doi:10.1029/2007jd008809.

Turpin, B. J., and H. J. Lim (2001), Species contributions to PM2.5 mass concentrations: Revisiting common assumptions for estimating organic mass, *Aerosol Sci. Technol.*, *35*(1), 602-610.

van der Werf, G. R., J. T. Randerson, L. Giglio, G. J. Collatz, P. S. Kasibhatla, and A. F. Arellano (2006), Interannual variability in global biomass burning emissions from 1997 to 2004, *Atmos. Chem. Phys.*, *6*, 3423-3441.

van der Werf, G. R., J. T. Randerson, L. Giglio, G. J. Collatz, M. Mu, P. S. Kasibhatla, D. C. Morton, R. S. DeFries, Y. Jin, and T. T. van Leeuwen (2010), Global fire emissions and the contribution of deforestation, savanna, forest, agricultural, and peat fires (1997–2009), *Atmos. Chem. Phys.*, *10*(23), 11707-11735, doi:10.5194/acp-10-11707-2010.

van Donkelaar, A., et al. (2008), Analysis of aircraft and satellite measurements from the Intercontinental Chemical Transport Experiment (INTEX-B) to quantify long-range transport of East Asian sulfur to Canada, *Atmos. Chem. Phys.*, *8*(11), 2999-3014.

Volkamer, R., J. L. Jimenez, F. San Martini, K. Dzepina, Q. Zhang, D. Salcedo, L. T. Molina, D. R. Worsnop, and M. J. Molina (2006), Secondary organic aerosol formation from anthropogenic air pollution: Rapid and higher than expected, *Geophys. Res. Lett.*, *33*(17), L17811, doi:10.1029/2006gl026899.

Wang, J., D. J. Jacob, and S. T. Martin (2008), Sensitivity of sulfate direct climate forcing to the hysteresis of particle phase transitions, *J. Geophys. Res.*, *113*(D11), D11207, doi:10.1029/2007jd009368.

Wang, J., S. Park, J. Zeng, C. Ge, K. Yang, S. Carn, N. Krotkov, and A. H. Omar (2013), Modeling of 2008 Kasatochi volcanic sulfate direct radiative forcing: assimilation of OMI SO2 plume height data and comparison with MODIS and CALIOP observations, *Atmos. Chem. Phys.*, *13*(4), 1895-1912, doi:10.5194/acp-13-1895-2013.

Wang, Q., et al. (2011), Sources of carbonaceous aerosols and deposited black carbon in the Arctic in winter-spring: implications for radiative forcing, *Atmos. Chem. Phys.*, *11*(23), 12453-12473, doi:10.5194/acp-11-12453-2011.

Wang, X., L. Zhang, and M. D. Moran (2010), Uncertainty assessment of current size-resolved parameterizations for below-cloud particle scavenging by rain, *Atmos. Chem. Phys.*, *10*(12), 5685-5705, doi:10.5194/acp-10-5685-2010.

Wang, X., Y. Wang, J. Hao, Y. Kondo, M. Irwin, J. William Munger, and Y. Zhao (2013), Top-down estimate of China's black carbon emissions using surface observations:

sensitivity to observation representativeness and transport model error, *J. Geophys. Res.*, n/a-n/a, doi:10.1002/jgrd.50397.

Wang, Y. H., D. J. Jacob, and J. A. Logan (1998), Global simulation of tropospheric O_3-NO_x-hydrocarbon chemistry -- 1. Model formulation, *J. Geophys. Res.*, *103*(D9), 10713-10725.

Warneke, C., et al. (2009), Biomass burning in Siberia and Kazakhstan as an important source for haze over the Alaskan Arctic in April 2008, *Geophys. Res. Lett.*, *36*, L02813, doi:10.1029/2008gl036194.

Warneke, C., et al. (2010), An important contribution to springtime Arctic aerosol from biomass burning in Russia, *Geophys. Res. Lett.*, *37*, L01801, doi:10.1029/2009gl041816.

Warren, S. G., and W. J. Wiscombe (1985), DIRTY SNOW AFTER NUCLEAR-WAR, *Nature*, *313*(6002), 467-470.

Wesely, M. L. (1989), Parameterization of surface resistances to gaseous dry deposition in regional-scale numerical-models, *Atmos. Environ.*, *23*(6), 1293-1304, doi:10.1016/0004-6981(89)90153-4.

Wofsy, S. C., H. S. Team, T. Cooperating Modellers, and T. Satellite (2011), HIAPER Pole-to-Pole Observations (HIPPO): fine-grained, global-scale measurements of climatically important atmospheric gases and aerosols, *Philosophical Transactions of the Royal Society a-Mathematical Physical and Engineering Sciences*, *369*(1943), 2073-2086, doi:10.1098/rsta.2010.0313.

Xiao, Y. P., D. J. Jacob, and S. Turquety (2007), Atmospheric acetylene and its relationship with CO as an indicator of air mass age, *J. Geophys. Res.*, *112*(D12), D12305, doi:10.1029/2006jd008268.

Zarzycki, C. M., and T. C. Bond (2010), How much can the vertical distribution of black carbon affect its global direct radiative forcing?, *Geophys. Res. Lett.*, *37*, L20807, doi:10.1029/2010gl044555.

Zhang, L., et al. (2008), Transpacific transport of ozone pollution and the effect of recent Asian emission increases on air quality in North America: an integrated analysis using

satellite, aircraft, ozonesonde, and surface observations, *Atmos. Chem. Phys.*, *8*(20), 6117-6136.

Zhang, Q., et al. (2009), Asian emissions in 2006 for the NASA INTEX-B mission, *Atmos. Chem. Phys.*, *9*(14), 5131-5153.

Zhang, Q., et al. (2007), Ubiquity and dominance of oxygenated species in organic aerosols in anthropogenically-influenced Northern Hemisphere midlatitudes, *Geophys. Res. Lett.*, *34*(13), L13801, doi:10.1029/2007gl029979.

Zhang, X. Y., Y. Q. Wang, X. C. Zhang, W. Guo, and S. L. Gong (2008), Carbonaceous aerosol composition over various regions of China during 2006, *J. Geophys. Res.*, *113*(D14), D14111, doi:10.1029/2007jd009525.